Automated Aerial Seed Planting using Biodegradable Polymers

A thesis submitted in fulfilment of the requirements for the degree

of

Masters of Engineering

in

Mechanical Engineering

at

The University of Waikato

by

Wade Cozens

THE UNIVERSITY OF
WAIKATO
Te Whare Wānanga o Waikato

2019

Abstract

The purpose of the thesis was to undertake a preliminary product design to assess the feasibility of using drone technology to aid reforestation for automated seed planting. This product would be able to increase productivity and reduce labour costs, especially when applied in difficult to reach terrains around New Zealand. Ultimately, the final product would be a weaponised drone or a swarm of drones that can fire plastic seed capsules into soil to a specific depth to prevent predation and ensure optimal germination conditions. The proof of concept hinges on the success of three objectives: Assessing and controlling the capsule's biodegradability in soil. A method of mass manufacturing projectile seed capsules that can be delivered at high velocity and the ability of it to be fired into soil to a specific depth to ensure safe germination.

Novatein was blended with poly(butylene adipate terephthalate) (PBAT) to aid sheet extrusion and improve water resistance. Biodegradability was tested by measuring the ability of bacteria and fungi to metabolise the polymer blends into CO_2 by enclosing samples in soil at 25 °C. PBAT showed very little biodegradation under these conditions, where approximately 3 % of the theoretical carbon content of the sample was converted to CO_2. Novatein reached 20 %, and the blends were intermediate, based on the amount of PBAT present. It was concluded that PBAT can effectively control the rate and extent of biodegradation in blends with Novatein.

A method for mass manufacturing seed capsules was evaluated by compression moulding spheres to test mouldability and manufacturing lap welded samples to quantify weld strength. Blends of Novatein and PBAT were successfully moulded and welded above the glass transition temperature of the material; optimal parameters were 105 °C with a three minute hold time. Lap welds were tested by varying the compression force and sheet thickness and thereby reducing the weld times to approximately eight seconds. Welded samples were tested for tensile and peel strength, where 0.68 mm thick sheets, welded at 750 N compression force, yielded the highest tensile strength (88 % that of an un-welded samples). Thicker sheets (1.52 mm) welded at 900 N compression force, resulted in the highest peel force. Producing capsules capable of penetrating soil would benefit from thicker sheets using sufficient pressure to prevent peeling at the seam.

Finally, seed capsule delivery was assessed using empirical modelling in combination with controlled soil conditions. Models created by Young and Lorenz used a dynamic cone penetrometer (DCP) to measure the soil's penetration resistance to predict the penetration depth of a known projectile. These models were developed for considerably heavier projectiles (> 2.2 kg) and penetration depths much greater than considered here. Considering the DCP measures the soils resistance to penetration at a depth of one meter, a comparison to a 10^{th} scale model was investigated. Contrary to expected, the standard DCP predicted the penetration depth of high velocity projectiles to a reasonably accuracy (~20 %) using two different types of homogenous sand, tested at three moisture contents. The scaled model failed to account for soil types, which was shown to have significant influence during high velocity testing. The work here highlighted the importance of considering realistic forestry soil, despite the accuracy of the prediction in homogenous sand.

Although an integrated product has not been developed, this project has shown that a strategy exists for controlling the rate of biodegradation of Novatein/PBAT. A plausible method for mass manufacturing seed capsules was demonstrated using compression moulding of Novatein blends. Penetration depth was predicted accurately for homogenous soil, this requires further research into applying the model to realistic top soil conditions. The final stage of the larger project is to integrate a firing mechanism with a drone for automated delivery of seed capsules produced from vacuum forming.

Acknowledgements

First and foremost, I would like to thank my supervisor associate professor, Casparus Johan Verbeek, for all the encouragement, support and guidance. Not only the support for this master's thesis, but during a summer scholarship, and with my honours research, you have certainly given me the skills to excel to heights I would not have expected when we first meet. Thank you very much for the over and above support and friendship.

I would like to thank members at the University of Waikato for their friendship, help and support. Technical support from Jonathan van Harselaar, and Peter Higgins. Samuel Hodder for the quality honours research that contributed to the results of Chapter 2, and for the technical support. Matthew Smith, Chanelle Gavin and Jim Bier for the guidance, advice and encouragement. Safiya Noorzai and Maria Flor, for sticking it out with me till the end. Alex Tibshraeny and Francis Bridge for the help, laughter, coffee and distraction when it was much needed.

I would like to say a special thank you to my parents, Garry and Jenny Cozens, who taught me that I have the ability to do anything I set my mind to. A lesson not forgotten. For the love and support, both financial and edible, that they have given me throughout my academic career.

Last but not least, to the amazing Lauren Paxton-Denny, encouraging me to take on this challenge, and giving me the love and support I needed to complete it.

Table of Contents

List of Figures

List of Tables

Nomenclature

PBAT	Poly(butylene adipate-co-terephthalate)	UAV	Unmanned aerial vehicle
FAA	Federal Aviation Administration	LDPE	Low density polyethylene
PCL	Polycaprolactone	PLA	Poly(lactic acid)
PBS	Polybutylene succinate	ASAE	American Society of Agricultural Engineers
DCP	Dynamic cone penetrator	Pa	Pascal (N/m^2)
ASTM	American Society for Testing and Materials	HDPE	High density polyethylene
EN	European Standard	PP	Polypropylene
PET	Polyethylene terephthalate	TPS	Thermoplastic starch
PBSA	Polybutylene succinate adipate	PHA	Polyhydroxyalkanoate
LLDPE	Linear low density polyethylene	TGA	Thermogravimetric analysis
FTIR	Fourier transform infrared spectroscopy	UV	Ultraviolet
PTFE	Polytetrafluoroethylene	IR	Infrared
pph	Parts per hundred	PVC	Poly(vinylchloride)
SEM	Scanning electron microscope	TEM	Transmission electron microscope
PHBV	Poly(hydroxybutyrate-co-hydroxyvalerate)	ASAE	American Society of Association Executives
OECD	Organisation for Economic Co-operation and Development	PLLA	Poly(L-lactic acid)
DMA	Dynamic mechanical analysis	TEG	Tri(ethylene glycol

T_g	Glass transition temperature (°C)	CAD	Computer aided design
CNC	Computer numerical control	ANOVA	Analysis of variance
F_D	Drag Force (N)	ρ	Density (kg/m^3)
V	Relative velocity (m/s)	A	Projected area (m^2)
C_D	Coefficient of friction	CI	Cone index
β	Viscous resistance of soil (m/s)	DCP	Dynamic cone penetrometer
P	Penetration depth (m)	m_p	Projectile mass (kg)
v_0	Initial velocity (m/s)	γ	Bearing strength of soil (N)
α	Inertial stress (kg/m)	D	Penetration depth (m)
S	Soil's resistance to penetration	N	Nose shape factor
W	Projectile mass (kg)	N_T	Tangent nose shape factor
N_C	Conical nose shape factor	CRH	Critical radius head
L_n	Ballistic length (m)	D_p	Diameter (m)
K_s	Mass correction factor	NZS	New Zealand Standards

Introduction

The purpose of this thesis is to develop a proof of concept for an automation technique that could increase the productivity of industrial seed planting ten-fold, while reducing costs equivalently. It will validate the potential use of a UAV or drone in combination with biodegradable polymers to contribute to the re-forestation goals set by the New Zealand government and around the world. Exciting developments in the quality and price of drones and biodegradable polymers has put this challenge in motion. Swarm technology could allow one pilot to be able to remotely operate a number of drones synchronously to plant thousands of trees in a day with minimal effort. This includes planting areas that are currently too rugged for a planter to do manually. However, the seed delivery device needs to be biodegradable to allow rapid degradation and seed germination.

It is well documented that deforestation has had a significant negative impact on the environment [1]. New Zealand has had a significant reduction in surface area of indigenous forest in the past 100 years from 82 % to 23 %. Forestry is a key contributor to the GDP of New Zealand, equating to 3.55 billion NZD, with plans for growth in this sector [2]. Government initiatives are driving this growth with the goal of planting 10 billion trees over the next ten years. However, 92 % of the forestry industry is privately owned and any increase in planting rates must be commercially viable. Current methods of planting forests for logging or natives are costly and labour intensive. For example, labourers in Canada were recorded to expend more calories than that of a marathon runner during a day's planting [3]. It is no surprise it is difficult to find labour willing to do such gruelling work, with relatively low pay in New Zealand.

Forestry is the third largest exporter in New Zealand and has over 1.7 million hectares of plantation forests, 90 % is Pinus radiata [4]. Due to this, there have been developments in forest planting leading to several techniques becoming more prominent within the industry. Open-pollination, where wind, insects or birds facilitate pollination, is the natural process. However, the vast majority of radiata pines are planted as cuttings. This allows forests of clones to be created from an older tree that is already showing good growing form [4].

Scion, located in in Rotorua, New Zealand, is home to one of the largest and longest running Pinus radiata experiments that began in the 1950s [5]. Initial selection

techniques were very simple and involved favouritism to desirable growth form, substantial grain size and high growth rate. In 1978 more rigorous trials were implemented that involved controlled pollination, propagation and cloning. One key problem with using propagated clones is that cuttings from trees older than 10 years have vastly lower growth rates. Scion is now able to use cryogenic embryogenesis to store vast quantities of clones from trees at a young age. This allows Scion to wait until favourable commercial characteristics have developed later in life, without compromising on the growth rate of clones [4].

With the return on investment in forestry being upwards of 20 years, it is clear that this is a major driving force for growing the best possible quality of trees. However, it is important to understand the balance between quality and investment in time with regards to return on investment. The price of planting trees was estimated in 1986 at 1 cent per thousand for open-pollination of P. radiate, whereas micro-propagated plants were at least five times the cost [6]. On average, 1200 stems/ha are planted and are thinned heavily, with final crop densities depending on several factors and are still up for debate. It was found that planting 50 stems/ha, trees had significantly increased stem diameter, however, the merchantable volume (m3/ha) harvested was drastically higher for 400 stems/ha. Final crops of around 400+ stems/ha are common in New Zealand [7]. Considering these thinned trees go straight to waste or are processed as pulp, it can be more cost effective to bulk plant seeds cheaply as opposed to expensive stems being planted from the perfect cloned species.

To achieve bulk planting at low cost, automation needs to be effectively utilised. Automation leading to increased productivity and quality whilst decreasing labour hours has been shown in a wide range of industries from producing electronics to farming [8; 9]. In forestry, mechanisation has seen a shift from manual labour towards working with machines that have resulted in decreased injuries. Among others, Sweden shifted approximately 90 % of its farming to industrial harvesting by the 1990s while reducing the risk of chainsaw accidents by 73 % [10; 11]. Technology is constantly improving to allow the production of new machines to make our lives safer and easier.

With growing awareness of the need for reforestation, a variety of emerging technologies are becoming available. Plant Tape Altea S.L has combined the conventional tractor, trailer combination with state of the art automation and

material science [12]. Figure 1 depicts the use of biodegradable film to house a wide variety of seedlings to be planted at specified intervals and depths. It uses multiple machines to sow 100+ seeds a second into the tape, packed in plastic trays holding 900 seeds that can be stored for transportation. Once watered they will germinate into seedlings, ready for transplanting [12]. In 2015 Tanimura and Antle [13] claimed that this machine allowed them to plant ten hectares of lettuces in a day using three people as opposed to using a more traditional trailer that planted four hectares using 15 people.

Figure 1: Plant Tape sourced from [12].

There are a few references to the use of drones for agriculture. One example is BioCarbon Engineering, a start-up company that is aiming to use drones to revolutionise the forestry industry. They are currently using fixed-wing UAV's to map planting environments to optimise available planting area. They intend to use this information to calculate flight patterns for a drone to plant seedpods. They claim they can plant 300 seedpods in 18 minutes whilst utilising a biodegradable seedpod with a nutritious hydro-gel to absorb impact forces and encourage germination [14]. Currently, they have filed patents in various countries with claims of novel inventions in relation to the data mapping system, optimised planting patterns, various seedpod bullet designs and seedpod delivery devices [15].

Figure 2: BioCarbon Engineering reforestation, sourced from [16].

DroneSeed is another start-up company that plans to tackle climate change by drastically reducing the cost of re-forestation. It boasts being the first company to become FAA approved to use swarm technology with drones to spray plantations. This allows one pilot to control up to 15 drones that can identify and manage weeds. It plans to expand its current operation, using its swarm technology to optimise planting efficiencies and reduce labour hours at least tenfold. They claim to have developed a biodegradable pod to encapsulate a seed that can be shot out of "effectively a paintball gun" [17].

These three companies are all utilising plastic to aid in increased automation. However, plastic is quickly becoming one the world's major environmental challenges. A major issue for the polymers industry is the common confusion around inconsistent definitions associated in the plastics industry. Biobased polymers, commonly thought to be degradable, while synthetic polymers are thought to be non-degradable, neither are 100 % true. Even the definition of biodegradability comes under contention. Therefore, it is uncertain if these emerging technologies are going to aid or hinder the environment.

Polymers have become an integral facet of every aspect of the world, which produced approximately 335 million tonnes of synthetic plastic in 2016. The European plastics industry had a turnover of approximately 350 billion Euros in 2016 [18]. The agricultural industry is no exception, estimated to consume almost 695,000 tonnes of plastic in Europe. Typical uses include single use silage or mulch wrap and sheets for greenhouses to name a few. Low density polyethylene (LDPE) is the polymer of choice as it is cheap and durable, however, not biodegradable [19].

If a plastic is termed biodegradable it is generally referring to degradation as a result of industrial composting at elevated temperatures of 50 to 60 ˚C, European standard, EN 13432 states under these conditions it must reach 90 % biodegradation within 180 days. Since the vast majority of plastics end up in landfill, most will biodegrade at similar rates to common plastics such as LDPE. A range of synthetic and biobased polymers have been given this standard such as; poly(butylene adipate terephthalate) (PBAT) and polycaprolactone (PCL) (synthetic polymers), or PLA (Poly(lactic acid)) , PBS (Polybutylene succinate) and starch blends (biobased polymers) [20]. However, in practice, the vast majority of biodegradable plastics will never reach the desired temperatures for degradation. Especially for the proposed product development that involves large quantities of plastic to be discarded into the soil. One key challenge of this study will be to evaluate ability for biodegradable polymers to biodegrade in a realistic environment.

For a seed to be accurately and safely fired into the ground, a method of encapsulation must be developed. The seed capsule must satisfy the following issues; a vessel that can be used as a projectile with the ability to penetrate the soil, a means of shock absorption, biodegradable, not interfere with germination and be affordable for mass manufacturing.

A case study of radiata pine seed growth found that 99 % of seeds germinated when planted 6 mm deep, at 3 mm they were susceptible to drying and bird predation, while germination reduced dramatically below 16 mm [21]. Generic methods of mass manufacturing plastics typically involve temperatures of 150 °C and above, therefore, if the seed is going to be encapsulated it may experience some heat. Calvo *et al.* [22] studied the effect of temperatures on germination rates of three pine species, when the seed was held at 200 °C for five minutes or at 300 °C for one minute the germination rate dramatically decreased. There was no substantial reduction when holding for 150 °C for five minutes or 200 °C for one minute. This gives a crucial processing parameter during manufacturing.

To accurately penetrate a wide variety of soils to a highly specific depth, it is first important to understand how different soil characteristics affect penetration. Important physical properties of soil are porosity, bulk density, water retention capacity, particle distribution and soil strength. Soil strength is characterised as the resistance of particles shearing past each other which is highly dependent on moisture content and directly relates to the ability for root growth and penetration

resistance [23]. Testing the soil's resistance to penetration is standardised by using cone penetrometers, which apply a force and measure the cohesive forces between soil particles and the frictional resistance to sliding past each other. Two main types of penetrometers are static and dynamic, one being pushed into the ground with constant force, the latter with an anvil that is dropped from a specific height [24]. When using a static cone penetrometer conforming to ASAE 1983 standard S313.1, some common values range from 0.5 to above 3.0 MPa for loose to extremely dense soil [23].

Ideally, the results of the dynamic cone penetrator (DCP) can be used to correlate the impact energy required to penetrate a desired depth. However, calculating the soil resistance is not an exact science and has a variety of mitigating factors. C.W Young developed a range of empirical formulae for predicting the penetration depth of projectiles using a DCP to characterise different soil types [25]. To ensure that this method of delivery is feasible, a study will need to be performed around the ability to effectively test the soil at a test site and relate this to an empirical equation for predicting the penetration depth, by varying the impact energy through velocity.

This study will endeavour to evaluate three key challenges around this prototype; plastic biodegradability, mass manufacture and accurate penetration control. It will be limited to segregated experiments delivering a proof of concept. The integration of a physical prototype will not be attempted. The study only considered Novatein and blends with PBAT, being preselected as part of a larger project. Novatein is a protein-based thermoplastic derived from blood meal and is generally considered biodegradable [26]. PBAT is also a biodegradable thermoplastic, but is petroleum derived. It is blended with Novatein to increase the material's water resistance. The polymer materials engineering to evaluate these blends was not part of this study [27].

Chapter 1

Biodegradability in Soil

In the 21st century, the use of plastics is integrated into every facet of life and will undoubtedly play a part in solving the pressing deforestation issue. However, widespread use needs careful consideration not to create more problems. It is crucial to understand how polymers are made, but more importantly how they degrade. This section will discuss a variety of polymers; non-degradable, biodegradable, biobased and fossil-based (Figure 1.1). By clearly defining these, we can determine what makes one polymer more susceptible to degrading opposed to another. The aim of this chapter is to put biodegradation of polymers in context of automated planting and to describe the rate at which blends of Novatein and poly(butylene adipate-co-terephthalate) (PBAT) biodegrades in soil. The purpose of blending Novatein with PBAT is to give the product designer the ability to tailor the rate of biodegradation of the device used to plant seeds. Novatein alone is known to be unsuitable due to its high water sensitivity and low impact strength, which is an additional advantage of blending it with PBAT.

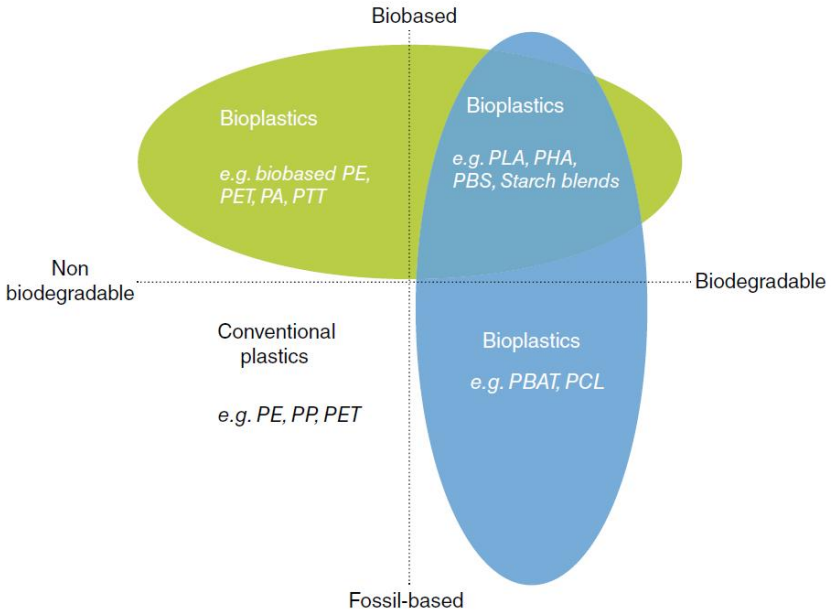

Figure 1.1: Definition of bioplastics according the European bioplastics, Sourced from [20].

1.1 Literature

1.1.1 Synthetic polymers

Fossil-based polymers are derived from petroleum and are commonly referred to as synthetic plastics and cover approximately 99 % of the plastic market [28]. They are essential in every part of our day from our clothing, food packaging and where we sleep. Typically made from crude oil, it uses 62 to 108 MJ/kg to produce, higher than common steel production but much more versatile [29]. High and low-density polyethylene (HDPE & LDPE) are very common synthetic plastics used in a variety of applications such as bottles, toys, wiring insulation, plastics bags and food packaging. HDPE has become highly popular due to its ease of processing and being able to be recycled, however, the US Environmental Protection Agency estimates only 27.5 % is actually recycled [30]. Therefore, as the vast majority of plastics end up in a landfill, it would be advantageous if they were biodegradable. If plastic is termed biodegradable, it is generally referring to degradation as a result of composting at elevated temperatures of 50 to 60 ˚C and EN 13432 states under these conditions it must reach 90 % biodegradation within 180 days.

I. Non−degradable polymers

Most common plastics are designed to resist biological attack, as one of the main uses is food packaging. They are designed to be durable to compete with other materials such as metal or wood, which was done with much success, taking centuries to decompose in landfills. Most common plastics like LDPE, polypropylene (PP) and polyethylene terephthalate (PET) have high corrosion resistance and longevity. They are even designed to be recycled. However, the environmental impact comes from one-time use that doesn't make its way into the recycling bin. Higher grade plastics that cannot be directly recycled can be ground down and used as fillers.

II. Degradable polymers

It is not commonly known that there a range of synthetic polymers that have a high level of processability whilst being biodegradable. As seen in Figure 1.1, PBAT and polycaprolactone (PCL) are synthetic, but biodegradable [31]. PCL has good chemical resistance to oil, chlorine and water, and it’s low viscosity and melting point (58-60 °C) allows a high level of processability [32]. PBAT is an expensive

co-polymer in comparison to LDPE, due to the industrial production requiring long processing times, high and vacuum and temperatures. It is highly processable due to low viscosity, giving an elongation at break of approximately 700 % [33]. Due to the high cost of these two polymers, using them as blends with other biodegradable polymers to improve processing is of interest. Luc and Christophe [31], successfully blended thermoplastic starch (TPS) with PBAT, PCL and polybutylene succinate adipate (PBSA). By using these blends, the dimensional post-injection stability of TPS was increased while maintaining the mechanical properties.

III. Biosynthetic polymers

Some synthetic polymers can be synthesised by bacteria opposed to the standard petrochemical way making them a more renewable source and can be considered more environmentally friendly. Polyhydroxyalkanoates (PHAs) are polyesters made from bacteria with good mechanical properties allowing them to be used as stents for heart valves or as fishing line whilst still being biodegradable [34]. Confusion comes in with biosynthetic polymers such as bio-PET can be made using biomass using bio-based ethylene glycol, which is not biodegradable. During a life-cycle analysis, it was found that there was a 20 to 50 % reduction in the greenhouse gases in the production of bio-PET as opposed to petroleum-based PET [35]. These new developments have allowed large corporations like Coca Cola switching to using bio-PET bottles reducing its environmental impact considerably [36].

1.1.2 Biobased polymers and Novatein

Biobased polymers are defined as polymers derived from biomass [37], sourced from organic or renewable sources. The most commercialised biobased plastic is thermoplastic starch, a polysaccharide [38]. It can be made from a number of abundant natural sources such as cassava, corn and potato. It has become more commercially favourable due to its cheap processability good mechanical properties. Potato starch, for instance, can be film blown which is essential in for the food packaging industry [39]. Alternatively, there have been numerous successful plastics made from sustainable protein sources such as gluten, zein, whey, soy and Novatein [40]. Currently, bioplastics make up less than 1 % of the total polymer industry, however, due to the increased public awareness and the recognised quality of bioplastics, this is projected to significantly grow [28].

Ethical debate has been raised about using plant sources for producing plastics, as it is potentially depleting food sources. The validity of this debate is yet to be determined, however, the ideal alternative is using waste products to produce plastics. Aduro Biopolymers Ltd developed a thermoplastic made from a waste product from the slaughter industry. Novatein is made from bloodmeal, which is 90 wt.% protein that is not suitable for human consumption, making it a perfect renewable material. Blood meal is also an effective fertiliser, containing approximately 12 pph nitrogen and has a 1 to 4 week release time, depending on soil activity, climate and moisture content [41]. It is capable of being injection moulded, with similar mechanical properties as LDPE [42].

Novatein's material properties have been improved by blending with a variety of commercial polymers, such as, linear low density polyethylene (LLDPE), PBS and PLA that increased mechanical properties, thermal stability and water resistance [43]. Continued studies have widened the range of processing techniques such as foaming and continuous sheet extrusion when blending with PBAT [27; 44].

Novatein is assumed to be biodegradable due to being a highly hydrophilic protein polymer. A composting study, at approximately 69 °C, was performed by Verbeek *et al.* [26] that investigated the effect of plasticizer content Tri(ethylene glycol) on biodegradation by mass loss, thermogravimetric analysis (TGA) and Fourier transform infrared spectroscopy (FTIR). Plasticized samples lost 47 ± 4 % dry mass loss over 12 weeks whilst non-plasticized samples only lost 36 ± 4 %. Plasticized samples started to disintegrate after six weeks, showing signs of surface cracking and pitting, whereas, the non-plasticized samples were still able to be removed intact. By week 12, both samples disintegrated (Figure 1.2).

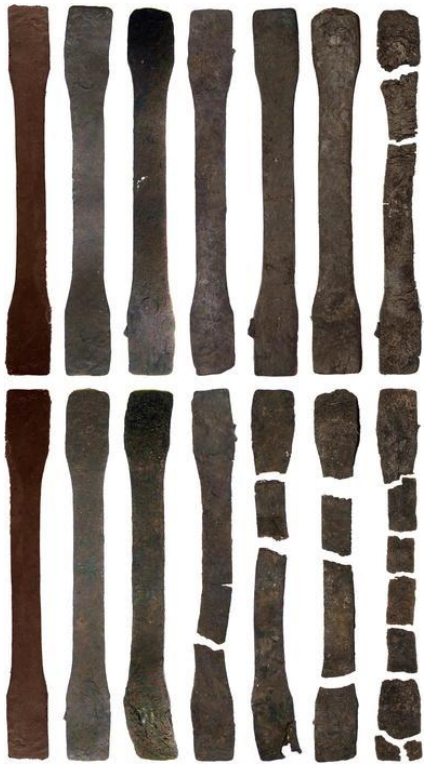

Figure 1.2: Composting trial with non-plasticized samples (top) and plasticized samples (bottom), sourced from [26].

After the trial had finished, samples were found to have a reduction in combustion temperature, via TGA analysis, indicating that stronger covalent bonds may have been reduced, inferring biodegradation. This was also confirmed by FTIR analysis [26]. This study was performed in typical common industrial composting facility, however, for the current project, compositing is insufficient. It is necessary to understand the variety of ways that polymer degradation occurs, such as, abiotic (UV or thermal disintegration) or biotic (bacterial and fungal metabolisation). The techniques by which these degradation methods are quantified will enable the suitable experimental method to be investigated.

1.1.3 Abiotic degradation

Abiotic degradation occurs via a variety of mechanisms such as ultraviolet (UV) radiation, hydrolysis, disintegration, or thermal decay. The majority of polymers will experience abiotic degradation while still in use [45; 46].

I. Thermal degradation

Thermal degradation refers to degradation as a result of heat, leading to bond scission. It typically occurs during processing, and many polymers have to be stabilised against thermal degradation. The activation energy required is

proportional to the bond energy of the macromolecular structure; e.g. polytetrafluoroethylene (PTFE) has higher thermal stability than PE, considering PTFE has a C-F bond of 116 kcal/mol compared to a C-H bond of 97 kcal/mol [47]. Thermal degradation can be used beneficially during pyrolysis, which is burning plastics in the absence of oxygen, and is a potential alternative for recycling plastics where the heat energy is used for steam generation and the hydrocarbon gases can be converted into fuel sources [48].

II. Photo−degradation

Varying levels of photo-degradation occurs in polymers due to UV, visible and Infrared (IR) radiation [49]. Radiation breaks down chemical bonds which cause polymers to become brittle, change colour and is detrimental to mechanical properties. Natural impurities present during processing tend to absorb more radiation than repeating units, increasing the photo-degradation. PE and PP have high resistance to photo-degradation whereas poly(vinylchloride) (PVC) becomes brittle if not protected correctly. Photo-degradation has also been applied as a mechanism to induce degradation and has led to the widespread misuse of the term degradable polymers. During photo-degradation, the polymer is simply fragmented and is not converted into water and CO_2. Additionally the products of photo-degradation has led to the widespread concern over the effect of micro-plastics in the environment [50].

1.1.4 Biotic degradation

Biodegradation is the result of microbiological activity such as bacteria or fungi, using plastic as a source of energy where the polymer structure is broken down to enter into the carbon cycle without the aid of external heating [46]. In aerobic biodegradation, there are two main mechanisms; oxidation and hydrolysis. Biological hydrolysis is catalysed by hydrolase enzymes reducing the polymer mass [51]. This is typically a two-stage process, first larger chains are broken in smaller ones via depolymerisation then complete mineralisation [52]. The degree of biodegradability is dependent on a variety of factors such as specific functional groups, morphology, solubility, molar mass and crystallinity [53]. Functional groups, such as peptide, amide, and esters are subject to hydrolysis and/or oxidation, and polymer containing these groups in its backbone are often more susceptible to biodegradation [51].

Due to synthetic polymers being relatively new, most organisms lack enzymes with the ability to transform them into an intermediate state, which is readily metabolised. Another key to being susceptible to microbial attack is the polymer's chemical and physical structure. Enzymes need a physical site to penetrate the polymer such as a pore, which is difficult when it is water-insoluble; they also need chemical groups that can be readily attacked. This is why simple polymers such as polyethylene with repeating C-C backbone are so resistant to microbial attack [54]. Griffin found by blending PVC with increasing amounts of starch there was a relative increase in fungal growth without a significant reduction in tensile strength. This was due to increased porosity and attack sites [55].

Biobased polymers generally have complex chemical structures that attribute to their lack of processability, but is also a key factor in the biodegradation. The following methods are used to evaluate the success of biodegradability.

I. Visual

Visual examination can accompany other test methods for added anecdotal evidence. The growth of fungus or bacteria implies biodegradation may be occurring in the plastic, however formation of cracks or crevices imply degradation but do not prove biodegradation. This can be more accurately quantified by using a scanning electron microscope (SEM) or transmission electron microscope (TEM) imaging [46]. Lopezllorca *et al.* [56] buried PHA in soil and used SEM to prove the presence of biodegradation via the colonisation of hyphae and surface cleavage by following hyphae tracks as seen in Figure 1.3.

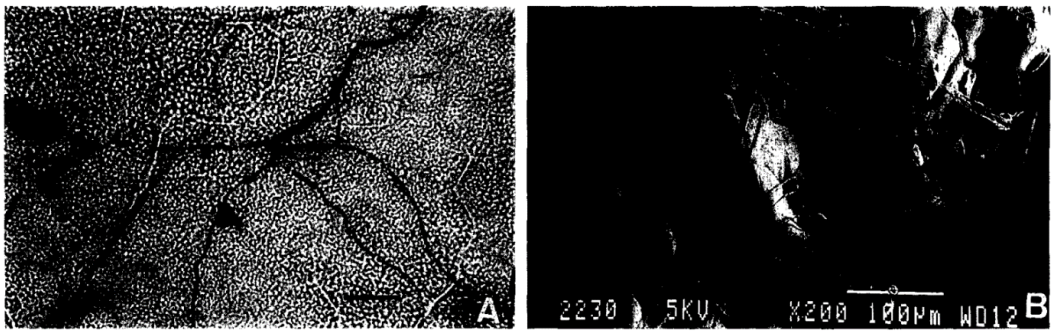

Figure 1.3: Hyphae colonisation and tracks on PHA films [56].

Weng *et al.* [57; 58] studied the biodegradation of PLA, PBAT and a blend of 40 : 60, PBAT to PLA in soil. The study left cast films 400 mm deep in soil that remained at approximately 20 ± 3 °C. Visual disintegration was observed over four months (Figure 1.4) while scanning electron microscope (SEM) images showed

numerous cracks in the surface of PBAT (Figure 1.5) and corrosive holes on PLA (Figure 1.5). PBAT and PLA independently degraded faster than the blended sample.

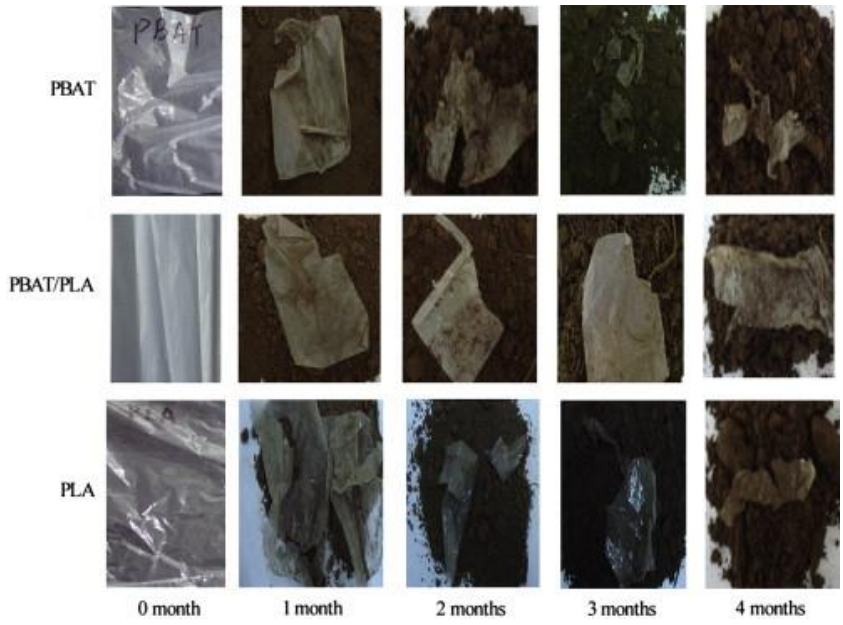

Figure 1.4: Biodegradation of PBAT and PLA films left in soil for four months, sourced from [58].

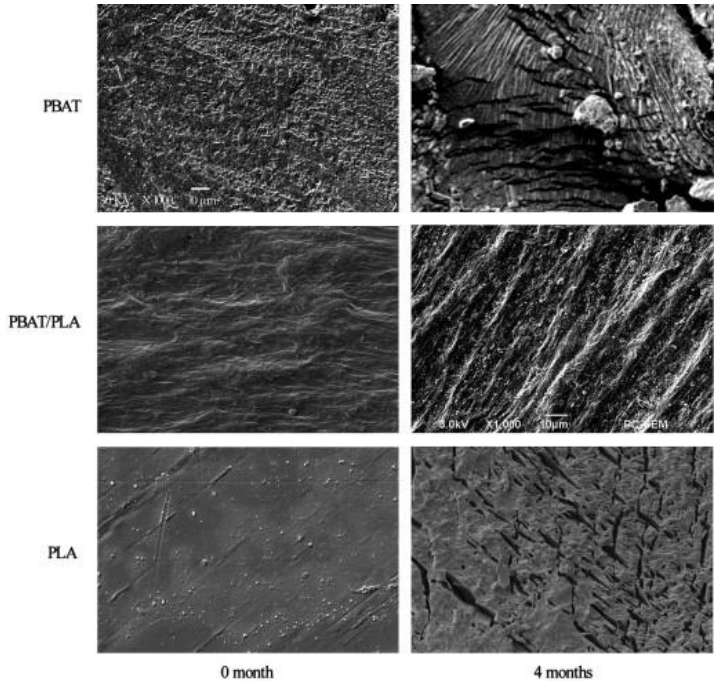

Figure 1.5: SEM images of the biodegradation of PBAT and PLA films in soil over four months sourced from [58].

II. Mechanical properties

As most plastics are designed with specific mechanical properties to be fit for purpose, observing changes in mechanical properties from degradation is crucial for longevity tests as well as inferred degradation. A reduction in tensile strength cannot prove biodegradation but is an effective way to test if degradation is occurring [46]. Luo *et al.* [59] studied the decrease in mechanical properties of poly(hydroxybutyrate-co-hydroxyvalerate) (PHBV) during a composting trial. Figure 1.6 shows the reduction in tensile strength from 30 MPa to 16 MPa after 30 days composting.

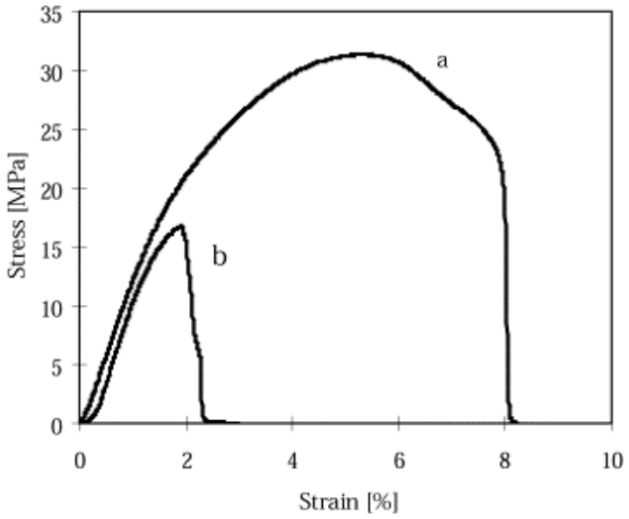

Figure 1.6: Stress-strain graph of PHBV before (a) and after (b) 30 days of composting [59].

Sabo *et al.* [60] investigated the effect of environmental conditions (exposure to 60 days of high humidity and submerged in water) on blends of PCL with wood flour and microcrystalline cellulose and found only minor reduction in mechanical properties. The mechanical properties of Novatein were found to deteriorate due to embrittlement after prolonged UVA exposure, the elongation at break reduced ten-fold and toughness reduced to 4.3 % of its original value for non-plasticized samples [61].

III. Mass loss

Mass loss studies have been commonly used for long-term soil biodegradation trials, but problems arise with the repetitive nature of sample cleaning, soil consistency and general disintegration of material leading to inaccurate results [46]. During a composting trial over 12 weeks at an average temperature of 69 ˚C, it is was found

that Novatein had a dry mass loss of 47 ± 4 % [26]. Huang *et al.* [62] investigated the mass loss of PBS and PCL in a composting system and found that the blend biodegraded faster than that of the individual polymers. The blend lost 32.7 % of its mass within 60 days. Luo *et al.* [59] found that PHBV lost approximately 80 % of its original mass during a 50 day composting trial.

Mass loss is also an integral part of the biodegradation/compositing standards. ASTM 5988 states that a compostable plastic should lose 70 % of its mass with in a six month period [63]. Although mass loss does not prove biodegradation, it is a reliable indicator thereof.

To avoid experimental error when collecting samples from soil it has been found to be more accurate to combine mass loss with measuring carbon dioxide evolution from microbial activity (when using a polymer as a food source). One of the definitions of being biodegradable is that the plastic returns to the carbon cycle, hence it makes sense that benchmark testing for the rate of biodegradation is to measure the amount of CO_2 produced via microbial activity. However, technical difficulties arise with synthetic polymers that have low biodegradation rates where measuring the amount of activity can be unreliable [46]. However, this method works very well when testing biobased plastics, like thermoplastic starch. Gang *Et al.* [64] found that TPS had 60 % of its CO_2 mineralised at room temperature within 14 weeks whereas LDPE had zero activity.

There are a number of standards that detail the experimental process involved, ASTM D5988 – 18, ASTM D 5209 – 92 and OECD 301 B & D [65; 66]. The tests typically consist of a closed gas system that controls the inlet and outlet with high precision (Figure 1.7). The sample polymers are put in a solution of water or soil, inside a closed vessel. The Sturm test uses an H_2O solution with municipal waste inoculum added whereas ASTM 5988 uses soil from three different fertile locations with a variety of soil specifications around PH and moisture content, to name a few [65; 66]. The results are obtained by calculating the amount of carbon evolved from each sample as a percentage of the total carbon within the system. Success is defined for ASTM 5988 as the sample and a cellulose control reach 70 % of the theoretical CO_2 content evolved during a 6 month period but is often reduced to 2 to 3 months [63; 67].

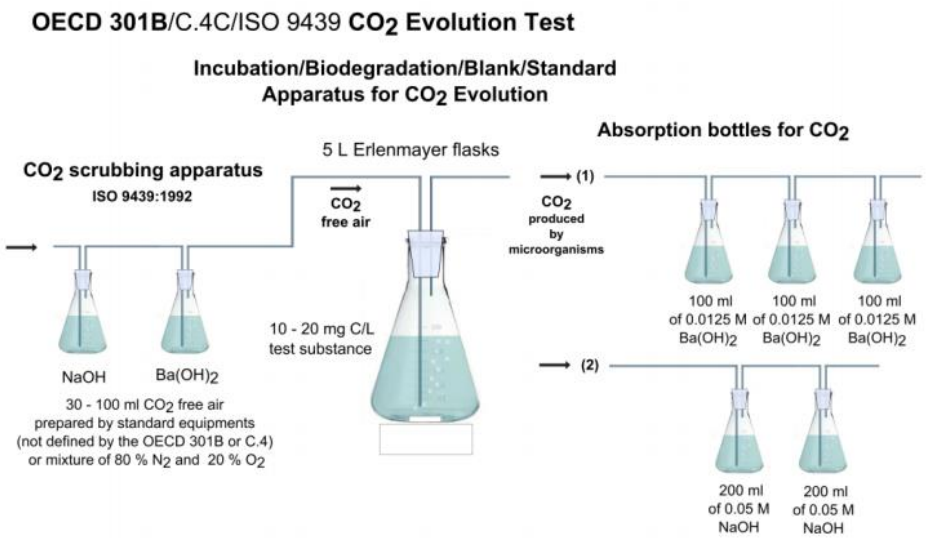

Figure 1.7: Sturm test based on OECD 301B/C/ISO 9493 CO_2 Evolution test, sourced from [68].

Briassoulis *et al.* [69] followed the French Norm test, which measures the expelled CO_2 from polymers in soil samples kept at 25 °C. Figure 1.8 shows that MATER-BI, a starch-based polymer, well known for biodegradability polymer only reached 38 % of its original carbon content over 6 months. The cellulose control reached the required 70 % and polyethylene appeared to have no change at all.

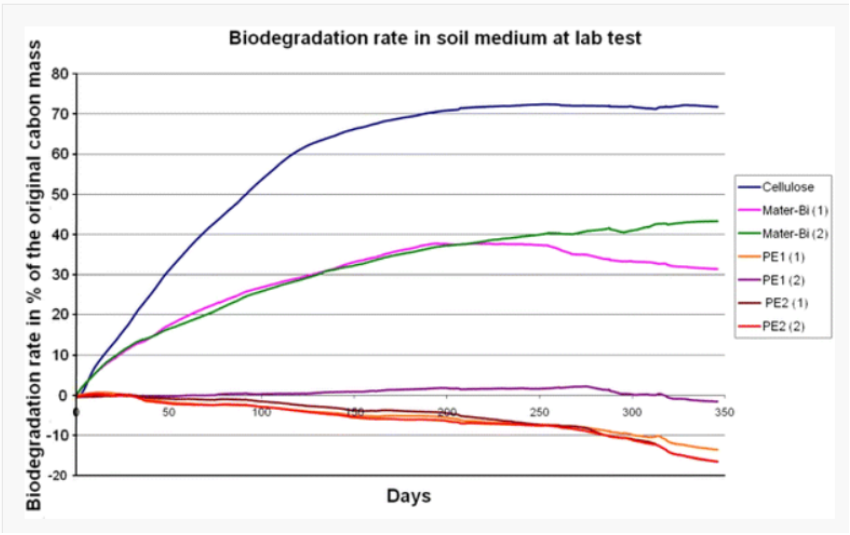

Figure 1.8: Percentage biodegradation of polymers in soil [69].

Feuilloley *et al.* [67] tested the biodegradation of three polymers using 10 standardised techniques, materials tested were; MATER-BI, Ecoflex® (PBAT), and PE modified with a peroxidant. The results (Figure 1.9) agree with those of Briassoulis *et al.* and showed that MATER-BI biodegrades to approximately 40 % on the same test, (Figure 1.9 experiment "headsp. 25 °C") and readily biodegraded

in all tests, apart from in the anaerobic environment. PBAT showed better biodegradation results than modified PE for the most part asides from “headsp. 25 °C” and “anaerobic test” (Figure 1.9). Whereas when the Sturm test was performed, PBAT showed significantly more biodegradation than headsp. 25 °C, this is likely due to the presence of more aggressive bacteria collected from the municipal waste. Possibly the most interesting finding is the agricultural soil test, where small films pieces were left underground for over 11 months and showed that modified PE was almost fully degraded whereas PBAT showed very little. This was attributed to a pre-treatment performed on the PE films of 90 to 100 °C for a few weeks, which would never naturally occur in the soil [67].

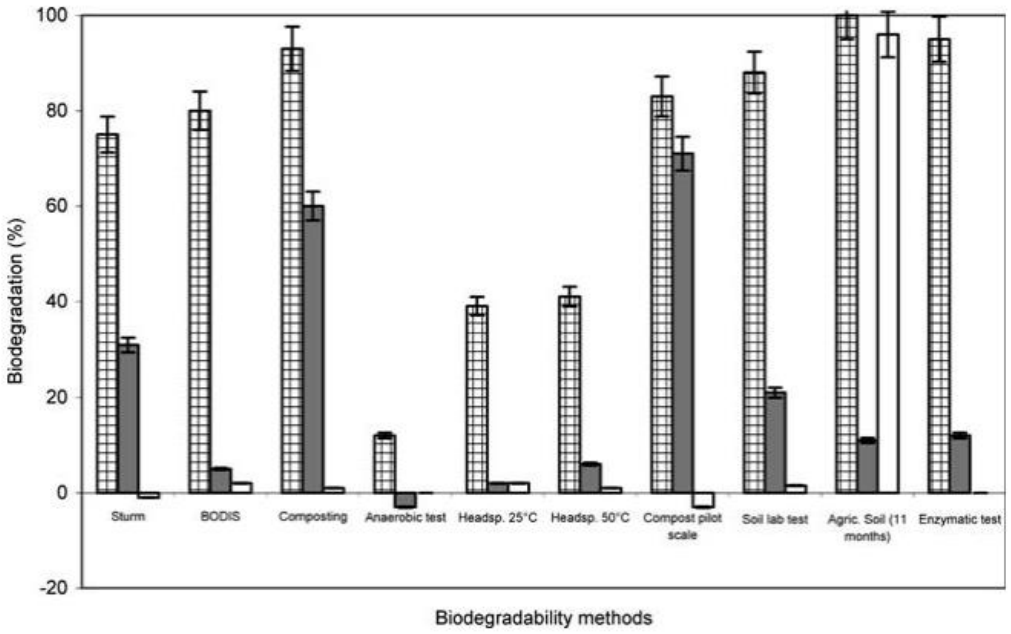

Figure 1.9: Biodegradation results for MATER-BI (checked), Ecoflex® (Black) and modified PE (white) [67].

From the literature above, it is concluded that a modified Sturm test that incorporates ASTM 5988 will be used to investigate the rate of biodegradation for different blends of Novatein and PBAT in soil.

1.2 Experimental Methods

The following section describes what materials and parameters were required to develop an apparatus that can accurately measure the rate of biodegradability in soil for a variety of samples.

1.2.1 Biodegradation method

This test evaluates the rate of biodegradation by measuring the percentage of the carbon content of polymer blends converted to CO_2 via microbial action over time. The method chosen was a modified Sturm test incorporated with ASTM D5988 and D2905 [63; 70; 71]. This method uses Schott bottles containing test material and soil. An experimental flow chart can be seen in Figure 1.10 and physical experimental set can be seen in Appendix A.

In short, the test involves supplying an equal amount of air to each test specimen after it has been scrubbed for CO_2. Microbial activity in the soil leads to biodegradation releasing CO_2, which is individually captured for each sample. The rate of biodegradation is assessed based on the rate at which CO_2 is formed.

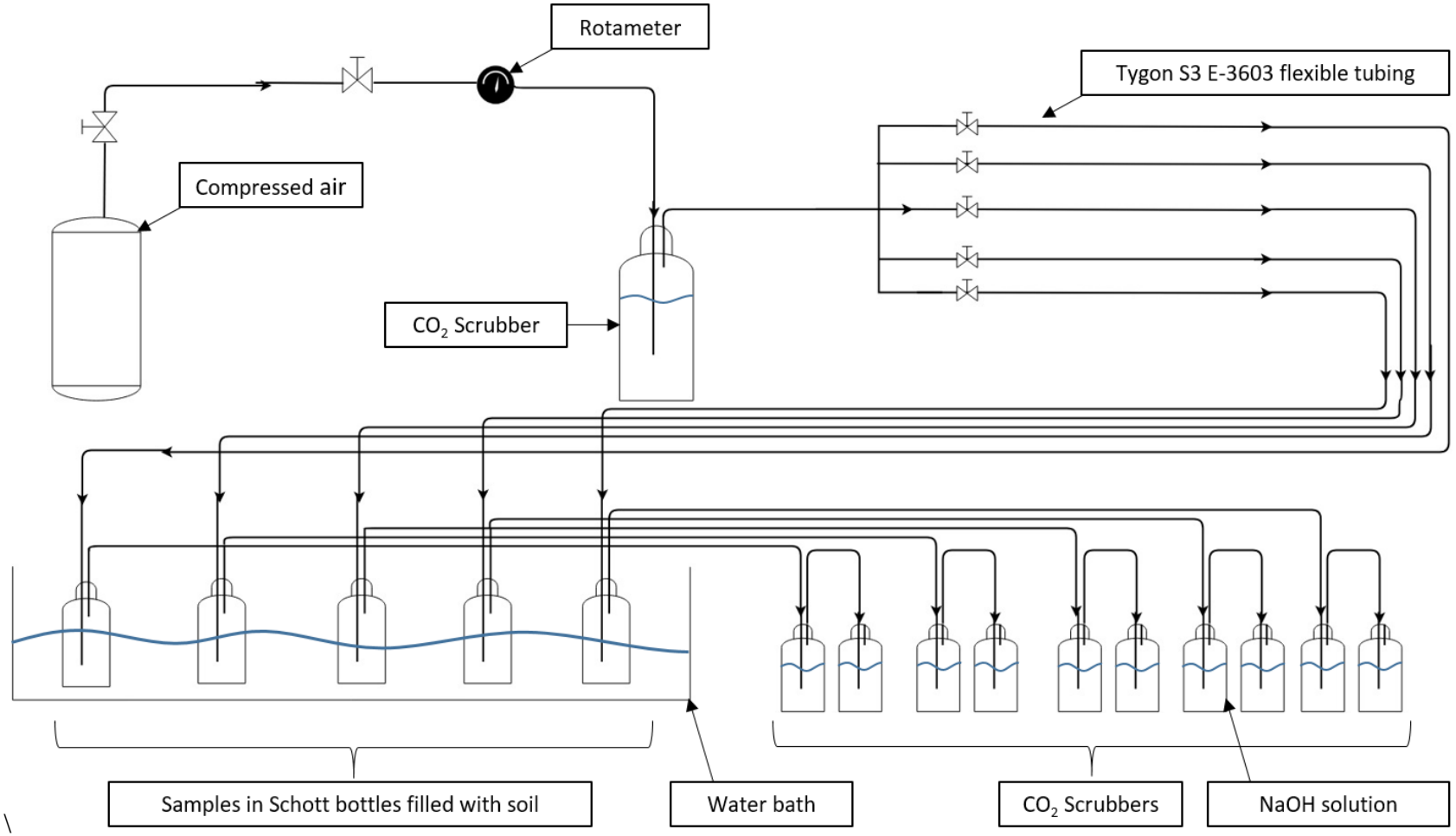

Figure 1.10: Flow diagram showing the configuration of the biodegradation test.

Four formulations were tested (Table 1.1). Formulations one to four were tested in triplicate while the control and positive control had only two repeats. The test mass of each sample was calculated to ensure 1 g of carbon is present in each sample (calculations can be found in Appendix A)

Table 1.1: Test formulations for biodegradability experiment.

Formulation	Novatein wt.%	PBAT wt.%	Corn-starch wt.%	No. of repeats	Test mass (g)
1	100	0	0	3	2.18
2	0	100	0	3	0.98
3	90	10	0	3	2.06
4	70	30	0	3	1.82
5	50	50	0	3	1.58
Positive control	0	0	100	2	1.50
Negative Control	0	0	0	2	0.00

A constant supply of CO_2 free air is equally distributed through a 19-valve manifold into each bottle where the air is bubbled through two CO_2 scrubbers attached in series. Each CO_2 scrubber has 200 mL of 0.1 M NaOH. CO_2 free air is abstained by scrubbing the inlet air is a 1.5 L Schott bottle, containing the same NaOH solution. Using a 1 M HCl titrant solution the phenolphthalein indicated endpoint that will enable the CO_2 content to be calculated. The efficiency of the scrubbers are calculated dissolving a known quantity of CO_2 into the system and then comparing with the titrated results using Equation 1-1.

$$efficiency\ (f) = \frac{CO_{2\ Scrub}}{CO_{2\ Total}} \qquad 1\text{-}1$$

Proof of biodegradability is defined as converting 70 % of the carbon content of the sample being converted into carbon dioxide over a reasonable timescale (90 days). The mass of CO_2 absorbed by the scrubbers was calculated using the following equation.

$$\frac{\left(\left((V_{CT} - V_{ST}) * HCL_{\frac{moles}{L}}\right) * MW_{CO_2}\right)}{f_{efficency}} = m_{CO_2} \qquad 1\text{-}2$$

Where V_{CT} is the control titrant volume, V_{ST} is the scrubber titrant volume. Using the corrected mass of CO_2 absorbed by the scrubber the mass of carbon can be calculated and converted into a total percentage degradation of the one gram of carbon in each sample (Equation 1-3).

$$\left(\frac{\left(m_{CO_2} * \frac{(MW_C)}{(MW_{CO_2})}\right)}{m_{sample\ total\ carbon}}\right) * 100 = total\ percentage\ degraded \qquad 1\text{-}3$$

1.2.2 Soil preparation method

The soil was collected from three diverse locations in accordance with ASTM D5988. Sample one was collected from a field in Cambridge, Waikato, where horses graze. Sample two, from Maungatautari Sanctuary Mountain, a dense native forest, which has become the largest pest-proof fenced restoration project in the world [72]. Sample three, a privately owned industrial pine forest in Kinleith. Each sample collected was a 300 * 300 * 300 mm (wide, long, deep). The locations and soil type can be seen in Figure 1.11.

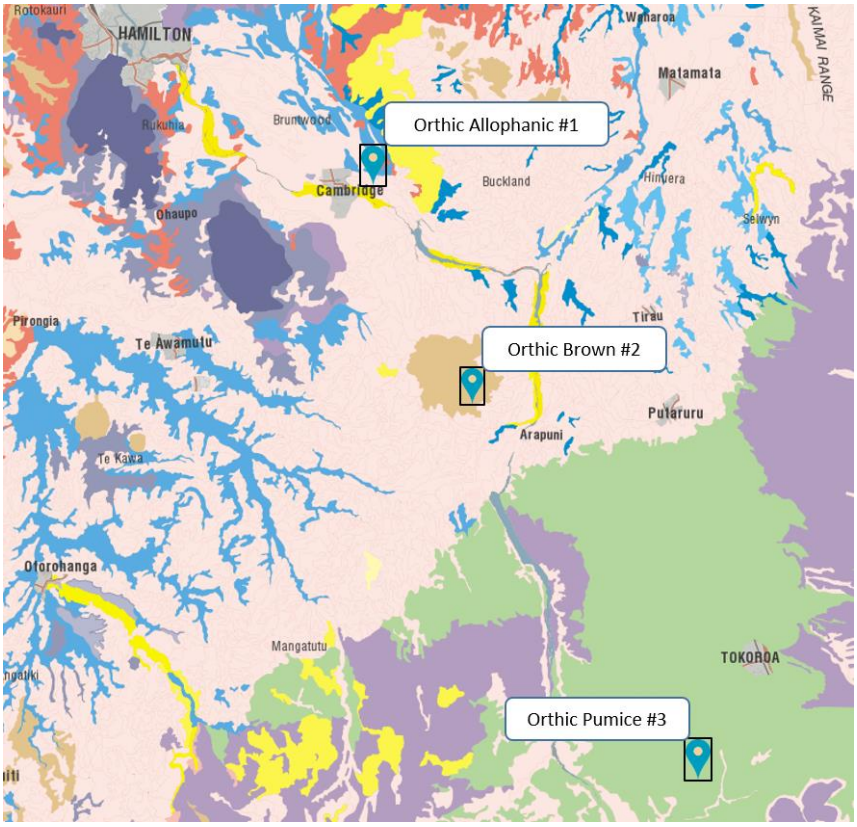

Figure 1.11: Soil map of New Zealand, sourced from [73].

The moisture content of each sample was measured upon collection. The moisture contents of Cambridge, Maungatautari and Kinleith were 32.3, 59.4, and 39.6 %, respectively. Each sample was stored in sealed buckets at 4 °C for no more than

two weeks before starting the experiment. Each sample was sieved 2 mm particle sized to remove any obvious plant material. Equal parts by mass of soil were mixed together and Ph tested in accordance with D4972 method A, using Eutech Instruments Ph 150, and the Ph of the mixed soil was on found to be 5.33. ASTM 5988 states that the Ph is required to be within 6.0 and 8.0. The soil Ph was not adjusted as the experiment favoured consistency with the environment opposed to standardisation. The C:N of the soil was not calculated.

1.2.3 Sample preparation method

Injection moulding grade Novatein IR3020 was obtained from Aduro Biopolymers LP (Hamilton, NZ). PBAT is produced by BASF under the tradename Ecoflex C1200 and was acquired from Clariant (Auckland, NZ). Novatein was rehydrated with H_2O to its initial MC of 32 % for consistency. PBAT was grafted with Joncryl and 2-methylimidazole (2MI), acting as a compatibiliser to improve blend morphology with Novatein [27].

A Labtech twin-screw extruder was used to produce the required blends. The temperature profile increased from 70 to 140 °C over 11 stages. It had an L/D ratio of 44 to 1. The screw speed was at 250 rpm with a feed rate 115 rpm that resulted in a mass flow of approximately 0.2 kg/min. Five blends were required for testing. Formulations are stated in Table 1.1. Blends were granulated using a tri-blade granulator with a 4 mm plate (Castin Machinery, NZ). The resulting specimens had their natural carbon content theoretically calculated, calculations can be found in Appendix A.

1.2.4 Experimental procedures

I. Scrubber efficiency and air flow calibration

During testing the CO_2 scrubbers efficiency, it was determined that accurately controlling the air flow of the 19 samples was critical for the experiment. It was established that having two air regulators in series was insufficient and a third more precise rotameter was required. Once this was in place, it was possible to know exactly what flow rate (L/min) of air was entering the system. Using this knowledge the scrubber efficiency test was performed by measuring the amount of CO_2 collected from two scrubber in series, when knowing the total CO_2 entering the system.

The absorption efficiency of two scrubbers in series was calculated to be 45.5 % using Equation 1-2, at a flow rate of 18 – 22 mL/min. The poor efficiency was to be expected and was attributed to the poor mass transfer due to small surface area to volume ratio of the CO_2 bubbles. Diffusers were not investigated, as the use of diffusers did not show significant increase in efficiency in a similar study [51]. Scrubber efficiency data and calculations can be found in Appendix A.

To calibrate the systems air flow through the manifold, each scrubber had to be filled and connected. At this stage the 500 mL sample Schott bottles were empty. By tweaking the individual ball valves on each sample line, the approximate number of bubbles per minute exiting each scrubbers could be equalised for the 19 samples. In practice, it was impossible to give all 19 samples the same amount of airflow. This was due to the ball valves being not finely tuned for the low flow rate (10 mL/min). This in turn made even the slightest fluctuations in back pressure cause one sample to stop bubbling completely, while others kept bubbling. This was partially resolved by increasing the total flow-rate through the system to 400 mL/min, this resulted in an approximate air flow of 21 mL/min for each sample. At this flow-rate it was possible to get all 19 samples to be continuously bubbling. When each sample was being connected to its respective manifold port, repeat samples were arranged in various sections of the manifold as to try reduce one formulation getting a disproportionate amount of air.

II. Experimental loss

Once the flow-rate was calibrated, the 19 samples were mixed into soil and placed within their respective bottles that were labelled using a colour coding system. During the initial set up of the experiment there was an experimental error that resulted in a number of samples being destroyed (Table 1.2).

Table 1.2: List of destroyed samples.

Sample
Positive control x 2
Negative control x 1
Formulation 2 x 1
Formulation 3 x 1
Formulation 5 x 2

Due to this experiment requiring a full three months and limited amount of soil remaining, it was decided to continue with the experiment with the remaining

samples. The only critical loss to the experiment was the loss of both positive controls. All other samples had at least two, with only formulation 5 and the negative control having no repeats. It was decided not to obtain more soil and create new a positive control, as it would have been different soil from that of the rest of the test.

III. Scrubber titrations

20 L batches of 0.1 M NaOH were made in bulk to reduce experimental error between samples. The mass of NaOH required was measured using an analytical grade scale with an accuracy ± 0.001 g. Each new batch of NaOH was titrated by the HCl to establish a base line concentration. The CO_2 titrations were performed by mixing the entire volume of the two scrubbers together and agitating. 25 mL was pipetted using a laboratory grade, 5 mL Eppendorf pipette into a 100 mL conical flask where it was titrated using 1 M HCl and three drops of pheophytin indicator.

IV. Testing intervals

It was expected that there would be a lag phase for the bacteria to start to digest the samples so the scrubbers were checked on the first day, then 3rd, and then 6th. Once variations of CO_2 were recorded in the scrubbers they were tested every day for the next week. After this stage the scrubbers were tested every second day, for two weeks. For the next month and a half the testing was performed every three to four days. Once observed that the majority of samples had appeared to plateau, testing was left for a week, then a further two weeks after that to ensure that no activity was present.

V. Plant growth

It became evident that some samples were growing weeds that had been dormant. The sprouts were first detected on day six. The presence of these weeds were determined to be an issue with respect to the unknown level of CO_2 that they would convert to O_2 during the test. A concern was that by opening the tests samples the CO_2 in the headspace of the containers would be lost to atmosphere. However, it was decided that this was a more controllable level of error that leaving the weeds to grow throughout the experiment. The vessels were opened on day ten, and the weeds were removed with sterilised tweezers.

1.3 Results and Discussion

A modified Sturm test was used to determine the rate of biodegradation of Novatein, PBAT and blends thereof in soil. Pure Novatein was expected to have a high rate of biodegradation while under the conditions here, PBAT was not expected to readily biodegrade although it is known to be compostable. If this material is to be used as a casing for delivering seeds in the proposed automated device, investigating the effect of biodegradation with increasing the PBAT content gives the ability to create a blend that tailors the rate of degradation to coincide with seed germination rates whilst confirming the materials effect on the environment.

Figure 1.12 shows the cumulative mass of CO_2 collected from the scrubbers for each sample, including the negative control. From initial inspection it is clear that Novatein released the greatest mass of CO_2 and that the cumulative mass of CO_2 decreased with increasing PBAT content. Approximately 1.4 g of CO_2 was collected from the biodegradation of Novatein, while PBAT was barely above the negative control (0.6 g). These initial results confirmed the expected trend and that PBAT's biodegradation under these conditions is almost zero.

The mass of CO_2 collected in the negative control is assumed to be a mix of carbon within the soil that was metabolised by bacteria present and a very small amount of CO_2 that enters the system via the air supply. The air used had a very low percentage of CO_2 content (0.2 %) and was scrubbed before entering the system, degradation of residual carbon in the soil was unavoidable. Using CO_2 free air was deemed unnecessary, considering that any residual CO_2 in the inlet air would be accounted for in the negative control. The other anomaly accounted for using the negative control was the rapid increase in CO_2 collected at around day 35. This was assumed to be as a result of a change in the inlet air velocity and (or) a decreased efficiency of the inlet scrubber. However, correcting for the negative control should give an accurate representation of the level of biodegradation.

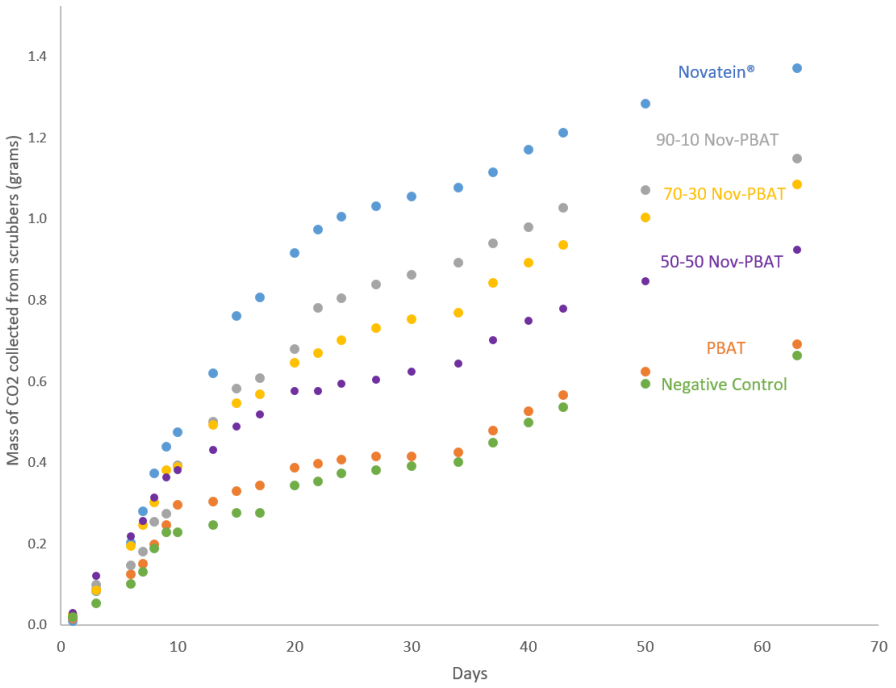

Figure 1.12: Mass of carbon dioxide collected from scrubbers during biodegradation experiment.

The results displayed in Figure 1.13 is the percentage biodegradation corrected for the negative control. It is measured by using the mass of CO_2 captured and knowing that the total degradable organic carbon in the sample is 1 g, from Equation 1-3 The percentage biodegradation data has been fitted with a non-linear curve that matches that of a standard growth cycle (Equation 1-4) the solid line, with data points overlaid. As expected from the results of the collected mass of CO_2, Novatein had the highest total percentage of biodegradation and PBAT had the lowest, with the blends intermediate of these.

$$\frac{\left(\left((V_{CT} - V_{ST}) * HCL_{\frac{moles}{L}}\right) * MW_{CO_2}\right)}{f_{efficency}} = m_{CO_2} \qquad 1\text{-}4$$

The experiment was run for approximately two months, the rate at which each sample reached a plateau varied, however, it can be seen that by day 40, there appeared to be no biological activity occurring. This experiment followed a classic bacterial growth cycle; lag, exponential growth and a stationary phase. The lag phase lasted approximately five days where after the bacterial growth increased exponentially, evident from CO_2 evolution. For Novatein, 90-10 and 70-30 (Novatein-PBAT) the bacterial growth appears to have stopped by day 25, indicated by the levelling off of percentage biodegradation. By day 40, the testing interval

rate was extended as it was assumed that the test had run its course. It is interesting to note that the last data point for the Novatein sample showed a slight increase in percentage degradation, suggesting that if this test was extended it may have biodegraded further.

It was expected from previous research that Novatein on its own would biodegrade substantially, however, with respect to ASTM 5988, defining biodegradation in this experiment as reaching 70 % total biodegradation within six months, all samples tested failed. Without the positive control, it is difficult to determine whether the lack of percentage biodegradation is with respect to errors in calculations or if the experimental set up had a fundamental flaw within it. However, the observed trend is as expected and a number of interesting discussion points can be drawn from this experiment.

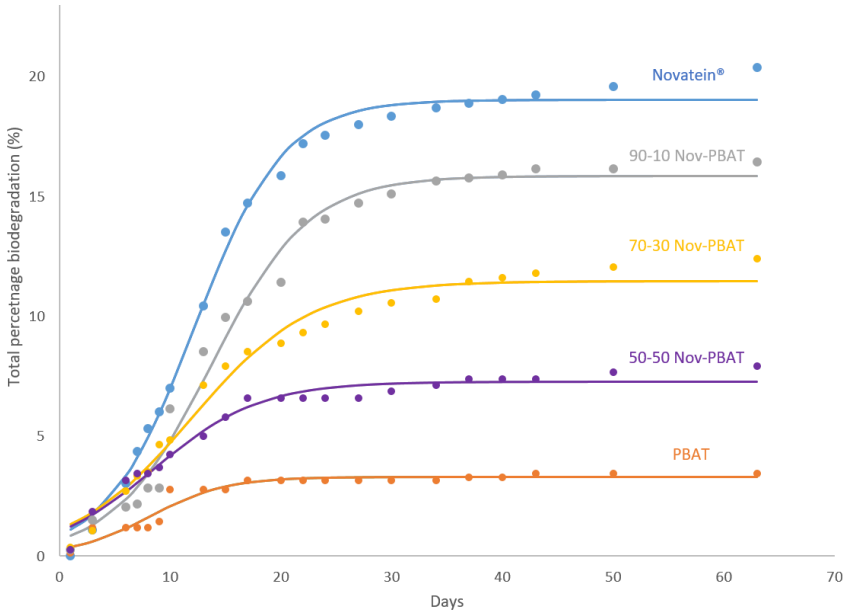

Figure 1.13: Percentage biodegradation results of different samples during the modified Sturm test.

Pure Novatein had the highest degree of biodegradation, reaching approximately 20 % (Figure 1.13) and biodegraded the fastest (steepest slope in the growth phase). Pure PBAT showed no significant biodegradation, reaching approximately 3 % with an almost non-existent bacterial growth curve. All the blended samples biodegraded less than pure Novatein, and decreased with increasing PBAT content. A relatively large drop in degree of biodegradation occurred with the addition of 10 wt.% PBAT, from 20 to 16 %. However, tripling the quantity of PBAT had only a minor effect, reducing it to 12 %. At equal proportion, the degree of

biodegradability reduced to 8 %. The decreased rate of biodegradation appeared to be linear with the addition of PBAT, this is quantitatively shown with an R^2 value of 9.85 in Figure 1.14.

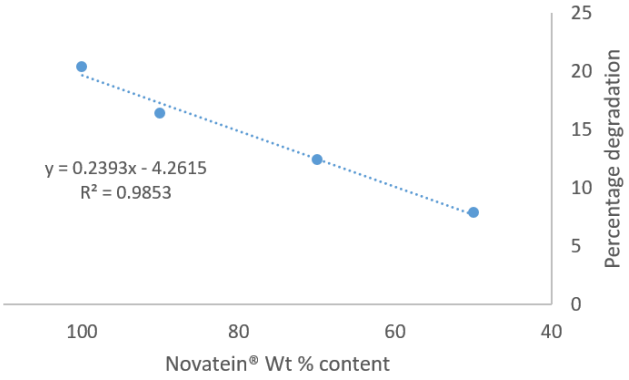

Figure 1.14: Linear relationship of the percentage degradation decreasing with decreasing Novatein wt.%.

It was expected that Novatein would biodegrade much faster than PBAT as it is a protein-based polymer. PBAT has a high molecular weight and a long chain branched molecular structure, which reduces its ability to biodegrade. However, literature has reported PBAT undergoing some biodegradation in similar soil conditions such as these [58; 67]. The consequence of the results is that the rate of biodegradation can easily be controlled by blending Novatein with PBAT. However, based solely on the results here, the material will not be 100 % biodegradable.

There are a wide variety of conditions that may contribute to biodegradation in soil; bacteria present, temperature, moisture, and the presence of oxygen [53]. It was expected that Novatein would readily biodegrade during this period, however, it did not even reach 30 %. However, this is not a crippling result, MATER-BI was tested in a similar study where it only reached 40 % [67]. Considering MATER-BI is a starch polymer and well known for its biodegradability, this test clearly holds the standard high for effective biodegradation.

When the samples were opened on day ten to remove weeds, it was discovered that there was considerable mould growth in some of the samples, of which pure Novatein had the most abundant mould growth (Figure 1.15, mould circled in black, and weeds in red). Small amounts of mould and weed growth was found in the blended samples. Weed growth was found in the pure PBAT and negative control samples; however, no mould growth was present. This mould growth was seen as a key indicator that Novatein was readily biodegrading whereas PBAT was not. The

results could not be corrected for CO_2 released as a result of plant/mould growth, other than what was observed in the negative control.

Figure 1.15: Mould and sprout growth, day 10, pure Novatein sample.

After the experiment had concluded, each sample was emptied and sifted to see if any of the original sample was still distinguishable. The left image in Figure 1.16, is soil from the Novatein sample, spread out for observation post experiment. The mould growth from earlier had completely disappeared during the course of the experiment, and no observable granules of Novatein were found. However, as Novatein is relatively indistinguishable from soil, it was unlikely to find any remnants.

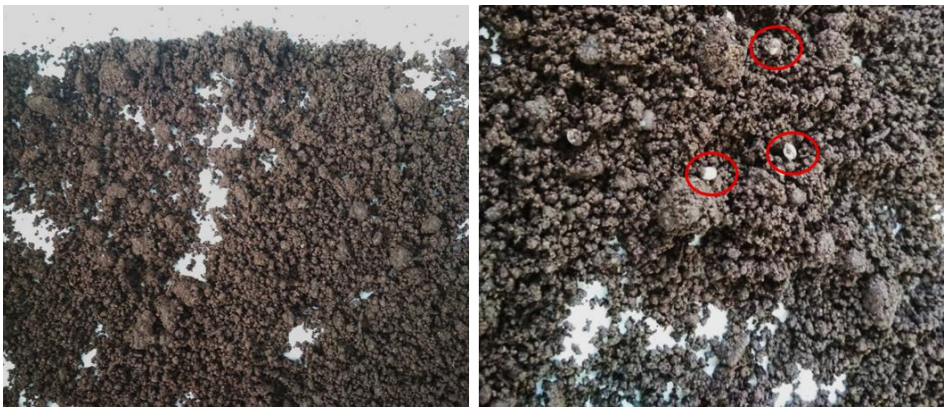

Figure 1.16: Sample soil post experiment for Novatein (left) and post experiment PBAT pellets circled in red (right).

Whereas when the pure PBAT sample was emptied, and the PBAT pellets look to have no biodegradation at all, right of Figure 1.16. No signs of PBAT or Novatein were found in the remaining blends. This too may be due to the soil and polymer blend being very similar in colour and texture.

1.4 Product Design Evaluation

The aim of this chapter was to gain a comprehensive understanding of different plastics and how their differences can lead to an environmentally friendly solution, to a modern problem. The use of plastics will undoubtedly play a part in every facet of industry if it does not do already. This chapter explored common misconceptions around polymers, giving more clear definitions to which polymers are better suited for specific applications. Understanding that biobased polymers can themselves be non-biodegradable and fossil based polymers can be biodegradable. The application and problem in question is; can a plastic projectile be produced that readily biodegrades in soil within a reasonable period in a controlled manner.

To solve this problem the mechanisms of biodegradability were investigated to understand why the lack of functional groups, high hydrophobicity, few cleavage sites and high molecular weight make LDPE highly resistant to microbial attack opposed to protein plastics that typically have the opposite characteristics. A variety of biodegradation techniques were evaluated, where mass loss by CO_2 evolution proved to be a benchmark in biodegradability testing as the test completes the carbon cycle, the definition of end of life. Modifying a Sturm test by incorporating ASTM 5988, which are both well-established test methods, the degree of biodegradation could be investigated. These methods calculate the percentage of biodegradation by measuring the mass of CO_2 bacteria and fungi have metabolised from a closed system against the known quantity of carbon. The bacteria used in the experiment was from soil collected from three diverse locations across New Zealand, a horse paddock, a native forest and a pine forest. The samples of interest were pure Novatein a biobased protein polymer, pure PBAT, a fossil based biodegradable copolymer, and blends of the varying quantities of both.

The results of this study showed that Novatein exhibited a high level of biodegradability in comparison to PBAT, PBAT showed very low signs of biodegradation during this experiment. The blended samples decreased in biodegradation with increasing the wt.% of PBAT. This was confirmed by the

presence of mould growing prolifically in the pure Novatein sample and its blends, but none present in the pure PBAT or negative control sample.

Post experiment investigations showed PBAT still physically present in the soil with no signs of deterioration. However, for Novatein and blends, there were no remnants observed. For the purpose of making a biodegradable product, it is believed that the Novatein sample biodegraded sufficiently and with as much as 30 wt.% PBAT the blend can still successfully biodegrade to a sufficient level. However, further studies are needed to confirm the absolute level of biodegradation. The results here assume that 1 g of carbon is fully converted to CO_2, which may not be the case within the time frame here. Also, carbon is converted to biomass, which is not reflected in the percentage biodegradation. A full biological evaluation of the bacteria and mould growth for each sample were not performed, but further studies would benefit from performing this.

The work presented here did not prove that Novatein itself or blended with PBAT met the acceptance criteria of ASTM 5988 (70 % biodegradation). This result needs to be confirmed, or a more suitable test method needs to be investigated if Novatein and PBAT are going to be used across the countryside. If biodegradation cannot be confirmed, the polymer selected for this application may have to be revised.

Chapter 2

Projectile Encapsulation & Welding

The current government's goal of doubling the rate of planting trees does not come without its challenges. Finding a feasible solution to automated planting will require mass manufacturing of a suitable capsule. Assuming that a Novatein PBAT blend can successfully biodegrade, the feasibility of manufacturing seed projectiles that can be used to penetrate the ground and avoid predation is still to be investigated.

One of the main reasons that plastic has become so widely spread is the ease it can be manufactured. Complex shapes can be produced in a one-step process with little to no finishing required, unlike metal or wood. These processes can be cyclically automated, or continuous, which is desired for mass manufacture. A variety of processing techniques are available, but they generally have these steps in common; heating, shaping and cooling. One of the most common is extrusion which uses a screw inside a barrel to melt polymer granules into a viscous flow that exits at a die. A single screw extruder can be seen in Figure 2.1 where the polymer is fed at the hopper and conveyed down the barrel. The polymer is heated and melts as a result of shearing forces, known as mechanical input, via the reduction in the depth of the screw channel, and is aided by external heating bands [74].

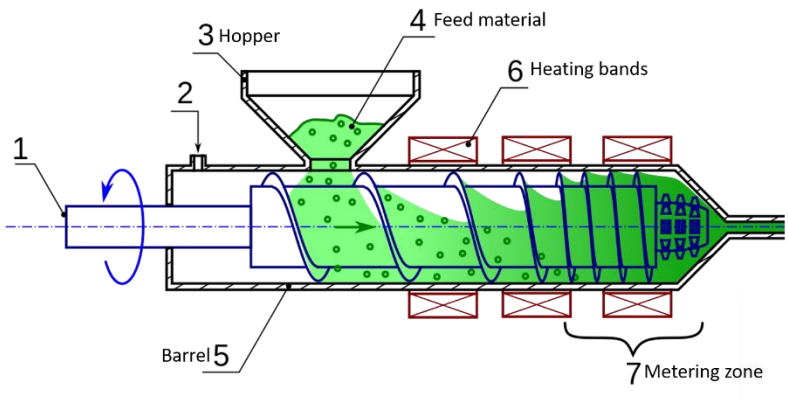

Figure 2.1: Single screw extruder, sourced from [75].

The polymer melt exits at the die where the die's shape can be easily changed to produce different products. Complex shapes can be made using simple die's to produce products such as those shown in Figure 2.2. Comprehensive understanding

of specific material properties, specifically thermal contraction during cooling is essential in profile extrusion in order to calculate the correct size of the die [74].

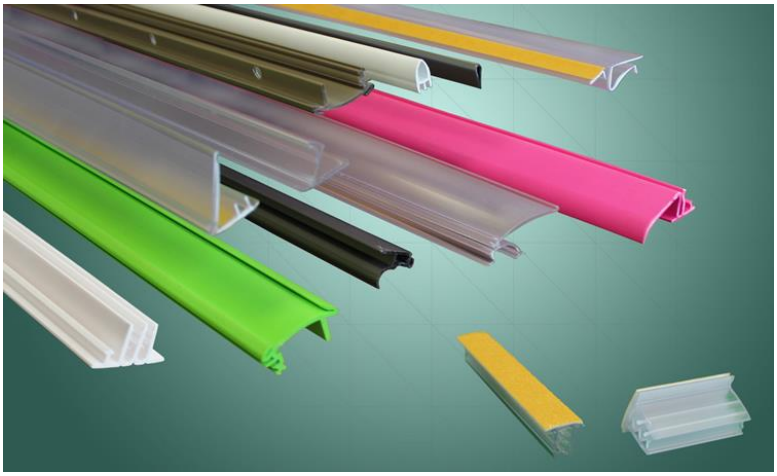

Figure 2.2: Continuous 2D extrusion of plastic profiles, sourced from [76].

This method of processing can be tweaked by introducing more complicated mixing sections, the addition of multiple barrels, secondary feeders, liquid dosing, non-Newtonian flow profiles and much more; however, during this study the intricacies of polymer processing will not be the focus [74].

Injection moulding is another very common form of mass production, a simple example can be in Figure 2.3. Using an extruder similar to Figure 2.1 molten polymer is forced in a cavity with high pressure, held to solidify, and then the mould opens. This processing method is desirable as complex parts can be made with rapid cycle times, depending on size and material they can be as quick as five to ten seconds. Areas of special attention are the gates, runners, and ejector pins. The gate is a small orifice where the melt enters the mould, this solidifies first to avoid backflow and is an easy place to break the part off from the runner when cold. The runner is where the material flows to the gate/part, in moulds with many parts the runners need to be designed effectively to reduce flow resistance but solidify at the same rate as the part. The ejector pins quickly remove the part from the mould once open to decrease cycle time [74].

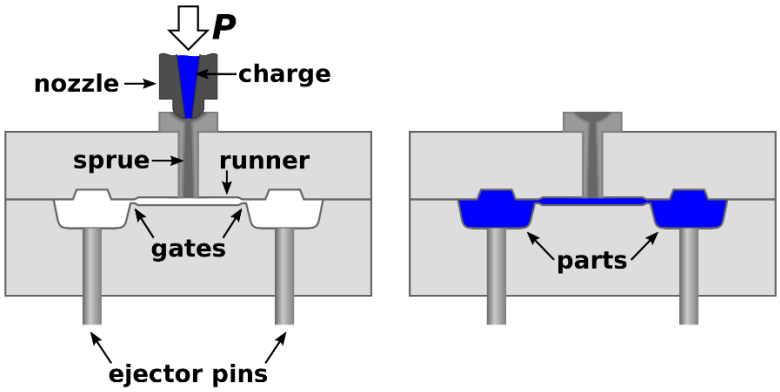

Figure 2.3: Injection moulding, sourced from [77].

A variety of other processing techniques are available, however, pure Novatein is limited to simple extrusion and injection moulding, so other techniques will not be evaluated [78]. From prior research it has been proven that when blending Novatein and PBAT with the appropriate compatibilisers, quality sheets can be produced. This provides two advantageous reasons for using PBAT, increased processability and improved biodegradation control.

During scoping for this chapter it was evaluated that injection moulding would be a complicated method for encapsulating seeds safely due to prolonged heat and processing parameters. It would require multiple parts that would need a secondary processing step and would likely not be cost effective. Due to the ability of Novatein and PBAT blends to be continuously sheet extruded, it was decided that a manufacturing method used to mass produce paintballs might work to encapsulate seeds continuously, seen in Figure 2.4 [27]. A gelatine sheet is fed into a cylindrical die roll where vacuum pulls the sheet into a semicircle shape [79]. The sheet with the two halves of the circle are then welded together. This is a continuous process designed to make large quantities paintballs easily.

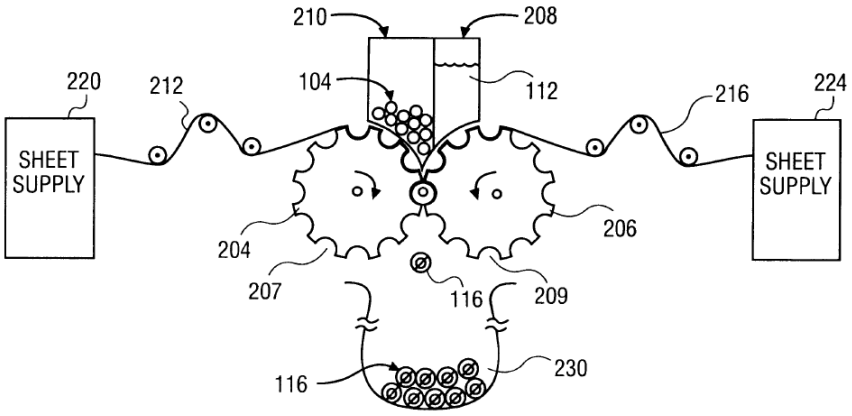

Figure 2.4: Paintball manufacturing technique, sourced from [79].

Figure 2.5 shows a close-up of paint being pumped into each side of the gelatine spheres. Using this method it can be easily retrofitted to produce the required seed projectiles. Gelatine sheets can be replaced with Novatein/PBAT sheets, where item 104 is the seeds and item 112 is a hydrogel for that could serve both as a nutrient source and shock absorption [80]. The polymer film itself could contain chemicals that encourage germination, such as the hormone kinetin [19].

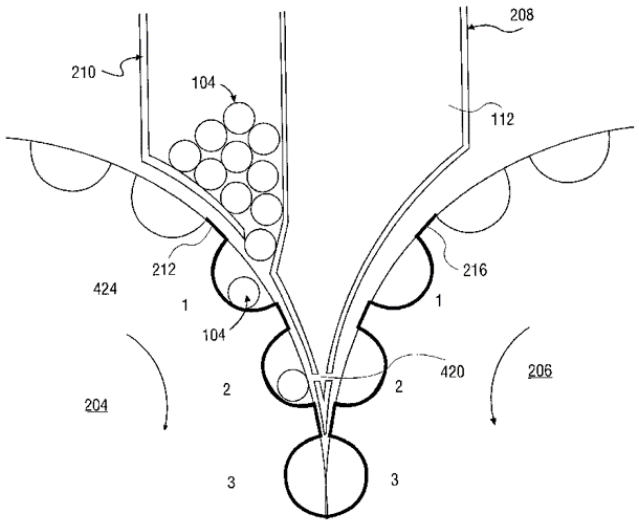

Figure 2.5: Detail view of paintball manufacturing technique that inserts an object within the paintball, sourced from [79].

The challenge of this chapter is to understand the mechanisms occurring during plastic welding, the different types, and how to replicate the paintball manufacturing technique. If the polymer blend can be successfully formed and welded, then quantitative testing is required to evaluate the strength of the weld, its repeatability and the process parameters required for a successful weld.

2.1 Literature

2.1.1 Plastic welding

Plastic welding is the process of forming a molecular bond between two parts, involving heat and pressure. Benefits of welding polymers opposed to using adhesives, or hinges with screws, is reduced manufacturing time and cost, reduced mismatch of thermal expansion or damage caused by drilling [81]. Just like other polymer manufacturing techniques, it involves heat, pressure and cooling. Heating is crucial as it allows the polymer chains to flow and entangle, allowing intermolecular diffusion, and the more heat, the more molecular diffusion, and therefore, faster weld times. Semi-crystalline polymers must be heated above their melting temperature where amorphous polymers only require being above their glass transition temperature. Asides from increasing intermolecular diffusion, pressure is often used during heating and cooling to hold the polymers in the correct position. Controlling the cooling rate allows the solidification of the polymer bonds and has a high influence on weld strength. Most techniques are relatively similar apart from how they are heated; hot plate, laser, implant, spin and seam are common examples that will be investigated [82].

I. Hot plate welding

During hot plate welding, two parts are heated by being pressed on a heated plate, or heated via radiation before being pressed together, weld times typically range from 10 to 20 seconds. Figure 2.6 shows a flow chart of the contact hot plate welding process and is used for relatively simple geometries although it can be used for larger objects but weld time increases dramatically [82].

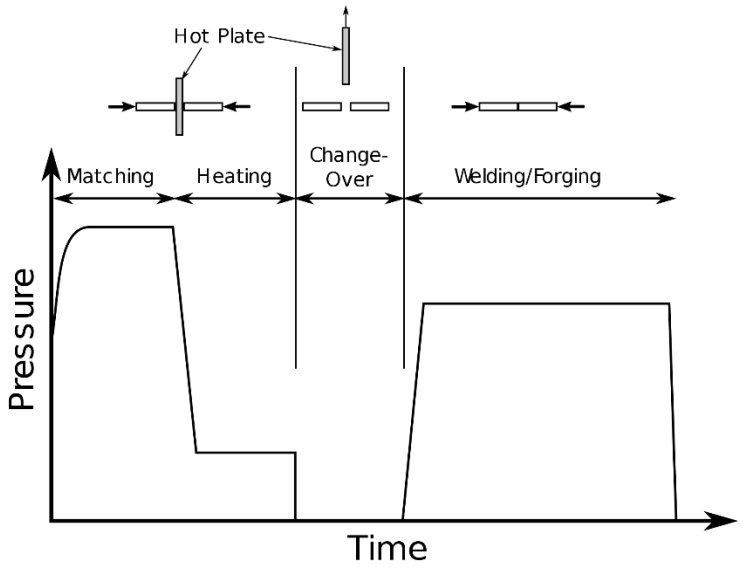

Figure 2.6: Hot plate welding flow chart, sourced from [83].

Liu *et al.* [84] investigated the influence of the contact angle for hot plate welding using virgin polypropylene (PP), 20 %, and 30 % glass fibre-reinforced PP composites (GF-PP). The 20 % GF-PP composite was found to have the highest joint strength, having an increase from 10 MPa for virgin PP to above 30 MPa for 20 % GF-PP, when using a square welding geometry. The effect of welding geometry was found to have a more drastic effect on the virgin PP, opposed to the composites. Nonhof C. J. [85] found a reduction in tensile strength from 23 ± 4 MPa to 17.0 ± 0.8 MPa when hot plate welding 30 wt.% short-glass filled PP.

Hot plate welding has several key factors that contribute to weld strength; time, pressure and temperature, however, Nonhof C. J. [85] determined that no single optimal parameter setting can be obtained for hot plate welding due to the large number of plastics, fillers and variation with joint requirements. One key insight for successful welding was that most welds rupture at the interface between the heated polymer and its solid parent material. This is due to a high shear rate at the interface that aligns the molecules in the direction of flow, creating a weak spot; this can be mitigated by lowering the welding force or having a slower application of force.

Ülker *et al.* [86] used a Taguchi method to optimise welding parameters when using hot plate welding of polycarbonate (PC) and acrylonitrile-butadiene-styrene (ABS). Statistical analysis of the tensile testing results showed that plate temperature had the highest influence on joint strength while weld displacement (sample compression distance) was second and the heating time had very little effect on joint strength.

II. Laser/Infrared welding

Laser welding applies highly accurate and localised heat that results in precision welds with short weld times of less than five seconds. By using one transparent material, that infrared will pass through, and one that's black, infrared welding has the unique ability to heat only the black material to bond to the transparent part (Figure 2.7) [82]. This can be useful for complex geometries, especially in the electronics or medical industries. Advantages of laser welding are non-contact, parts with different viscosities and stiffness's can be welded and no mechanical stress is put on the part [87]. Knapp *et al.* [88] evaluated the shear strength of a PP matrix reinforced with 40 wt.% glass fibres with different bonding techniques. The maximum shear strength of the base material was 44 MPa, reduced to 32 MPa for laser welding, and a considerable reduction to 15 MPa when using a chemical bond.

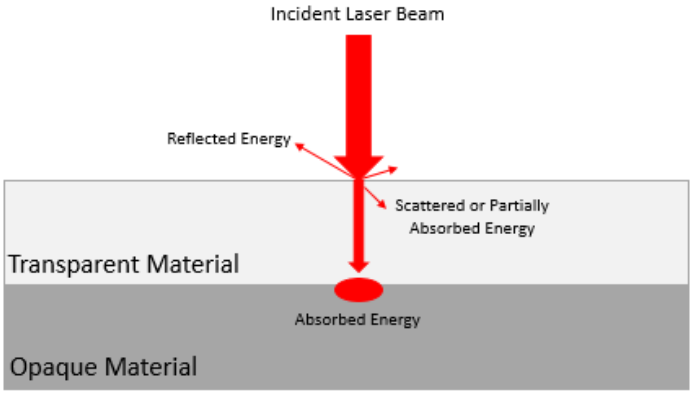

Figure 2.7: Laser welding, sourced from [89].

III. Implant welding

Implant welding involves applying an external heat source via induction or electrical resistance. Electrical resistance typically involves a wire located at the weld joint to melt the surrounding parts. A key difference for this technique is that in larger parts the implanted wire is generally left within the weld joint once complete (Figure 2.8). Implant welding generally takes longer, up to a minute, but has the distinct advantage of handling large parts. It has been used in the aerospace industry for lightweight thermoplastic composites and the automobile industry for car bumpers because it is not restricted to flat surfaces such as vibration hot plate welding [90]. However, when Knapp *et al.* [88] compared implant to laser welding, the maximum shear strength of the PP matrix reinforced with 40 wt.% glass fibres was 22 MPa opposed to 32 MPa, implant to laser welding, respectively.

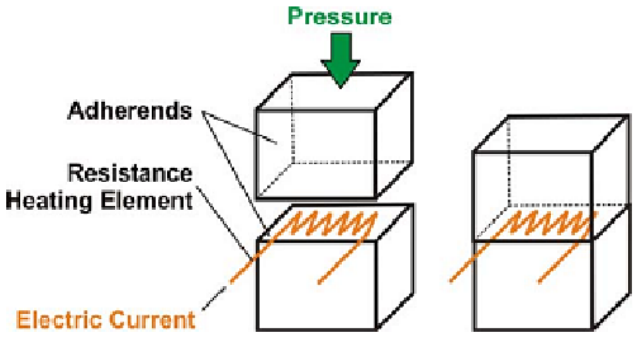

Figure 2.8: resistance welding, sourced from, [91].

IV. Spin welding

Spin welding works by creating heat and friction at the joint of two parts, causing the surface to melt, by applying rotational movement to one part while holding the other still (Figure 2.9). This is an established method of joining for metals and has recently gained momentum for thermoplastic joining [92]. This method is unique in that the welding step is split into an unsteady and steady state with respect to temperature; melting and flow. Although it can be done on a lathe to get high-quality welds, the rotational energy needs to be controlled carefully. Common rotational linear speeds vary from 1 to 20 m/s with pressures ranging from 80 to 300 kPa. It is common practice for tubes or round bars as it is highly reproducible with high quality welds [93].

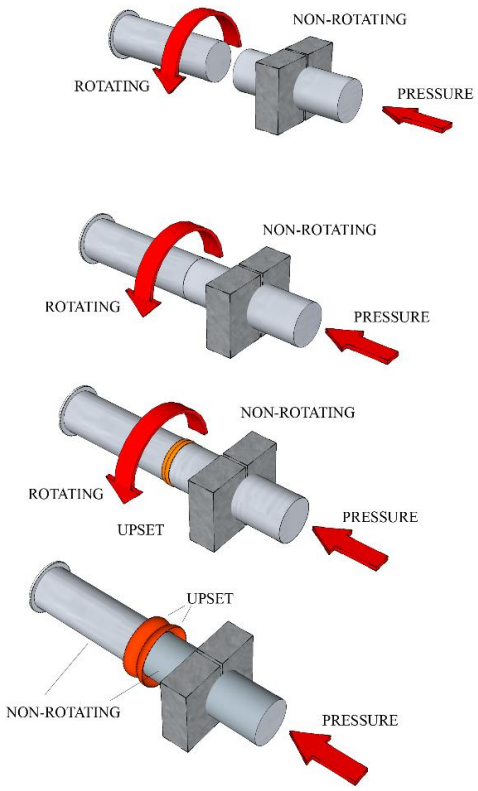

Figure 2.9: Rotational welding, image courtesy of Gatwick Technologies [94].

V. Seam welding

Seam welding is a form of continuous welding, specifically for plastic sheets and is an industrially trusted technique. There are various ways to apply the heat and pressure, it typically uses rollers, made from electrodes to continuously spot weld. This allows a consistent feeding rate, pressure and weld time (Figure 2.10) [95]. This technique can be used on PVC coated fabrics, vinyl films, PP, PE, and polyurethane. A variety of seam welds are achievable, overlap, hem, tubing and much more [96].

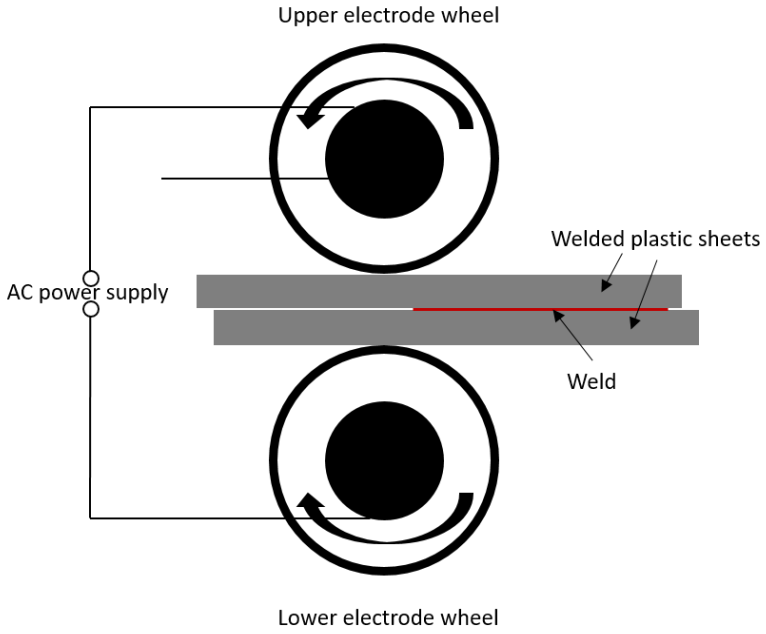

Figure 2.10: Seam welding of plastic sheets.

2.1.2 Welding of novel polymers

From literature is it clear that fusion welding of common thermoplastics such as polypropylene and composites is common, but further investigation is required for proof of fusion welding for more novel polymers, such as biobased, biodegradable or both.

Hattori *et al.* [97] developed a bioabsorbable thread made from poly(L-lactic acid) (PLLA) and PCL for fixation of broken bones. This was achieved due to PCL having a low melting temperature where as PLLA has a relatively high melting temperature. Knots were tied from the thread, heat applied that melted the PCL which becomes a matrix for PLLA to adhere to. This thread had a tying strength of 39.7 N which was comparable to that of the stainless steel. Solvent welding is another valid form of bonding thermoplastics and recent developments in ionic liquid (IL) solvent bonding is being developed for biobased fibres [98-100]. Ionic liquids are a unique class of solvents for the dissolution of biopolymers. IL have successfully fibre welded cotton, cellulose and chitin and chitosan on a cloth substrate [99; 100].

2.1.3 Material properties of Novatein

Although no literature was found on welding protein polymers it is important to understand the material properties of Novatein to estimate how it may be welded.

Novatein's material properties have been extensively investigated [42; 78; 101; 102]. Bier *et al.* [42] studied the effect of plasticizers on the thermal and mechanical properties of Novatein, Figure 2.11 is a dynamic mechanical analysis (DMA) of conditioned Novatein showing that with increasing plasticizer content, (Tri(ethylene glycol) (TEG)) the glass transition temperature (T_g) was reduced from 72.4 to 59.8 °C. This was characterised by a peak in tan δ and a drop in the elastic modulus by two orders of magnitude. The crystallinity was found to be reduced from 35 to 22 %. Novatein is unique in that it is semi-crystalline, but the crystalline frication does not melt before it degrades, however, it softens well enough above the T_g, enabling it to be processed.

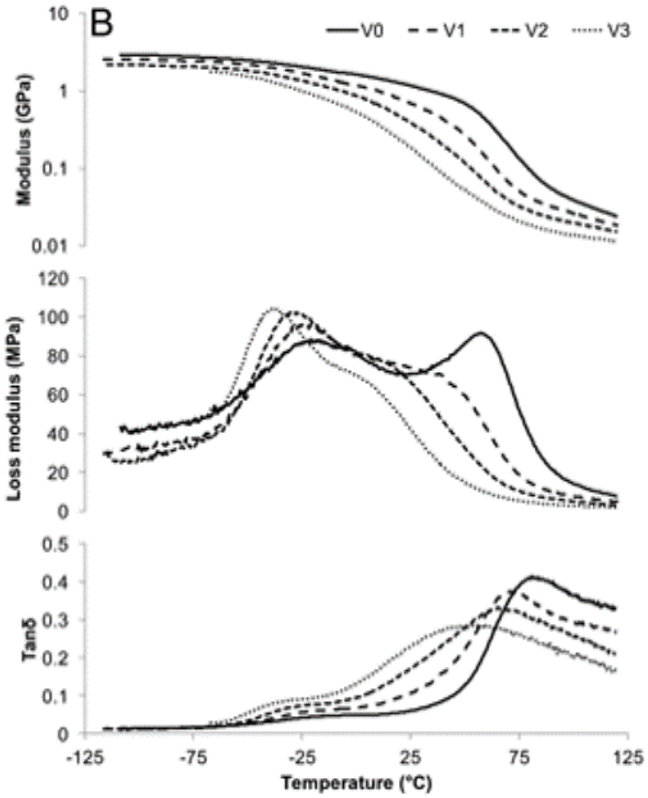

Figure 2.11: DMA of conditioned Novatein, V0 to V3 is increasing TEG content from 0 to 30 pph bloodmeal, sourced from [42].

2.1.4 Material properties of PBAT

No literature was found on welding of PBAT specifically, but its material properties are well known, which would allow for some prediction about welding conditions. PBAT (Ecoflex® FBX7011) From BASF has a T_g of -29 °C, a melting point of 115 °C and a cold crystallization temperature of 80 °C [58]. Arruda *et al.* [103] found that PBAT sourced from Ecoflex® (F BLEND C1200) was approximately

19.1 % crystalline. Tavares *et al.* [104] investigated the effect on thermal properties of adding kraft lignin to PBAT (C1200). The DMA in Figure 2.12 found that the T_g was reduced from -29.8 to -25.6 °C and the storage modulus was increased from 466 MPa to 2113 MPa when increasing lignin content from 0 to 5 wt.%.

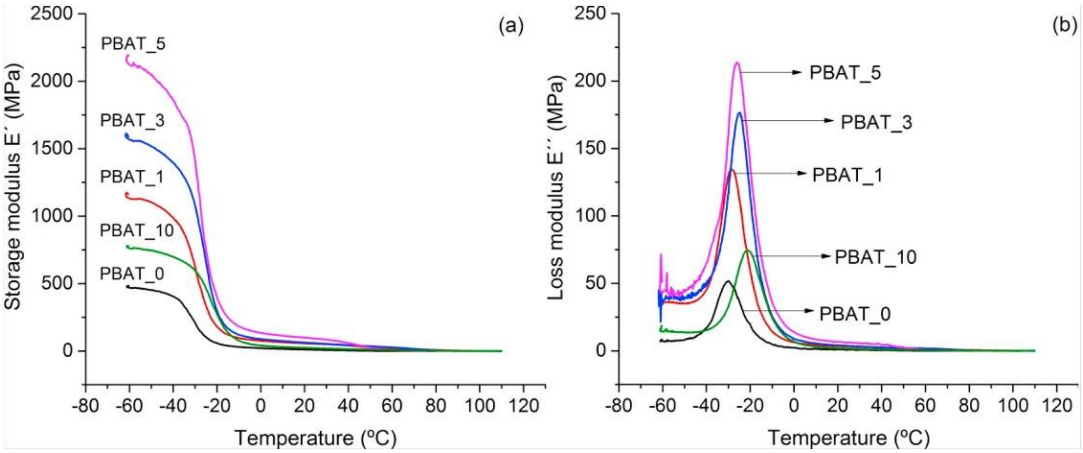

Figure 2.12: DMA of PBAT and kraft lignin blends, PBAT_0 to 10 is increasing lignin content, sourced from [104].

2.2 Weld Testing Methods

There are a variety of methods for testing the bond strength of welds or adhesives in polymers. Grouve *et al.* [105]used a compaction roller with a laser heat source to laminate carbon-fibre onto polyphenylene-sulphide. The validity of using a mandrel peel test to measure fracture toughness of composites was investigated and was found to work for hybrid interfaces when a double cantilever beam failed (Figure 2.13).

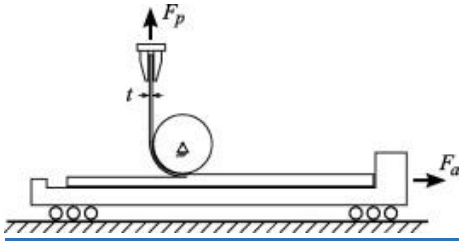

Figure 2.13: Mandrel peel test, sourced from [105].

Zhao *et al.* [106] used a double-lap shear test on laminates made from carbon fibre-reinforced poly-ether-ether ketone (Figure 2.14). The laminates were made using compression moulding at 385 °C at 1 MPa for 20 minutes, ultrasonically spot welded together and had a max peel force of 8 kN. T-peel testing using ASTM D1876-08 is a standardised test method that is commonly used for testing the

adhesive bond strength of thermoplastics [107; 108]. This method uses an Instron tensile tester to pull apart the samples.

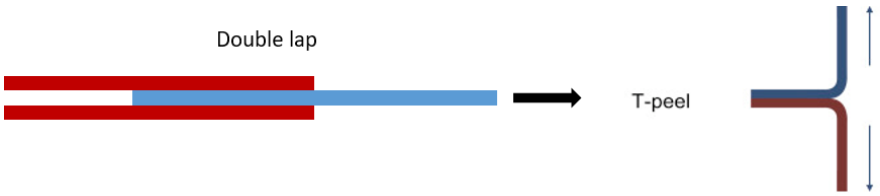

Figure 2.14: Experimental set up for double-lap shear test, T-peel test, experimental set up, sourced from [109].

2.3 Experimental Methods

After investigating the different types of welding it was determined that hot plate welding is the most appropriate for replicating the paintball manufacturing method. The following section describes the methods used to evaluate the feasibility of welding Novatein/PBAT sheets. The experimental section is divided into two sections. Firstly, a feasibility study was undertaken to establish if sheets can be moulded and welded around a steel ball bearing in a simple aluminium mould. This method of experimentation replicated welding and moulding of the paintball manufacturing technique, in a batch format. Success of this experiment is defined as the ability of the sheets to stretch around the ball bearing and weld to each other. A second, more precise experiment, uses test samples punched from sheets to evaluate the effect of welding parameters (time, pressure and sheet thickness). The test samples were punched to be the correct size for tensile testing according to ASTM D638. Preparing overlapped welds allowed for tensile and peel tests to be performed, giving quantifiable weld strength data.

2.3.1 Equipment

I. Aluminium mould design

An Aluminium (grade 6061-T651) mould was designed using SolidWorks CAD, and manufactured with a Fusion360 kitset CNC. The clamshell mould can be seen in Figure 2.15 with SolidWorks drawings in Appendix B. Two identical moulds were made, that can be pressed together, with guide pins to encapsulate a spherical free volume with a diameter of 17.3 mm (the calibre of paintball bullets). The mould was designed with three identical cavities appropriately spaced to minimise any interference.

Figure 2.15: Clamshell Aluminium mould with ball bearings (open).

II. Sheet extrusion

A 70:30, Novatein-PBAT blend was made using the same process as described in Chapter 1. After granulation, the blend was re-extruded with a sheet die attachment. The temperature profile was 70 – 150 °C with the sheet die set at 140 °C. Sheets were extruded using a 200 mm wide die, with inserts capable of producing 0.5 to 1.5 mm thick sheets. The sheets were rolled up as seen in Figure 2.16, this kept constant tension on the sheets drastically improving sheet quality. An internal image of the sheet die can be found in Appendix B.

Figure 2.16: Physical sheet extrusion process.

III. Sample preparation

Samples of 250 by 100 mm were required for testing within the aluminium mould. The sheet was cut long ways into 250 mm long sections, then cut in half. Samples were left under a large square vessel with weights inside it to flatten.

The specimens used for controlled welding had the same flattening process as above, after which, the samples were pressed out using a Lloyds tensile tester, fitted with a die that conforms to the dimensions stated in ASTM D638 type one (Figure 2.17) [110].

Figure 2.17: Dog bone sample preparation process.

Due to melt flow properties during sheet extrusion there was more material in the centre of the sheet, therefore the sheets were thicker in the middle than the outside (exaggerated in Figure 2.18). Samples were cut long ways down the sheet so that each sample had a relatively consistent thickness.

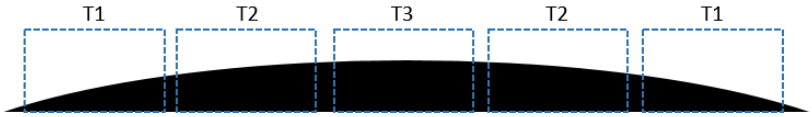

Figure 2.18: Dramatised sheet extrusion profile that resulted in the three different thicknesses.

Due to the symmetrical way the dog-bones were cut, the vast majority of samples fell into three thickness categories T1, T2 and T3 (Table 2.3.). Samples outside these boundaries were discarded.

Table 2.3.: Categorisation of sheet samples with tolerances.

Category	Median thickness (mm)	Tolerance (mm)
T1	0.675	± 0.075
T2	1.090	± 0.060
T3	1.515	± 0.115

IV. Dynamic mechanical analysis (DMA)

Dynamic mechanical analysis was performed in a TA instrument and was carried out in the range of 1–150 °C at a rate of 4 °C.min^{-1} under multi-frequency strain mode. Strip specimens were 16 (L) x 6.2 (W) c 1.02 (D) in dimensions. The exact thickness was measured by an electronic thickness gauge. The static and dynamic controls were set at 0.2 % strain and 0.1 % strain, respectively, and the sample was tested at a frequency of 1 Hz. Liquid nitrogen was used to maintain an isothermal environment outside the furnace.

2.3.2 Experimental procedures

I. Feasibility study

A 50 tonne heated press was used for compression welding sheets in the aluminium die. During initial scoping tests it was found that the pressure control was not accurate enough to be able to vary the applied force without pressing out the sheets entirely. Due to this, it was decided that pressure would not be varied, the press was held at 1.5 MPa for each test. Test parameters was therefore limited to time, temperature and internal bearing size.

Black electrical tape was placed on the aluminium mould and heated press for increased accuracy of an infrared temperature sensor. The aluminium mould was heated in an oven, then moved to the heated press for the experiment. A sheet was placed on top of the mould, the bearings were manually softly pressed into their correct position and held for three seconds. This stopped the bearings rolling out of their cavity. Another sheet was placed on top while the mould was pressed into place. Figure 2.19 shows an example of how the experiment was setup.

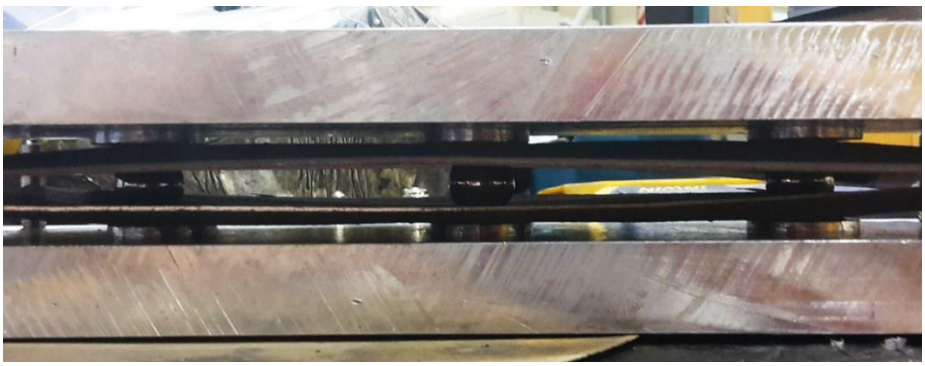

Figure 2.19: Clamshell mould, with two sheets and ball bearings.

During scoping experiments, it was found that after the pressing, cooling the mould before opening it improved the results. After each test, the mould was water cooled under a tap, taking care to not wet the samples before opening. During scoping it was found that the use of 'CRC 808' silicon spray aided in mould release and was sprayed onto the top and bottom of the mould before each test.

The study included three diameter bearings, three different weld durations, at a variety of temperatures were investigated (Table 2.1). The mould had three cavities, yielding three test specimens, and each experiment was repeated twice.

Table 2.1: Feasibility study experimental design.

Bearing size (mm)	Temperature (°C)	Press time (min)
14.3	16 75 90	0.5
15.0	95 100 105	1
15.9	110 115 120 125	3

Compression tests were performed for the successfully bonded spheres. Due to the ball bearing being inside, the samples were cut perpendicular to the weld to create a semi-circle sample. This enabled the samples to be compression tested to determine the force required to buckle (Figure 2.20).

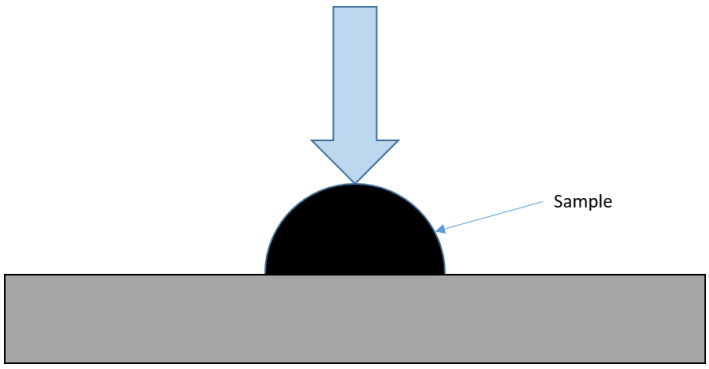

Figure 2.20: Compression testing successfully welded samples.

II. Compression welding

A Lloyds tensile tester was used in compression mode to give accurate control of the welding force. However, this machine did not have a heating function, therefore the temperature was not varied. Test samples were cut in half, overlapped and placed under a semi-circle aluminium insert (Figure 2.21) for compression.

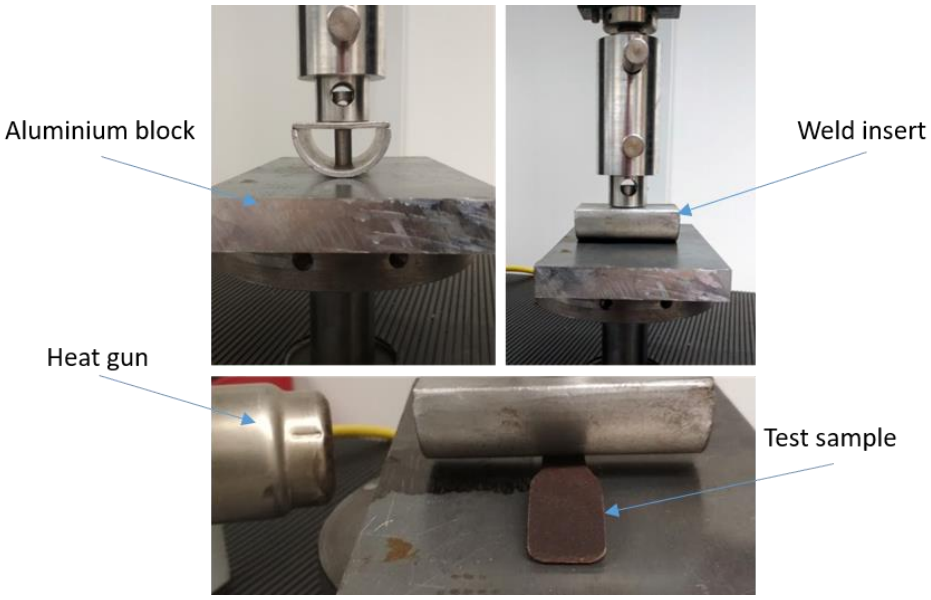

Figure 2.21: Experimental set up for welding dog bone samples.

During scoping experiments, it was found that increased heat resulted in improved weld quality with shorter weld duration required. A heat gun, set at its max temperature (240 °C) was used to heat samples in-situ. Both the aluminium block and rounded weld insert were heated in an oven at 130 °C. The temperature of the aluminium block was measured using an infrared sensor (on a black surface). This was to ensure that the temperature was relatively consistent during the experiments. When the temperature dropped 10 °C below the average (120 ± 10 °C), the aluminium block and weld insert were returned to oven for an extended period of

time. However with a heat gun set to 240 °C. Measuring the sample temperature itself was found to be highly inaccurate but it is assumed that it was higher than 120 °C.

The compression welding method was, 60 seconds sample preheat, and a loading speed of 16 mm per minute, which resulted in approximately ten second cycle times. The extended preheat time was necessary due to the limited heating capabilities of the system. A full factorial experimental design can be seen in Table 2.2. Compression forces for high medium and low are 900, 750 and 500 N, respectively. Each experiment was repeated three times. Tensile and peel tests were performed on comparatively for quantitative analysis.

Table 2.2: Full factorial experimental for welding and testing 70-30 Novatein - PBAT dog bone samples.

Test	Sheet thickness	Compression force (N)	Repetitions
Tensile	T1	High	3
		Medium	3
		Low	3
	T2	High	3
		Medium	3
		Low	3
	T3	High	3
		Medium	3
		Low	3
Peel	T1	High	3
		Medium	3
		Low	3
	T2	High	3
		Medium	3
		Low	3
	T3	High	3
		Medium	3
		Low	3

Tensile tests were performed at 10 mm per minute extension rate using vice grips (Figure 2.22A) (using a 30 kN load cell). Moisture contents were measured before tests were performed. And sample thickness was measured with digital callipers. Peel tests were performed at 10 mm per minute extension rate using vice grips (Figure 2.22B). Thickness was measured with digital callipers.

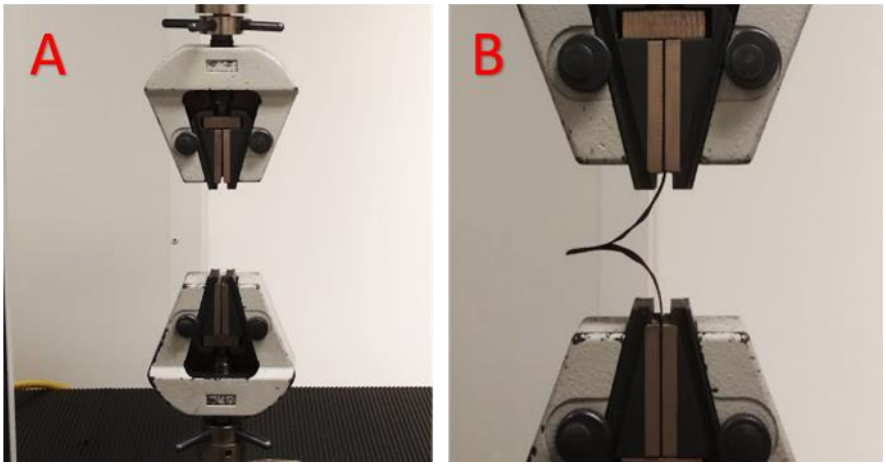

Figure 2.22: Tensile test experimental set up (A), and peel test (B).

2.4 Results and Discussion

2.4.1 Feasibility experiments

During the feasibility study a variety of observations were made regarding the weldability of Novatein/PBAT sheets. Cold pressing was unsuccessful regardless of time or sheet thickness. However, a partial bond was achieved at as low as 75 °C. This result was consistent to what was expected in light of the material properties of Novatein and PBAT. The lowest temperature where a fully successful weld was formed was 105 °C. At the highest temperature of 125 °C a successful weld was also formed. Future studies would require more precise heating control to quantify the effect of heating.

The smallest bearing size did not show any success, regardless of time, temperature or thickness and was therefore removed in subsequent experiments. Figure 2.23A displays a thin sheet that ripped during moulding. It was assumed that when the polymer was given too much room to stretch, as seen in Figure 2.23B, without complete support it would tear. This was confirmed with the medium sized ball bearing having some successful welds but all samples tore when being removed from the bearing for compression testing.

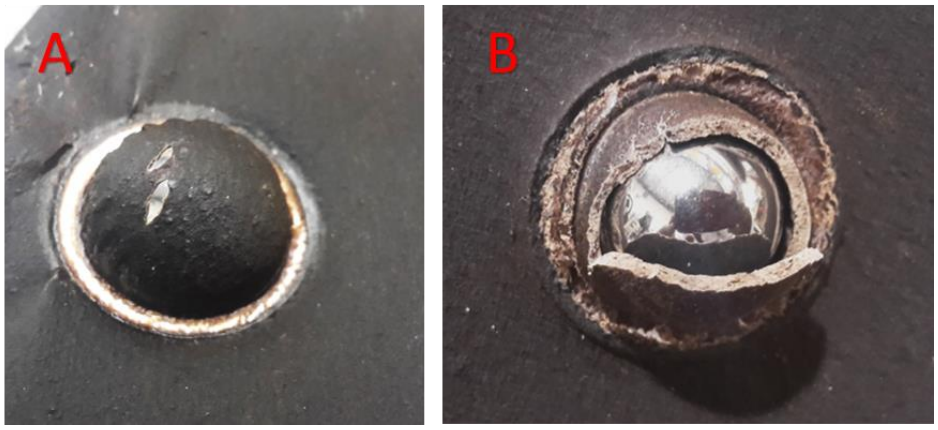

Figure 2.23: Failed feasibility welds with small ball bearing, thin sample (A), thick sample (B).

The results presented below are from the largest bearing (15.9 mm diameter), with an internal free thickness of 0.7 mm. Due to the cavity size being similar or slightly less thickness of the sheet it was able to be formed effectively (Figure 2.24). Successful weld adhesion was achieved for sheets as thin as 0.5 mm, but performed poorly during compression testing. Sheet thicknesses of 0.85 to 1.15 mm resulted in the best overall performance.

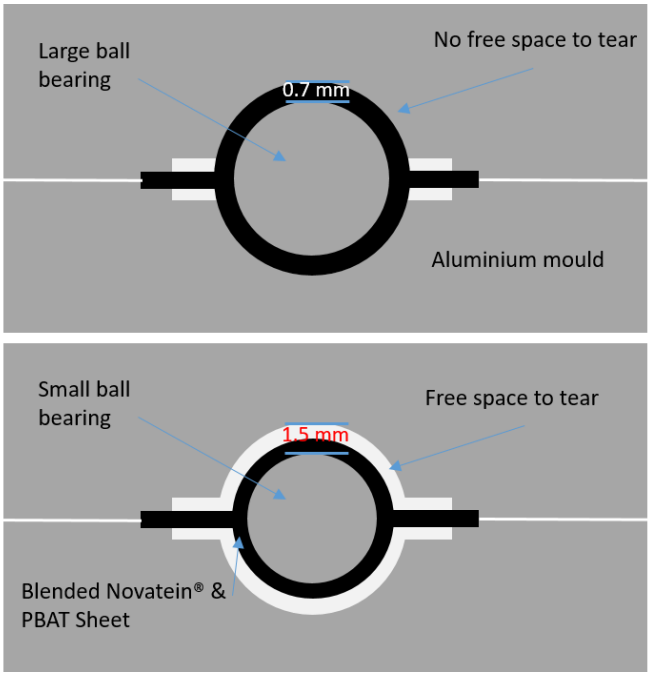

Figure 2.24: Visualisation of how the effect of bearing size on the weld quality.

The successful results are summarised in Table 2.3, grouped by temperature with decreasing hold time (a full list of results can be seen in Appendix B). The test highlighted with a red box was the most successful in two ways; it resulted in the largest average compression force (44.9 N) and most consistent in that all six

samples were able to be tested. Closer inspection of the compression results indicated that longer press times resulted in higher compression resistance of the hemispheres. Press times of 0.5, 1 and 3 minutes resulted in average compression resistances of 23.5, 26.8 and 31.4 N, respectively. This was expected as more samples were successful and able to be tested at a 3 minute hold time opposed to 0.5 minutes. No significant trend was noticeable with respect to the difference in temperature within the range of 105 to 125 °C. However, the second best individual result (39.2 N), indicated by the green box, was only held for one minute, but 10 °C higher. They both had sheet thickness of 1 mm which may have been a contributing factor. However as the experiment was not done in a full factorial design, and statistical analysis was not able to be performed. It was apparent that below 105 °C, the results were significantly reduced. This is of no surprise as plastic welding is typically done above the glass transition or melting point. Cold pressing resulted in no intermolecular diffusion which resulted in chain entanglement, therefore having no effective bonding.

Table 2.3: Summarised feasibility results.

Approx. Press Temp (°C)	Approx. Release Temp (°C)	Press Time (min)	Sheet Thickness (mm)	Weld Adhesion (%)	Average Compression Resistance (N)	Standard Deviation
105	27	3.0	0.90	100	23.1	4.88
105	30	3.0	1.00	100	44.9	4.01
105	30	3.0	1.10	50-90	21.6	2.61
105	26	1.0	1.05	60-80	15.7	N/A
105	31	0.5	0.95	0-70	25.5	N/A
110	21	1.0	1.00	100	31.7	7.12
115	30	3.0	1.15	100	33.4	N/A
115	28	3.0	1.10	100	32.4	1.41
115	27	1.0	1.05	100	20.8	11.22
115	32	1.0	1.00	100	39.2	16.14
115	33	0.5	1.00	80-100	21.6	6.93
125	24	3.0	0.85	100	33.4	N/A

Figure 2.25 shows the results of successfully welded samples around the bearings. Figure 2.25C shows how the ball bearing is cut perpendicular to the weld seam so that it can be tested. Figure 2.25D shows how the weld seem failed during the compression testing.

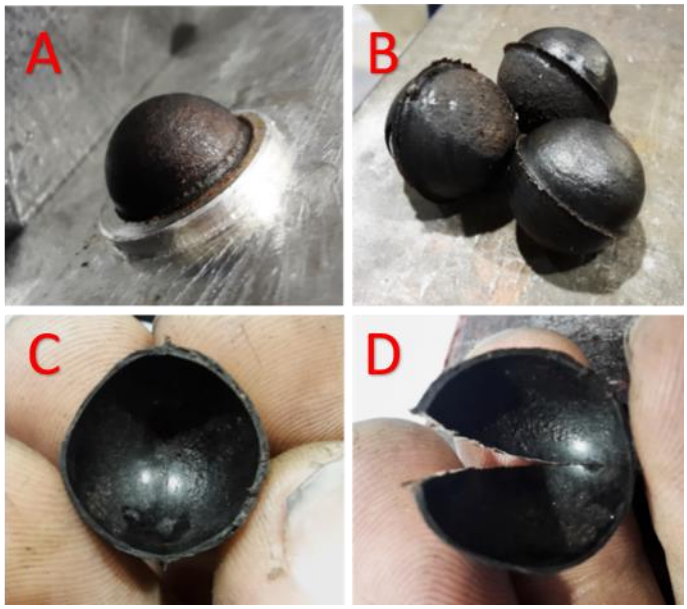

Figure 2.25: Successfully welded samples.

2.4.2 Weld strength

The first successful scoping experiments used a three-minute process that involved pre-heating, holding and cooling. In the interest of economic feasibility, extensive scoping was performed to find the lower limit of processing time and force required. Figure 2.26 shows the results of the boundary conditions during more accurate scoping experiments.

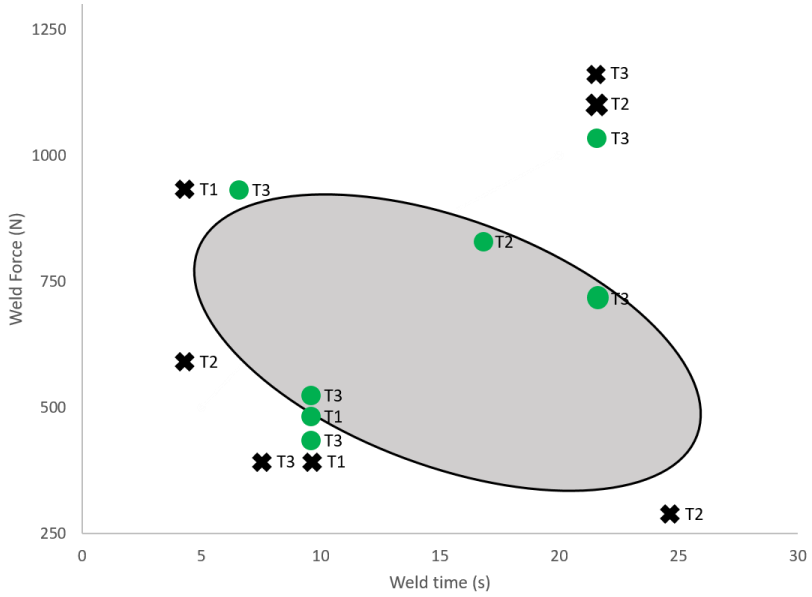

Figure 2.26: Scoping results for finding boundary conditions for welding 70-30 Novatein - PBAT. Green dots designate successful welds while black crosses designates failed welds.

Figure 2.27 displays the results of a DMA of Novatein/PBAT over the temperature range of -100 to 140 °C. The steep drop around -20 to -10 °C is characteristic of softening as we would expect for a blend of these two polymers. The exponential increase of Tan δ at 115 to 120 °C, is characteristic of the PBAT phase melting. From these results, it was determined that welding should be performed at 120 °C, but also explains the moderate successful welding observed at 75 °C.

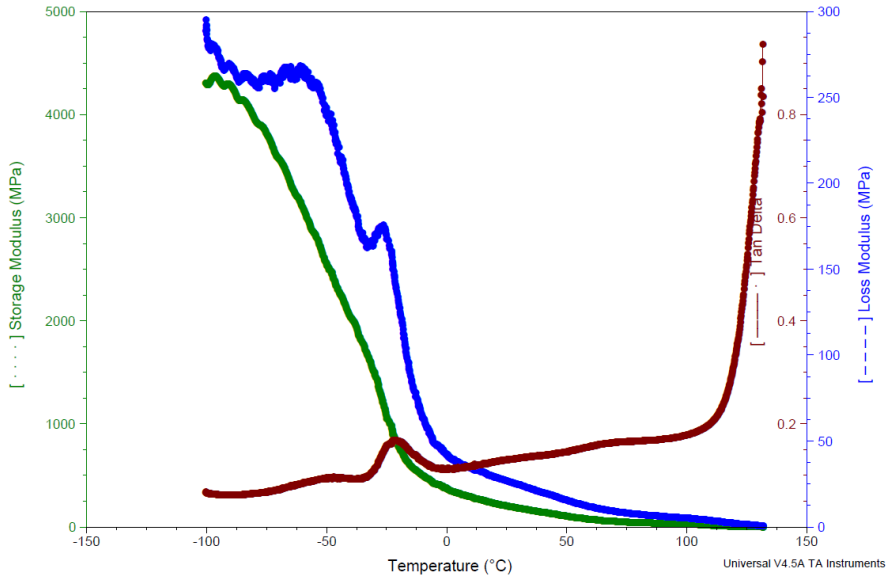

Figure 2.27: DMA of Novatein/PBAT sample.

Based on the scoping experiments, a more precise experiment was designed to test the strength of welded sheets. This section details the results of these compression welded samples in tensile and peel mode.

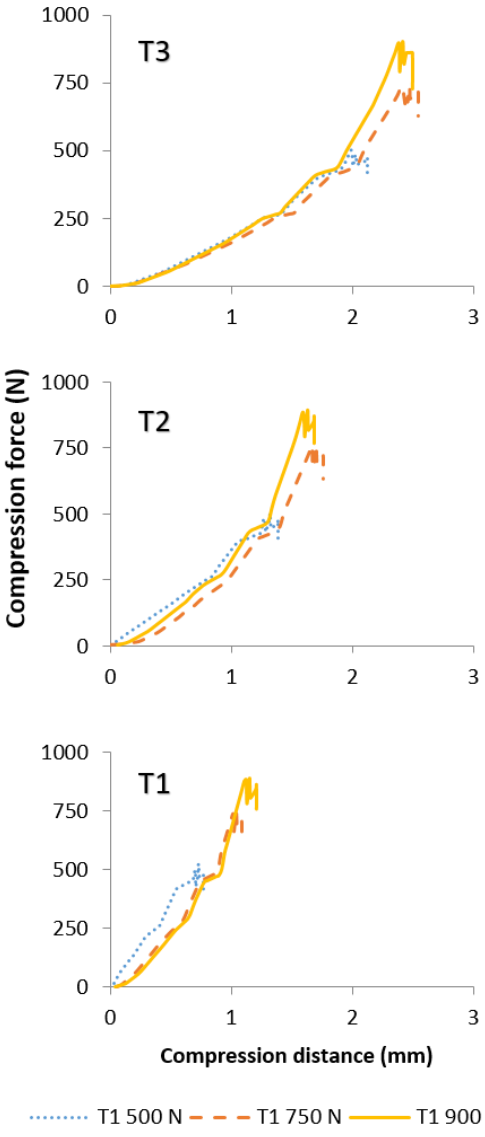

Figure 2.28: Compression force vs compression distance during welding.

Figure 2.28 shows the evolution of the compression force as a function of displacement for each sheet thickness tested. During welding, the maximum force is not applied instantaneously. Rather it is let to increase with displacement, at a rate of 16 mm/min. It is clear that at the lowest maximum allowable force, sheet compression was the lowest, irrespective of thickness (shown with the blue dotted line). There was very little difference in compression distance between 750 and 900 N. The compression distance decreased with decreasing sheet thickness accordingly. T3 samples would be approximately 3 mm thick when overlapped and the maximum compression was at least 0.5 mm less than this. On the other hand, T1 samples welded with 900 N had approximately 1.2 mm compression, with a thickness of only 1.35 mm.

From these results, it is no surprise that the only experimental combination that failed completely was T1 with a high weld force, the thin sheet had its material completely pinched during the welding process and therefore was not able to be tested (Figure 2.29). This was anticipated during scoping, however, it could not be avoided as the results from the high weld force gave a good weld quality using thicker samples.

Figure 2.29: T1 900 N failed weld.

The results from the peel and tensile tests can be seen in Figure 2.30A and B, respectively. The standard deviation of the experiments was reasonably large, and was attributed to poor temperature control and inconsistent material properties of the sheets. However, some general trends can still be observed.

In Figure 2.30B, the solid black bar is the average tensile strength of five control samples, i.e. samples cut from a single sheet and not welded. Not surprisingly, this is larger than the average of any combination of welded samples. Interestingly, it can be seen some of the thin samples (T1) with medium weld force (750 N) had individual results higher than the average of the control. Figure 2.30A shows the average peel force increasing with weld force. However, it was almost the complete opposite for the tensile strength, high weld forces resulted in the two lowest average results. The peel force also showed a trend of increased sheet thickness, resulting in increased peel force. The average peel force of the thin sample with low weld force increased 80 % when increasing the medium thickness level. It did show a slight reduction in peel force for the large peel force but this was the only result that did not align with this trend.

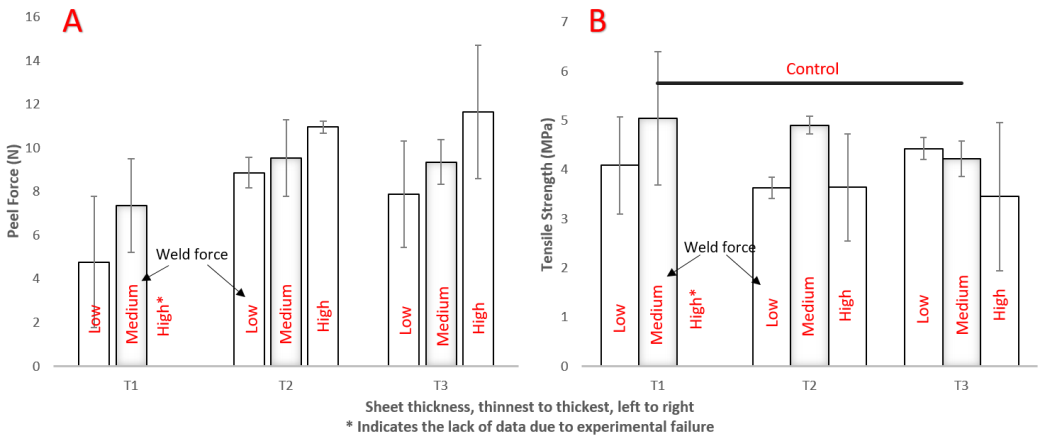

Figure 2.30: Peel force testing of welded samples (left), tensile strength of welded samples (right).

T3 samples showed the largest reduction in tensile strength and most inconsistent results. The largest average peel force recorded was 11.65 N, this was from the thickest sample with high weld force (Table 2.4). This is in total contrast to the same sample that had the largest reduction in tensile strength of 40 % (Table 2.4). The results for the tensile strength show a less obvious trend for improvement, however, it can be seen that the medium force had the highest average value of 4.72 MPa. It is clear that the right balance of weld force needs to be acquired to obtain the greatest tensile strength. Whereas increasing the thickness and weld force should optimise the peel force.

Table 2.4: Average results of the different experiments for the tensile and peel experiments.

Sample	Weld force	Average Tensile strength (mPa)	STANDV	Percentage reduction (%)
	Low	4.08	0.98	0.29
T1	Medium	5.04	1.35	**0.12**
	High	N/A	N/A	N/A
	Low	3.63	0.22	0.37
T2	Medium	4.90	0.18	0.15
	High	3.64	1.12	0.37
	Low	4.43	0.23	0.23
T3	Medium	4.22	0.36	0.27
	High	3.45	1.69	**0.40**
Control	N/A	5.76	0.88	0.29
			Average	0.28

Sample	Weld Force	Average Peel Force (N)	STANDV
	Low	4.77	3.01
T1	Medium	7.36	2.15
	High	N/A	N/A
	Low	8.86	0.69
T2	Medium	9.52	1.75
	High	10.95	0.27
	Low	7.88	2.44
T3	Medium	9.35	1.03
	High	11.65	3.05

An analysis of variance (ANOVA) was performed to determine whether there is any statistical difference between the means of the tensile and peel strength with respect to the parameters of weld force and sheet thickness. The results of the ANOVA can be seen in Table 2.5, the null hypothesis for this test is that the means of the results are not significantly different. The response table for means, ranks weld force to have the highest influence on tensile strength, however, the P value for both weld force and thickness were above 0.05, thus we cannot reject the null hypothesis and conclude that the uncontrolled error had more influence on tensile strength of the weld than the weld force or sheet thickness.

Table 2.5: Tensile statistical data: Analysis of Variance for Means (left), Response Table for Means (right).

Source	DF	Seq SS	Adj SS	Adj MS	F	P
Weld Force	2	8.574	8.574	4.2869	2.54	0.194
Thickness	2	1.889	1.889	0.9445	0.56	0.610
Residual Error	4	6.747	6.747	1.6869		
Total	8	17.210				

Level	Weld Force (N)	Thickness
1	4.047	3.073
2	4.720	4.057
3	2.397	4.033
Delta	2.323	0.983
Rank	1	2

The main effects plot for the means in Figure 2.31 shows the medium weld force (750 N), resulted in the greatest tensile strengths, this agrees with the results in

Figure 2.30. It shows that there is little difference in results between T2 and T3. It also indicated that the thinnest sheet and the 900 N weld force gave the poorest results. These results may be skewed as the high weld force for the thin sheet were not present and therefore set to zero.

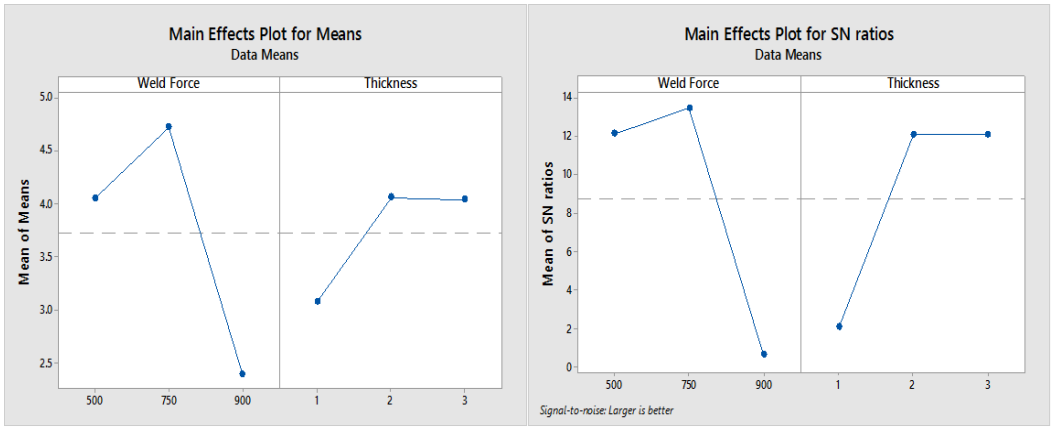

Figure 2.31: Tensile statistical results for main effects plot for means (left) and SN ratios (right).

Table 2.6, shows the statistical results from the peel force tests, the response table for means has thickness ranked the most influential on peel force, this contrasts with the tensile strength results. However, again the P values seen in the analysis of variance for means are both above 0.05, therefore the null hypothesis cannot be rejected and no statistical difference with these two parameters. This implies that the uncontrolled error had more influence on peel force of the weld than the weld force or sheet thickness.

Table 2.6: Tensile test statistical data. Analysis of Variance for Means (left), Response Table for Means (right).

Source	DF	Seq SS	Adj SS	Adj MS	F	P
Weld Force	2	4.102	4.102	2.051	0.25	0.788
Thickness	2	63.622	63.622	31.811	3.93	0.114
Residual Error	4	32.379	32.379	8.095		
Total	8	100.103				

Level	Weld Force	Thickness
1	7.177	4.077
2	8.763	9.797
3	7.567	9.633
Delta	1.587	5.720
Rank	2	1

The main effects plot seen in Figure 2.32 indicates that the medium force weld (750 N) resulted in a greater peel force. Again, it sees little difference between T2 and T3, although the zero value for the T1 sample skewed the results, indicating that the T1 thickness does not perform well overall. Interestingly the 900 N weld force does not see such a reduction in peel force, as the overall trend would agree with.

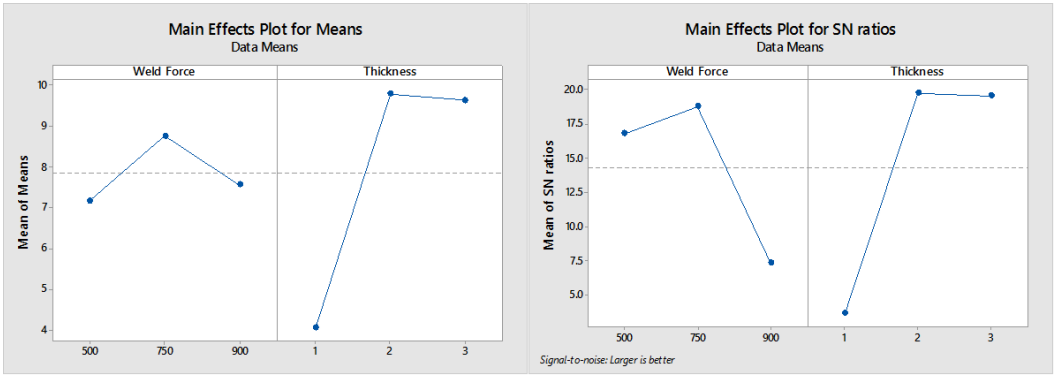

Figure 2.32: Peel test statistical results for main effects plot for means (left) and SN ratios (right).

Although the results of this experiment are statistically insignificant, the observed failure modes agree with relevant literature. The T3 samples when welded with more force looked visibly stronger than others, however during tensile testing performed the worst.

Images of the tensile tests can be seen in Figure 2.33, Figure 2.33A was the highest average result and Figure 2.33B, the lowest. When looking at the weld quality, B1 appears to have a higher quality weld than A2. However, when looking at where the fracture occurred, it can be seen that B1 is completely outside the weld zone, whereas A1 is highly centralised. This indicates that during the 900 N welding, the compression force was either too high or needed to be applied at a slower rate. This high load causes a high shear rate in the interface where the temperature gradient is highest, aligning molecules and creating a weak spot [85].

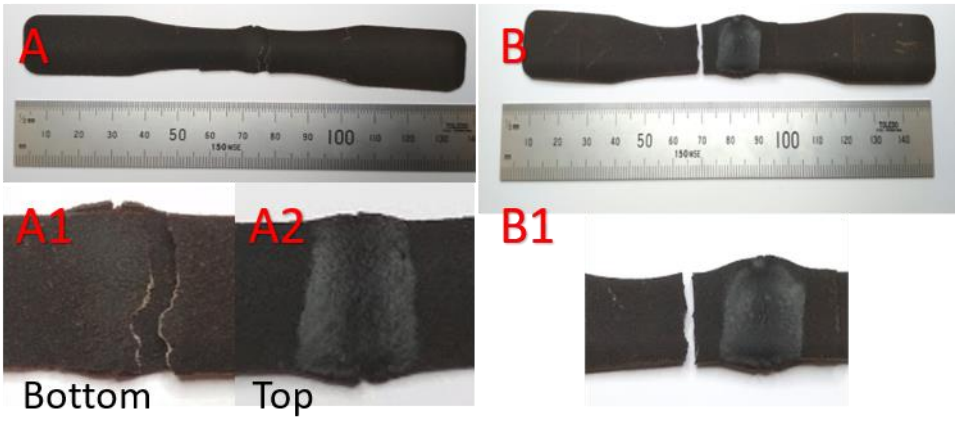

Figure 2.33: T1 750 N tensile test (left), T3 900 N Tensile test (right).

When graphing the compression force versus time (Figure 2.34), it is clear to see that the rate of loading for the 900 N force is much steeper than the rate of loading

for the 500 N force, shown by the solid yellow circle and the dotted blue circle, respectfully.

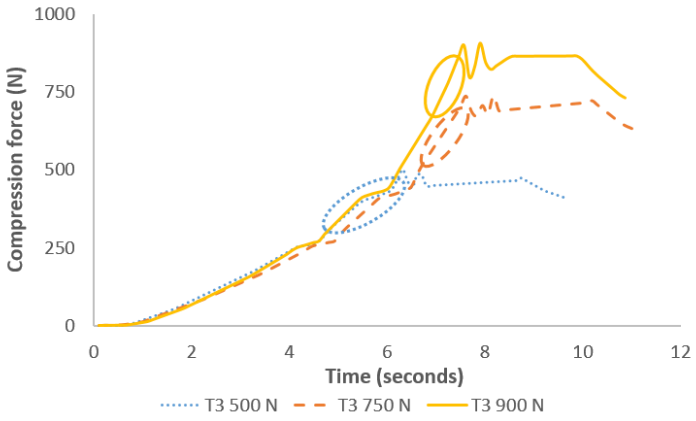

Figure 2.34: Compression force vs time during welding the T3 samples.

However, when the weld quality is judged by the highest peel force, the thicker and higher force the better. Figure 2.35, shows how during the peel test the sample on the right shows comprehensive tearing at the weld, whereas the sample on the middle and left, spit apart with barely any interaction at all.

Figure 2.35: T3 500 N Peel test (left), T1 500 N Peel test (middle), T3 900 N Peel test (right).

2.5 Product Design Evaluation

The aim of this chapter was to evaluate a method of mass manufacturing a projectile that can be utilised to dramatically decrease the labour cost of planting trees by automating the system. The method chosen was to replicate manufacturing paintballs, where seed injection can be incorporated into the process. The challenges around this manufacturing technique are the ability to continuously produce sheets, mould them and effectively be welded to itself. From prior research, the ability to continuously sheet extrude compatibilised 70-30 Novatein-PBAT

sheets has been successfully investigated [27]. This chapter investigated the forming and welding of this polymer blend.

Sheets of 70-30 Novatein and PBAT were extruded with compatibilisers to improve sheet morphology and quality. A scoping experiment was performed to evaluate if the blended sheets could formed around a ball bearing and if welding was at all possible. This experiment used a 50-tonne heated press to investigate the effect of temperature, press time and the bearing size. Several key results were obtained; initial welds were achieved when increasing the heating to the 75 °C which were just above the T_g of the sheets, larger ball bearings reduced the free volume which improved the forming ability and cold releasing the mould greatly improved weld success. The samples that were successful were evaluated by testing the compressive strength of semi-circles when cutting perpendicular to the weld. The most successful and repeatable was a 1 mm sheet, pressed for 3 minutes, at 105 °C, with an average compressive strength of 44.9 N. A key result was that the compressive strength was found to increase by 34 % when the press times were increased from 0.5 to 3 minutes. However, due to economic manufacturing, this would be impossible to do on the scale required. There was clearly a number of different variables that need to be controlled in a more accurate study; a smaller heated press would be required to vary the weld force, the mechanics behind the forming with respect to the sheet thickness needs to be investigated and a full factorial design needs to be implemented to perform a statistical analysis.

Once a window was found for successful welding and forming, a more precise method of quantifying the weld strength was tested. Due to one of the limiting factors of the heated press was its pressure control and from literature knowing that weld pressure plays a significant role, a test method using an Instron in compression mode was developed. This used the sheets, cut into dog bone testing strips that could be lap welded, investigating the effect of weld force and thickness on tensile strength and peel force. Both methods are widely used to evaluate the strength of welds on thermoplastics. During scoping the weld time was optimised to a 6 to 9 second compression cycle with a 60 seconds preheat. This preheating time would be easily reduced or removed with the appropriate equipment and giving dramatically decreased cycle times. Knowing this, it was decided not to vary the preheating or weld durations as this would be ideal for a further experiment with more controlled heating.

Initial results for tensile strengths found that compared to un-welded control samples, the average tensile strength was reduced by 28 % when lap welded, the best result was a reduction of 12 % and the worst by 40 %. The most successful weld (12 % reduction) had an average tensile strength of 5.04 MPa, produced by a thin sheet approximately 0.675 mm thick, with a weld force of 750 N. The only test that consistently failed was using this same sheet thickness with a slightly higher weld force of 900 N, indicating that this sample is on the upper limit of force that it can withstand before breaking. From the results, it is not clear why the thin sheets showed an increasing tensile strength with increasing weld force whilst the thick sheets showed the opposite trend and the middle thickness (T2) sheets appeared to have no trend. From the statistical evaluation, the error during the experiment had a more significant effect of the average tensile strengths than the parameters changed, therefore indicating more precise temperature control, force application and homogeneous sheets are required. The peel test showed more significant trends of improvement with increasing weld force and sheet thickness, the largest average peel force was 11.65 N for the thickest sample welded with the largest force. Compared with the lowest recorded of 4.08 N, from the complete opposite, thinnest sample with lowest weld force. These parameters were not confirmed to be statistically significant due to error, however, it is clear to see that increasing the thickness and weld force increases the peel force.

From this study, we can conclude that a polymer blend of Novatein and PBAT can be successfully welded together using a standard plastic welding method which is relatively cheap and reliable. The ability for this polymer blend to be moulded around a ball bearing was also found to be successful, from this it can be assumed that vacuum forming could be used to produce the semi-circles would be achievable and that this method of mass manufacturing is ideal for producing seed pods in the form of projectiles.

This project would benefit greatly from the following future investigations; accurate pressure control during heated press forming, temperature controlled welding, vacuum forming sheets, and failure mode evaluations. If the results of these further investigations are successful like the study performed during this project, I believe that this method of production can be successful.

Chapter 3
Penetration Depth Predictions using Empirical Modelling

To successfully automate reforestation, a seed planting method of penetrating the soil accurately is required. It was found that if radiata pine seeds were planted too deep (< 16 mm), or too shallow (> 3 mm), the chance of seeds germinating was reduced significantly [21]. Therefore, if a projectile is to be used to deliver a seed within a bullet capsule a method of calculating the penetration depth will need to be developed.

This chapter will investigate, soil characteristics which affect penetration, projectile flight, and empirical and theoretical formulae for predicting penetration depth. The objective of this chapter is to develop a relationship between a method of testing soil and predicting the depth of penetration of a known projectile into a known granular medium.

3.1 Literature

3.1.1 Newton's law of penetration

A projectile is defined as an object that has been given an initial velocity by an outside force where the only other force acting upon it during flight is gravity [111]. To achieve stable flight, projectile aerodynamics and ballistics must be considered. When considering the aerodynamics, one must first understand simple projectile motion where the flight pattern and trajectories can be modelled with simple kinematics equations. However, this does not take into account the medium for projectile flight. Because flight is not in a vacuum, a drag force acts on the projectile, which is a function of its shape, density of the fluid and a drag coefficient, as seen in Equation 3-1.

$$Drag\ force\ (F_D) = \frac{1}{2}\rho V^2 A C_D \qquad 3\text{-}1$$

Where; ρ is the density of the fluid medium, V is the relative velocity of the projectile to medium, A is the projected area, C_D is the coefficient of friction, a function of the shape.

When evaluating the forces around projectiles there are four external reaction forces to be considered; [112] lift, drag, thrust and gravity (Figure 3.1). Lift and drag are generated from the relative motion of a stationary fluid with a moving object or vice versa. The resultant force will determine which direction the object will be accelerating, dependent on the thrust. The left of Figure 3.1 shows how different common geometric shapes result in different drag coefficients, which is used in Equation 3-1 to calculate the drag force experienced by the object.

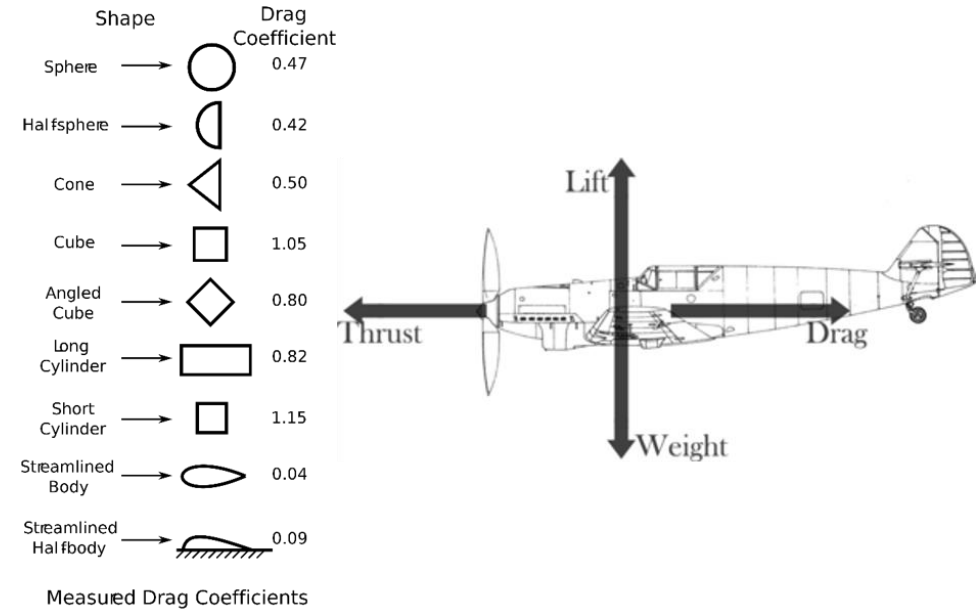

Figure 3.1: Drag coefficients of generic shapes (left), sourced from [113] and the four forces acting on an object during flight (right), sourced from [114]

3.1.2 Methods of thrust

For this project, an appropriate method of thrust needs to be evaluated. The thrust needs to be sufficient to achieve penetration into hard soil, light for transportation and be able to deliver at least 100 projectiles per flight. Most importantly, the method of thrust needs to be adjustable to ensure that the same penetration depth can be achieved when planting in hard clay, or soft, wet soil.

I. Spring

Air rifles use a simplistic spring powered pneumatic device that fire pellets up to 500 m/s [115]. Air rifles typically use 0.177 calibre pellets, 4.5 mm diameter, weighing approximately 0.5 g. An air rifle is mechanically very simple with few moving parts which make them ideal. However, they require a cocking force, which can be up to 120 Nm [115; 116]. Domingo Tavella, investigated the internal

ballistics on spring action piston airguns, and found that with a 0.177 calibre pellet, 0.67 g, with a max barrel pressure of 5273 kPa, the muzzle velocity was approximately 250 m/s with 20 J of linear kinetic energy [117]. Werner *et al.* [118] investigated the penetration depth of differently shaped pellets into gelatin gel (Balistic 2 type A) with varying kinetic energy. It was found that as low as 4 J penetrated up to 50 mm, and 20 J penetrating up to 100 mm deep. Although this method has the required simplicity and muzzle velocity, it is not easily adjusted and would also require a mechanical system to recock the spring run off a battery.

II. Combustion

Using combustion for a method of thrust involves a dense energy source usually referred to a propellant, such as gunpowder. This creates a controlled explosion or combustion, the same way a petrol engine works. Combustion allows for a much higher power, for instance, a rifle will have an average muzzle velocity of a 1000 m/s, ten times that of a paintball gun [119]. Using combustion for thrust could decrease the overall weight by using a high-density energy source, however for this project the impact velocity could be significantly too high and difficult to adjust. This would also cause issues around recoil if the UAV were not of sufficient mass.

III. Compressed CO_2

Compressed CO_2 is commonly known for firing paintballs at high velocity with a loader that can carry 200 to 300 paintballs [120]. It was found that the muzzle velocity of a paintball gun with 870 kPa pressure was approximately 85 m/s and the impact velocity decreased with distance by a linear function of the natural log [121]. The US military investigated the depth of paintball penetration into clay for two different calibres and a range of impact velocities. It was found that the penetration depth did not significantly vary between 6 and 8 gram paintballs, but did decrease linearly with decreasing velocity [122]. The lowest impact velocity tested was approximately 38 m/s where the 6 g paintball that penetrated to a depth of 15 mm.

Compressed CO_2 is the obvious choice for this project, it can shoot a relatively large number of projectiles with a relatively small canister, easily adjustable, has the required muzzle velocity for penetration and will have less recoil than that of combustion.

3.1.3 Impact analysis

If we assume that the seed pod will be delivered by compressed air similar to a paintball gun with a muzzle velocity of 100 m/s, and 4 g mass, we can assume it will have an impact force of approximately 20 J. Past research has tested the limits of impact forces for a range of nuts and seeds. It was found that locust bean seeds took on average 174 N to crack [123], wheat seeds 93 N [124], and mustard seeds as low as 17 N [125]. However no past research was found that evaluated the breaking force of radiata pine seeds, it is approximated they will have a breaking force similar to the locust bean due being a similar size. However, if this was found to be a problem it could be investigated easily. A solution would be to fill the bullet with shock absorbing liquid made from dense colloidal suspensions [126].

3.1.4 Penetration analysis

As discussed above different shape projectiles result in different drag coefficients, however, it is the effect that shape has on penetration that is of interest here. The effect on the ballistic limit of the projected area or nose shape has been comprehensively studied with different materials [127; 128]. The ballistic limit is the velocity a projectile needs to penetrate its target more than 50 % of the time. These tests are typically conducted when firing a projectile into metal plates with varying thickness. There is conflicting literature of the ballistic effect of different nose geometries such as, flat, hemispherical and conical. The conclusions of this field of research are not entirely compatible, but highly situation dependent.

Børvik *et al.* and Wingrove, A. L. found that the ballistic limit of the conical and hemispherical shapes were similar whereas the blunt nose required much lower velocity when testing on 12 mm thick steel and aluminium sheets [127; 129]. On the other hand, Wilkins [130] found that sharp projectiles such as the conical shape gave a lower ballistic limit to blunt projectiles when fired into metal plates. It was confirmed that when the target thickness to projectile diameter ratio is less than one then the blunt nose has a lower ballistic limit (requires less velocity to penetrate). Simply, when penetrating thin metal plates a blunt nose works best, thick metal plates require sharper nose shapes. This is due to the blunt projectiles causing material failure by plugging, dominated by shear banding, a localised intense shearing strain during severe deformation of ductile materials [127]. The top image

of Figure 3.2 displays plugging where an almost circular plug was ejected, whereas the conical pushed the material in front of it, to the side and creates petals.

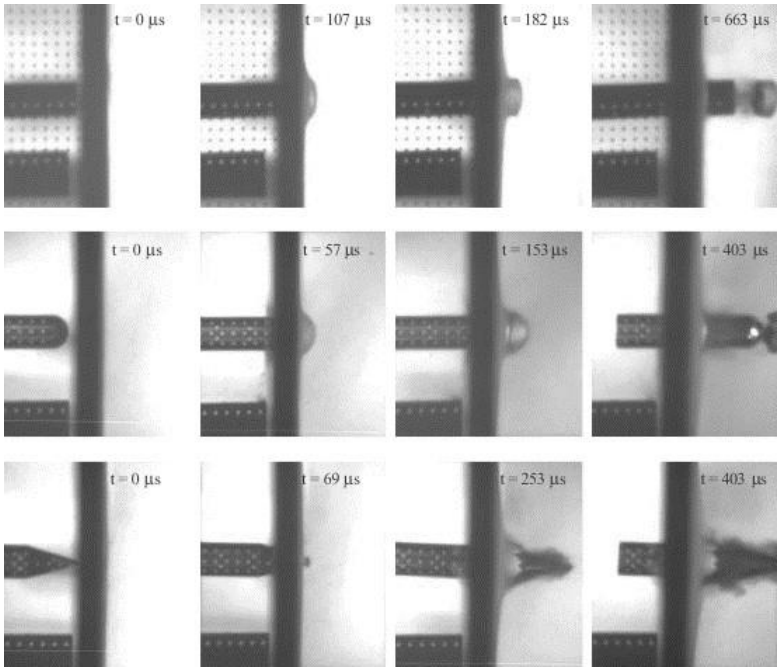

Figure 3.2: Failure modes of blunt, hemispherical and conical (top to bottom) projectiles penetrating through metal plates, sourced from [127].

3.1.5 Penetration into granular media

Soil is classified as a granular media and the study of how projectiles behave when impacting into granular media is referred to as phenomenology [131]. This field has been of interest predominantly for military purposes, but also for deep sea anchors, nuclear waste disposal and subsurface investigations of extra-terrestrial surfaces, such as the moon [132-134]. Models to predict projectile behaviour are broadly known as phenomenological models and are based on Newton's second law of motion. Newton's equation is modified for penetration of granular media and can be seen in Equation 3-2. Although the field has been studied extensively, it is still difficult to use a single model to accurately predict penetration with respect to different medium and projectile variables [131; 135].

$$m_p \frac{dv}{dt} = F = m_p g - \alpha v^2 - \beta v - \gamma \qquad 3\text{-}2$$

Where, v is the impact velocity, m is the projectile mass, α represents the contribution of inertial stresses (with units of mass over length), β controls the contribution of viscous resistance of soil (with units of mass over time), γ is a parameter (with units of force) dominated by the bearing strength of the soil.

To calculate the penetration depth of soil, the physical soil properties must be understood. Important physical properties of soil are air porosity, bulk density, water retention capacity, particle distribution and soil strength. Soil strength is the resistance to the particles shearing past each other which is highly dependent on moisture content and is directly related to root growth and penetration resistance. Particle distribution is the relationship of relative amounts of gravel, sand and clay within the soil. This relationship affects the surface area of the soil; clay, for instance, has a surface area in the range of 5 - 750 m^2/g whereas coarse sand is approximately 0.01 m^2/g [23].

Water retention capacity is expressed as the mass of water evaporated per 100 grams of oven dry soil as a percentage. The bulk density of soil is the oven dry weight of soil per unit volume (g/cm^3). Typical values of bulk density range from 1 - 1.8 g/cm^3. The bulk density of standard agricultural soil from literature was calculated to be 1.4 g/cm^3 with an available pore space of 47 % [23].

I. Methods of testing soil properties

Penetration tests are the most common methods of testing soil strength to predict important characteristics such as cultivation performance, water retention, root growth and for geotechnical engineering [136; 137]. Penetration tests can be dynamic (drop tests) or static (constant applied force or under own weight).

Campbell *et al.* [138] investigated a static drop-cone method on different soils at different moisture contents. A 30° cone of 80 g mass was placed at the top of the medium and allowed to plunge for five seconds, measuring the penetration depth. It was found that for a sandy loam (soil that is predominantly sand) the penetration depth was decreased when increasing moisture content up to 25 wt.% (Figure 3.3).

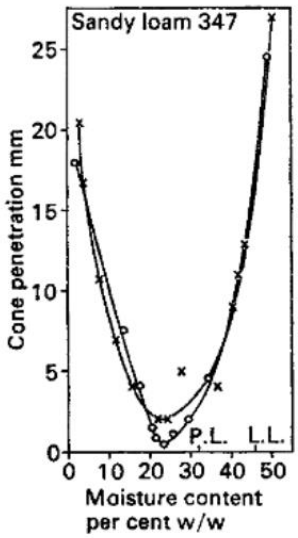

Figure 3.3: Penetration depth of a drop cone method in sand with increasing moisture content, sourced from [138].

A standardised penetration test method is to use a cone penetrometer, the results of which are typically converted into a value in the MPa range or a cone index (CI) [137]. By applying a force on a cone shape the cohesive forces between soil particles and the frictional resistance to sliding past each other can be calculated. The can be static or dynamic, being pushed into the ground with constant force, or the latter with an anvil that is dropped from a specific height [24]. When using a static cone penetrometer conforming to ASAE 1983 standard S313.1, some common values range from 0.5 to above 3.0 MPa for loose to extremely dense soil [23]. Equation 3-3 calculates the soil resistance when using a dynamic cone penetrometer (DCP) (Figure 3.4).

$$R = \frac{mgH}{A\Delta z}\frac{m}{m+m'} \qquad 3\text{-}3$$

Where, R is the soil's resistance to penetration (Pa), A the cross section area of the cone (m^2), g is the gravitation acceleration constant of 9.81 m/s^2, m is the mass of the hammer (kg), m' is the mass of the shaft (kg) and Δz is the change in depth from the impact (m).

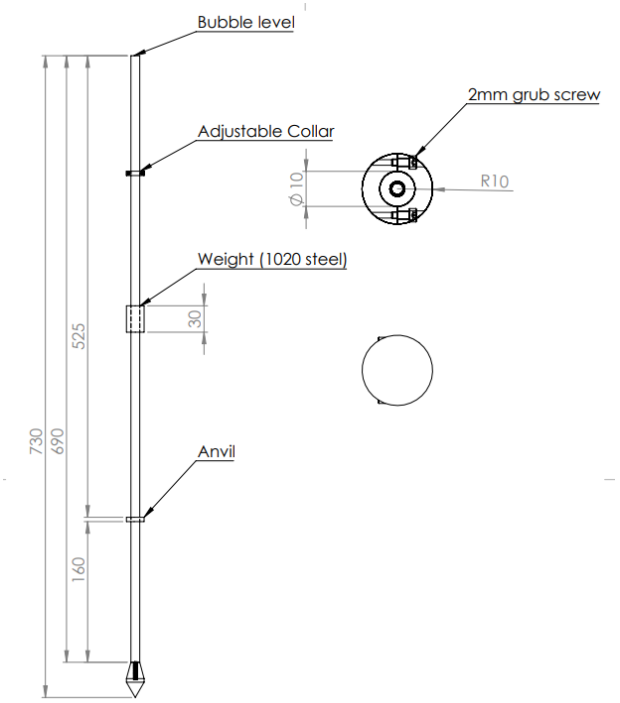

Figure 3.4: Dynamic Cone Penetrometer.

Vanags *et al.* [24] used the DCP to study the penetration resistance of soil that was used for cultivation and pasture (Figure 3.5). It can be seen that with both soil types, the resistance increased with depth, with the pastured soil being higher. Of particular interest was the sudden increase in penetration resistance at 10 to 12 cm, indicating the variability of soil. It was assumed to be from either localised compaction or the presence of calcium carbonate precipitation.

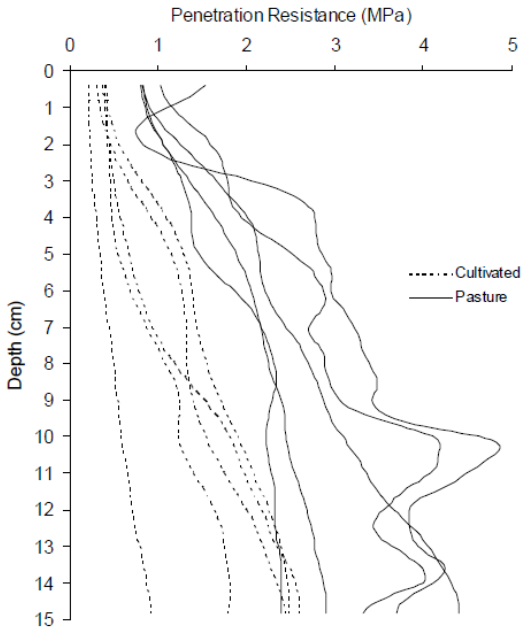

Figure 3.5: Penetration resistance of soil under cultivation and pasture, sourced from [24].

The soil resistance is highly dependent on moisture content, bulk density and organic matter, due to this it makes it difficult to relate one test to another. Vanag *et al.* [24] described the relationship between moisture content and penetration resistance to be exponential due to the water molecules decreasing the cohesion between the particles, acting a lubricant and therefore reducing the frictional forces. Investigators commonly try to ensure that the moisture content kept constant between different testing sites when possible. Busscher *et al.* [139] (1997) found that a single equation to correct for moisture content did not always fit the data and proposed multiple corrections may be required. Vaz *et al.* [140] continued his work using a cone penetrometer that used time domain reflectometry to measure the real time moisture content during the test. This was used to validate the theory proposed by Upadhyaya *et al.* that suggested an exponential-power function can be used to relate the measured penetration resistance to bulk density and moisture content. A recent study into the effect of moisture content of soil strength was performed by Weider *et al.* [141] who failed to validate the work of Sullivan *et al.* from 1997 on the relationship with moisture content to soil strength due to factors previously mentioned such as bulk density and organic matter. Ideally, the DCP could be used to correlate the impact energy required to penetrate a desired depth, however, the bulk density and moisture content will likely need to be known in order for the correlation to work.

II. Theoretical formulae

Modelling of impact and penetration into granular media (soil) has been extensively studied in the field of Phenomenology [131]. Equations are based off Newton's second law of motion. Soil resistance is characterised by three physically interpretable components in Equation 3-2.

Four penetration models derived from Equation 3-2 are historically referenced, Euler (3-4), Poncelet (3-5), Resal (3-6) and Petry in empirical units (3-8) [131].

$$P = \frac{m_p v_0^2}{2\gamma} \quad 3\text{-}4$$

$$P = \frac{m_p}{2\alpha} ln\left(1 + \frac{\alpha v_0^2}{\gamma}\right) \quad 3\text{-}5$$

$$P = \frac{m_p}{\alpha} ln\left(1 + \frac{\alpha v_0}{\beta}\right) \quad 3\text{-}6$$

$$P = \frac{m_p}{A} log\left(1 + \frac{v_0^2}{2 * 10^4}\right) \quad 3\text{-}7$$

Where, P is the penetration depth (m), m_p is mass of projectile (kg), v_0 is the initial velocity (m/s), γ is a parameter (measured in Newton's) dominated by the bearing strength of the soil, α represents the contribution of inertial stresses (with units of mass over length), β controls the contribution of viscous resistance of soil (with units of mass over time).

From the objective of this project, it was determined that performing a theoretical analysis of the penetration depth was not in the main interest. This was decided due to the lack of modelling experience, and a more experimental approach to the problem was required. Therefore, investigating empirical models that could be experimentally studied was the focus.

III. Empirical formulae

Calculating soil resistance is not an exact science and is strongly dependent on bulk density, moisture content, grain size and organic matter. To determine that the prototype considered in this study is feasible, an ability to evaluate soil characteristics at the desired planting site and predict penetration depth needs to be examined. The study of Terminal ballistics is well known, however, it is still sufficiently difficult to accurately calculate the penetration depth of a projectile with respect to different shapes and mediums [131; 135].

In 1967 C. W. Young developed a range of empirical equations for calculating the penetration depth into a variety of mediums, one being soil. In 1997 he updated these equations and increased the accuracy to within 15 %, unless the conditions were close to the specified boundary conditions. The boundary conditions were that the projectile remains intact, has a stable trajectory, a maximum velocity of 1200 m/s, penetration depth be more than three projectile diameters deep, and the projectile must be at least 2.2 kg. The final boundary condition is significantly larger than the mass of projectiles for this project.

To predict penetration depth the projectiles, velocity, mass and shape had to be known. However, different to theoretical models this used a dimensionless coefficient (S) to test the soil's resistance to penetration. The penetration resistance of the soil was calculated using a DCP or selected from his literature values (Table 3.1).

Table 3.1: Penetrability of typical soils, sourced from [25].

S-number	Target Description
2 - 4	Dense, dry, cemented sand. Dry caliche. Massive gypsite and selenite deposits.
4 - 6	Gravel deposits. Sand, without cementation. Very stiff and dry clay.
6 - 9	Moderately dense to loose sand, no cementation, water content not important.
8 - 10	Soil fill material, with the S-number range depending on compaction.
5 - 10	Silt and clay, low to medium moisture content, stiff. Water content dominates penetrability.
10 - 20	Silt and clay, moist to wet. Topsoil, loose to very loose.
20 - 30	Very soft, saturated clay. Very low shear strength.
30 - 60	Clay marine sediments, either currently (Gulf of Mexico) or recent geologically (mud deposits near Wendover, Utah).
> 60	It is likely that the penetration equations do not apply.

Dense, dry, cemented sand has an S value of 2 to 4, whereas, moist silt, clay, loose or very loose topsoil will range from 10 - 20 [25]. The DCP used for the calculation has a 12.7 mm diameter steel rod, 30-degree cone nose and uses a 5 kg anvil. The number of drops (N_D) to reach 0.3 m is used in Equation 3-8 to calculate S.

$$S \sim \frac{60}{(N_D^{0.55} - 2)} \qquad 3\text{-}8$$

For projectile velocities above 60 m/s, Equation 3-9 is used to predict penetration depth, below 60 m/s, Equation 3-10 is used, both in SI units. Both equation use the

hardness value (S), mass to area ratio, velocity and a shape factor the prediction [25].

$$D = 0.0000178\, S\, N \left(\frac{W}{A}\right)^{0.7} * (V - 30.5) \quad 3\text{-}9$$

$$D = 0.0008\, S\, N \left(\frac{W}{A}\right)^{0.7} * ln(1 + 2.15V^2 * 10^{-4}) \quad 3\text{-}10$$

Where, D is the penetration depth (m), S is the dimensionless soil hardness, N is a dimensionless shape factor, W is the projectile mass (kg), A is cross sectional area (m^2), V is the impact velocity (m/s).

Equations 3-11 & 3-12 are corrections for shape factor, N_T for a tangent nose and N_C for a conical tip, as seen in Figure 3.6.

$$N_T = 0.18(CRH - 0.25)^{0.5} + 0.56 \quad 3\text{-}11$$

$$N_C = \frac{0.25L_n}{D_p} + 0.56 \quad 3\text{-}12$$

Where, L_n is the ballistic length (m) and D_p is the diameter (m). For blunt nose shapes use conical with $L_n = 0$. CRH is the critical radius head = to the radius of curvature/D_P as seen in Figure 3.6.

When the projectile mass is less than 27 kg, Equation 3-9 or 3-10 (dependent on projectile velocity) is multiplied by a correction factor, K_s from Equation 3-13.

$$K_s = 0.27\,(W)^{0.4} \quad 3\text{-}13$$

Where, W is mass in kg.

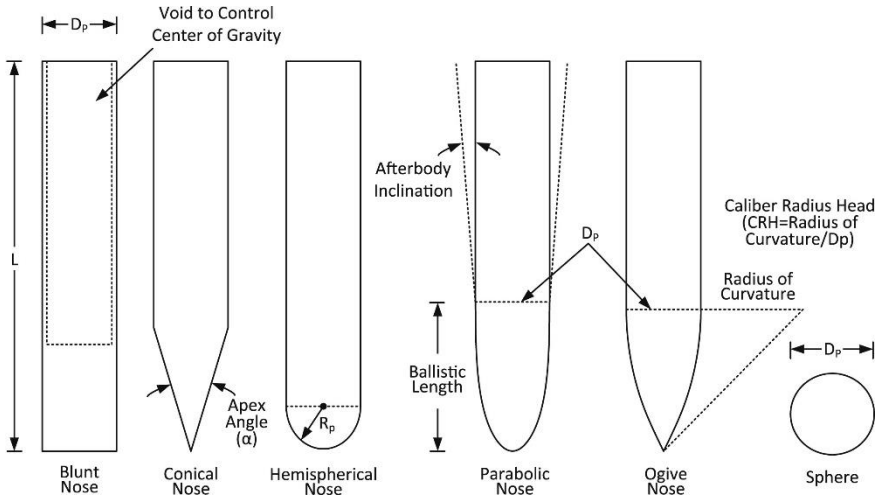

Figure 3.6: Typical impact shapes, sourced from [131].

Lorenz *et al.* [135] modified Young's penetration Equations (3-9 or 3-10) using a 150 mm diameter airgun, to determine his own empirical formula that was found to be more accurate (Equation 3-14). He used the same method for calculating soil resistance. It was determined that the shape factor did not show a strong influence on results and hence was removed for added simplicity.

$$D = 4.5 * 10^{-8} S^{0.5} \left(\frac{W}{A}\right)^{0.7} * V^2 \qquad 3\text{-}14$$

It was omitted that none of these methods are dimensionally consistent and needs further work in increasing accuracy. Due to subtle differences in the geometry and mass of penetrometers the non-unity of the S term was not a surprise and further work was required to obtain a more accurate method of testing [135].

Preliminary modelling of Lorenz and Young equations against each other with respect to increasing velocity and soil hardness within the set boundary conditions show obvious discrepancy (Figure 3.7).

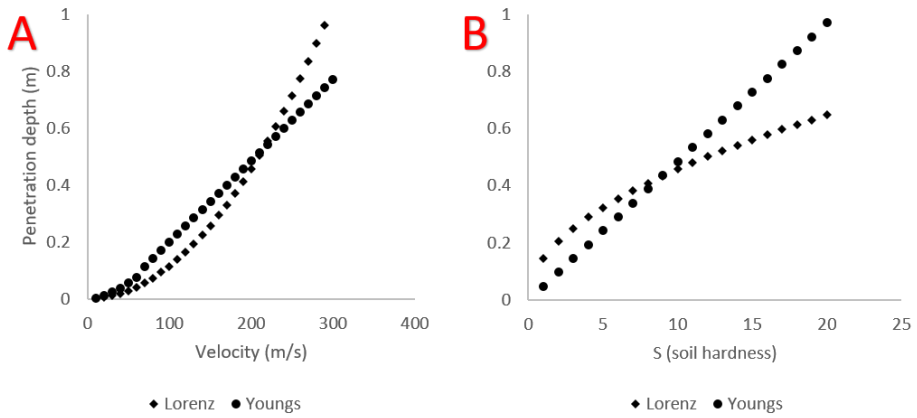

Figure 3.7: Modelled penetration depth of Young vs Lorenz, as a function of velocity (A) and soil hardness (B).

The aim of this literature was to prove the feasibility of predicting the penetration depth of a projectile into various soil mediums for planting seed capsules. This is proven successful by demonstrating that a tried and tested model exists between a practical method of testing the penetration resistance of soil, and relating it to a simple model for predicting the penetration depth of a projectile. This method is now required to be tested outside of its boundary conditions to evaluate its credibility.

3.2 Experimental Methods

3.2.1 Experimental procedures

I. Dynamic cone penetrometer

Figure 3.8 is a diagram of a dynamic cone penetrometer with dimensions conforming to NZS 4402, it was used to measure the penetration resistance of soil in locations across New Zealand. This method involves repeatedly dropping a weight (9 kg) onto an anvil from 508 mm and measuring the distance the rod enters the ground up to one meter. The full experimental method can be found Appendix C. The penetration resistance is measured in MPa and is calculated using Equation 3-3.

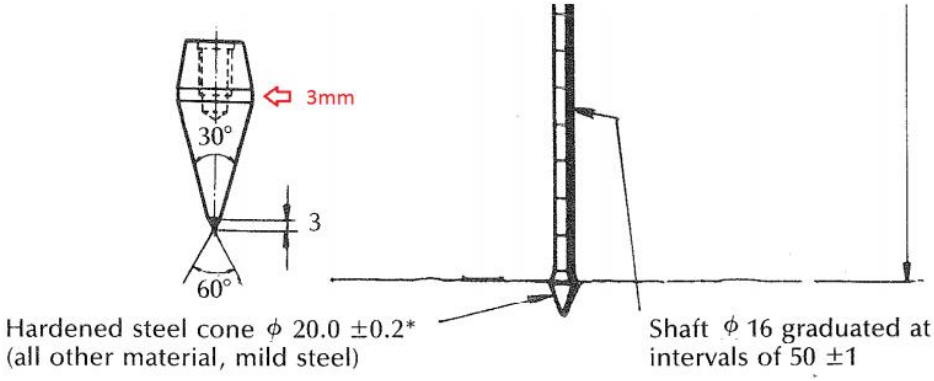

Figure 3.8: DCP conforming to NZS4402, sourced from [142].

Table 3.2: Locations of field-testing

Cambridge (horse paddock)
Muangatautari (native forest)
Kinleith (pine forest)
Waikato river (sand)
Waikato river bank (grass)
University of Waikato field (grass)

The experiment was repeated in a controlled experiment that used a PVC drain pipe with an internal diameter of 105 mm, clamped and levelled as seen in Figure 3.9A. The granular medium (sand) was filled from the top, then the DCP was used three times in the strike points indicated in Figure 3.9B, then the outside of the tube was hit with a mallet. This compacted the sand, during this process more sand was added. After the final addition of sand, a compaction pressure of 2 kPa was applied five times. The measurements were recorded the same way as stated in field tests.

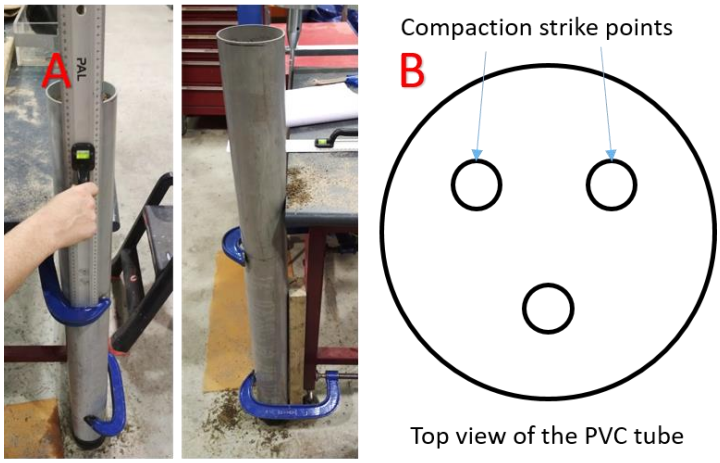

Figure 3.9: Laboratory DCP experimental setup.

Each test was performed with two different types of sand at three different moisture contents with 2 to 3 repetitions (Table 3.3).

Table 3.3: Variety of test mediums to be investigated.

Moisture content (wt.%)	
Coarse	Fine
0	0
5	5
10	10

The coarse sand had a bulk density of 1485 kg/m^3 and the fine sand, 1429 kg/m^3. The sand is characterised by ASTM D2487-11 as both being 'medium' sand. However, they will be referred to as fine and coarse. The fine sand had more than 50 % of its grains pass through a 0.71 mm sieve and the coarse sand had 50 % of its grains pass through a 1.18 mm sieve.

II. Drop tests

The DCP is designed for testing the penetration resistance of the top metre of soil, this method was scaled to investigate the top 100 mm. The scaled DCP will have the same nose and shaft dimension, 3D printed with a Flashforge® Creator Pro, out of PLA at 40 % fill density. The experimental set up used a linear guide rail and ball bearings to drop a 3D printed scaled penetrometer into a perspex box (Figure 3.10). The mass of the PLA DCP with linear guide rail was a 10th of the mass, a 10th of the anvil mass was dropped a 10th of the height as in specified in NZ4402. The sand was compacted with a distributed load that results in approximately 2.2 kPa, applied five times. The mini-penetrometer was slowly lowered onto the top of the sand, an initial measurement was taken, and subsequent measurements were taken after the 0.9 kg mass was dropped from 51 mm, until 100 mm was reached.

Figure 3.10: Experimental set up of scaled penetrometer drop tests, top view (A), post test (B), drop demonstration (C).

This test was performed with three different geometries, the mini-penetrometer, parabolic and hemispherical (Figure 3.11).

Figure 3.11: 3D printed parts for drop tests, hemispherical, parabolic and mini-penetrometer, left to right.

III. High velocity testing

High velocity penetration testing was performed using a Tippmann 98 pneumatic paintball gun with compressed CO_2 at 6.9 MPa, with an approximate muzzle velocity of 90 m/s [121; 143] (Figure 3.12).

Figure 3.12: Tippmann 98 Custom paintball gun.

The projectiles were 3D printed PLA, 0.68” calibre (17.3 mm Ø). The effect of density was also studied using a solid, 1 mm thick shell and a 3 mm thick shell (Figure 3.14). The corresponding mass of each projectile was 2.0, 1.0 and 2.1 g for solid, 1 mm and 3 mm, respectfully.

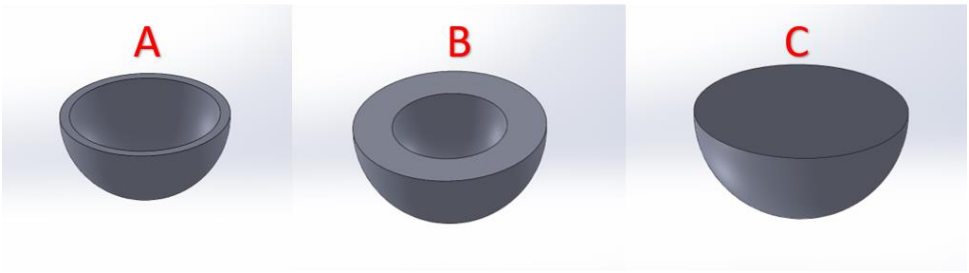

Figure 3.13: Cut view of the 3D printed spheres, 1 mm thick shell (A), 3.5 mm thick shell (B), and solid infill (C).

The effect of different nose shapes was assessed using an ogive (A), spherical (B) and parabolic (C) nose.

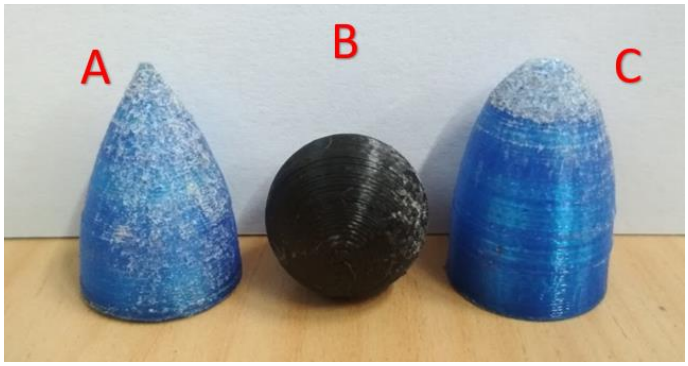

Figure 3.14: High velocity projectiles, ogive nose shape (A), hemispherical nose shape (B), and parabolic nose shape (C).

The paintball gun was fired from at a vertical distance of 0.3 m, downwards and the penetration depth was measured in the same set of sand samples as before, compacted the same way as during the drop tests.

3.3 Results and Discussion

The results are presented in two parts; firstly, a relationship was established between the soil resistance of several locations around the Waikato Region and sand with controlled properties using a dynamic cone penetrometer (1 m depth). These results were compared to a 10^{th} scale penetrometer, using the same sand. Secondly, the accuracy of the two models presented earlier were estimated under the shallow penetration conditions considered in this work.

Soil penetration in New Zealand for civil engineering purposes is determined as the number of impacts it takes to drive the cone to a depth of 1 m, and the results for the soil tested are presented in Figure 3.15 [144]. Considering the shaft has a weight of 13 kg, when placed on the soil it penetrated to a certain depth, displayed in Figure 3.15A as the zero depth. Figure 3.15B compares the penetration of the top soil with the number of impacts to reach a meter. The penetration depth under its own mass for sand was considerably higher than other locations tested, however, it still took the third most number of impacts to reach a depth of one meter.

The general trend observed was that penetration depth logarithmically increased, in other words, the most significant penetration occurred during the first few impacts. The initial penetration (as a result of the shaft only) is displayed in Figure 3.15B where it can be seen that the rugby field had the smallest penetration and the river sand had the highest. Contrary to this, considering the number of impacts required to reach 1 m, the same was not observed (Figure 3.15). Here the native forest was the softest soil recorded, reaching 1 m after only 10 impacts, whereas the river bank soil required 25. In between these the soil samples did not follow the same trend considering initial penetration compared to penetration at 1 m. This would immediately suggest that the soil properties measured using the dynamic penetrometer may be dramatically different depending on the depth at which it is measured and would have serious implications when predictions are required for firing seed capsules into the soil.

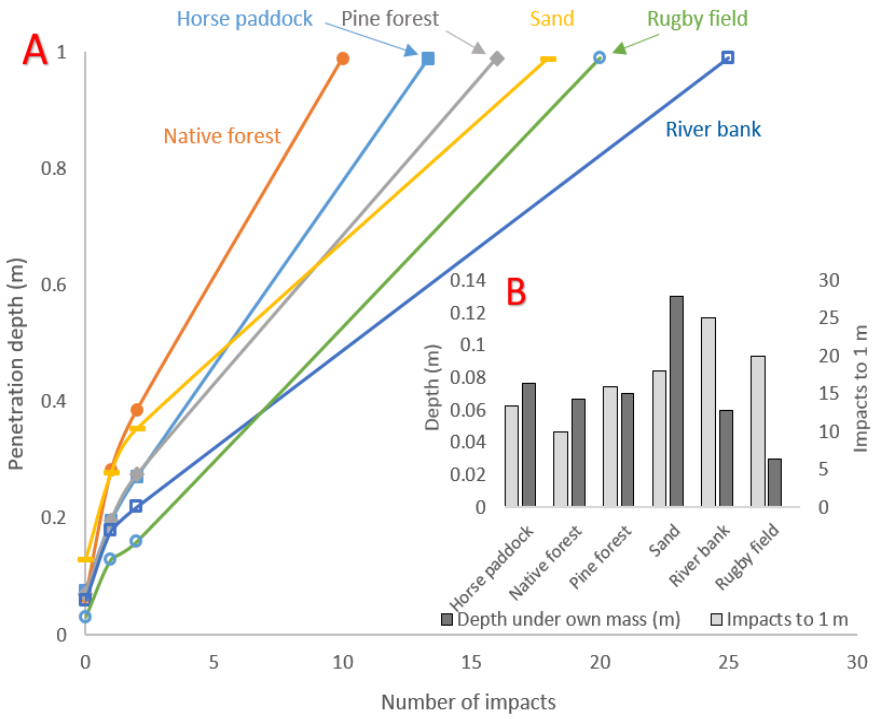

Figure 3.15: Penetration depth of a DCP in different locations around the Waikato region (A), impacts to 1 m penetration compared with initial depth when under own mass (13 kg) (B).

This experiment was repeated in a controlled environment using sand of known particle size and moisture content, as described in the experimental section. Figure 3.16 shows the penetration depth as a function of the number of impacts for the six sand samples tested. The same trend was observed as for the field testing; a logarithmic increase in penetration depth with an increasing number of impacts. The number of impacts to reach one meter during the controlled experiment was approximately the same as for the field tests, with lowest recorded being 12 and highest 29 (the river sand tested earlier required 18 impacts). This would suggest that the controlled experiment's data is realistic and comparable to soil found around the Waikato.

Some interesting observations were made during the controlled experiment. The coarse sand was significantly harder to penetrate than the fine sand, of which 5 wt.% moisture was the easiest. However, Figure 3.16B shows that for the fine sand increasing the moisture content appeared to have a dramatic increase in penetration depth for top soil, with little consequence on the number of impacts to one meter.

On the other hand, the hardest to penetrate was the coarse sand at 0 wt.% moisture. It would appear that 5 wt.% moisture increased the ease of penetration, but

increasing this further either made penetration more difficult or it made little difference (depending on particle size). The coarse sand also experienced a significant increase in penetration depth at the top layer with increasing moisture content. This was potentially because of variability in compaction at each moisture content. The effect of moisture appeared to have had more effect on the penetration for the coarse sand, resulting in a dramatic reduction in the number of impacts. The results highlighted the importance of consideration of soil properties; the same soil on a dry day may behave very differently and should be considered when a product, like the one proposed here, is implemented.

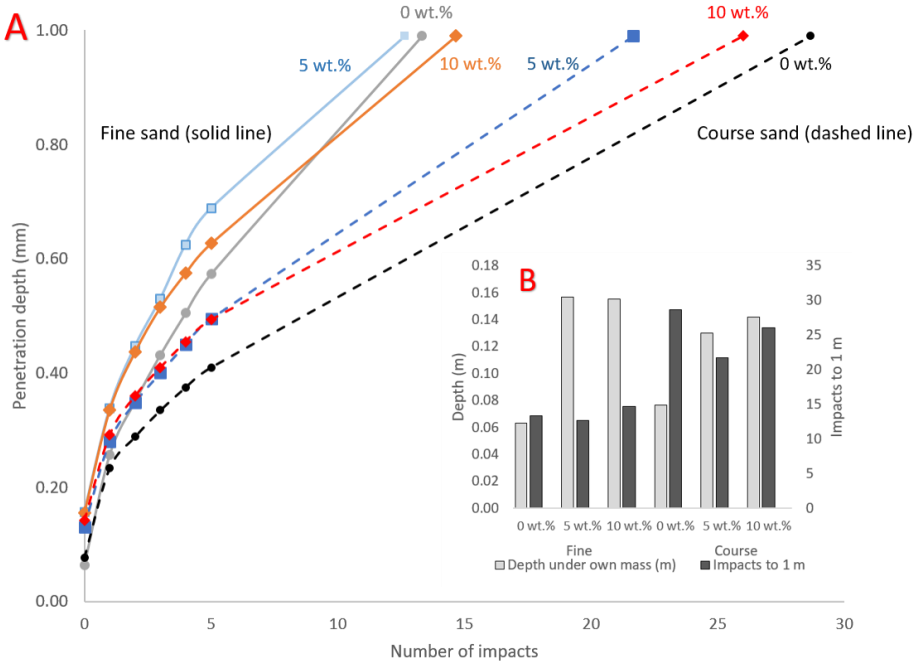

Figure 3.16: Penetration depth of fine and coarse sand using a standard DCP over increasing moisture contents, 0, 5 and 10 wt.% (A) impacts to 1 m penetration compared with initial depth when under own mass (13 kg) (B).

What is more, in the interest of this project, penetrating the top of layer is more important as opposed to a meter deep. However, it is important to understand the correlation between the two if Lorenz or Young's predictions are to be adjusted. Figure 3.17 shows the results of the scaled version of the test, recording the number of impacts to reach 100 mm. The results broadly observed similar trends compared to the field and controlled penetration experiments. A logarithmic increase in penetration was observed. In contrast, most tests reached 70 to 80 % of the penetrometer length with the first impact (with the exception for the 5 wt.% moisture fine sand that took approximately twice the impacts to reach the same

depth). Although most samples took four drops to get 100 mm, the 0 wt.% moisture coarse and fine sand took the least. Comparing this to the controlled experiment (Figure 3.16), 0 wt.% moisture coarse sand took the most impacts.

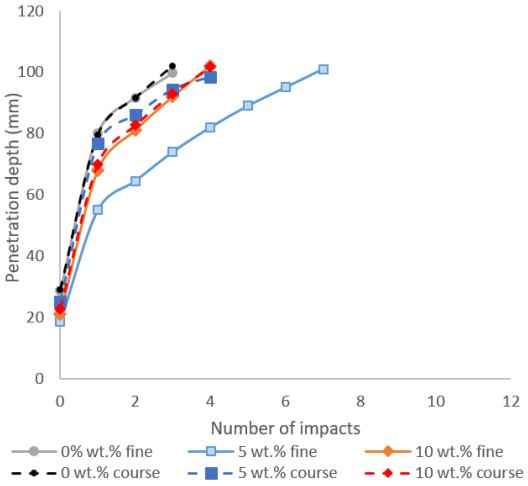

Figure 3.17: Penetration depth of controlled sand for the scaled DCP.

The results for the scaled test appear not to follow a similar trend for the difference in penetration with respect to coarse or fine sand. Ideally, a correlation between the regular DCP and the scaled version could have been made which allows a correction factor to be implemented for the empirical formulae of Lorenz and Young's models. However, it would appear that it would be more appropriate to test soil resistance within the top layer of soil, rather than the recommended full penetration depth, as typically required.

The effect of nose shape was investigated using the scaled impact test. Impact tests were performed with a hemispherical nose (Figure 3.18B) for comparison with the spherical balls during high velocity testing and the parabolic nose shape (Figure 3.18A) was used for comparison for the parabolic bullet. Both presented a similar logarithmic trend, parabolic took approximately double the impacts to reach 100 mm as the scaled penetrometer, the hemisphere nose required more again.

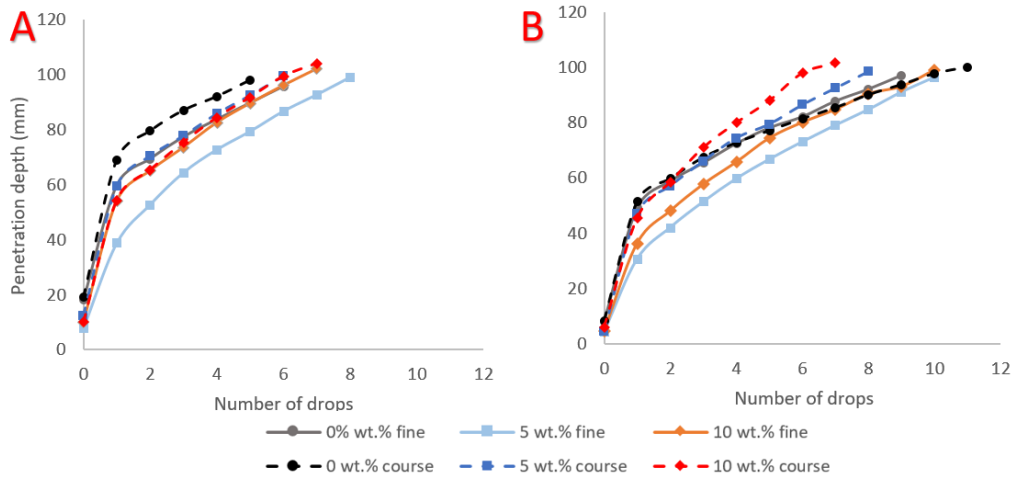

Figure 3.18: Effect of nose shape on penetration for the different mediums, parabolic nose (A) and hemisphere nose (B).

Knowing the soil properties using both the regular and scaled penetrometer, penetrations were assessed under high velocity conditions, using different projectiles to investigate the effect of mass and nose shape (Figure 3.19). Five different cone configurations were used; a solid sphere, two spheres with decreasing wall thickness, parabolic and a pointed nose. Increasing moisture content increased the penetration depth across all the projectiles. It appeared to have been more dramatic for the solid sphere and the parabolic nose. The solid sphere had double the penetration after increasing the moisture content from 0 to 10 %. The penetration depth typically decreased with decreased shell thickness due to a reduction in mass, as expected. Moisture content and sand type appeared to have had less influence with decreasing mass (dotted cluster). The parabolic nose also appeared to be less affected by the change of medium, whereas, the pointed nose was. On average, the parabolic nose penetrated the deepest, which was to be expected.

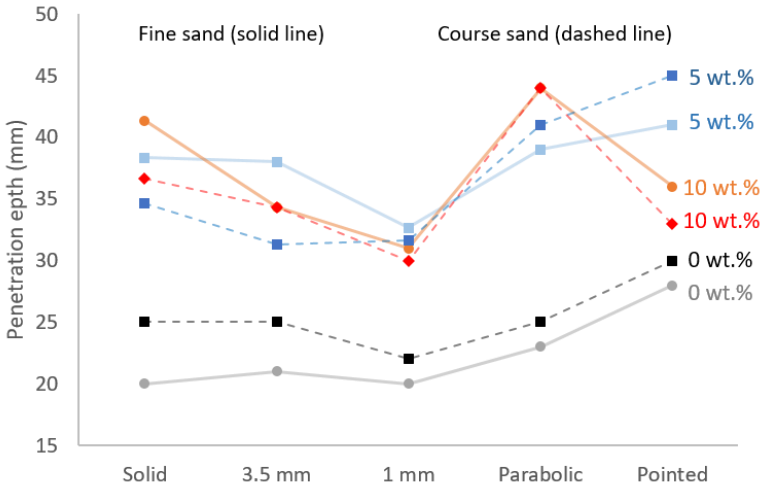

Figure 3.19: High velocity penetration depth of different projectiles, solid, 3.5 mm and 1 mm are spherical with different internal dimension, parabolic and pointed refer to the projected area.

Using Equation 3-3, the penetration resistance was calculated for soil around the Waikato region with the DCP (Figure 3.20). Due to the experimental error, only two data points could be calculated as Equation 3-3, requires the change in depth for the calculation, therefore when this testing was done, only the first few depths were measured and the number of impacts to one meter. It is difficult to see the trends with only two data points, however, as expected the penetration resistance increased with penetration depth for all test locations. It was found that for the UOW rugby field that the penetration resistance increased the most.

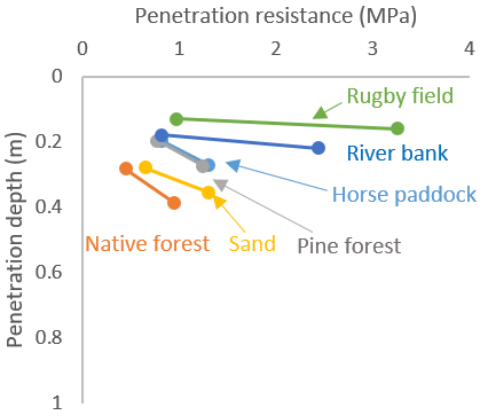

Figure 3.20: Penetration resistance of locations in the Waikato region.

Figure 3.21 is the penetration resistance with increasing depth for the DCP and the scaled model, using controlled sand. The general trend for both is that with increasing depth the penetration resistance increased, as expected. The penetration resistance for the scaled model is approximately a 10^{th} of the standard DCP. For

Figure 3.21A the penetration resistance appears to be grouped by coarse and fine sand whereas, Figure 3.21B showed less dependence on this and more on moisture content with the 0 and 10 wt.% moisture for fine and coarse being very similar.

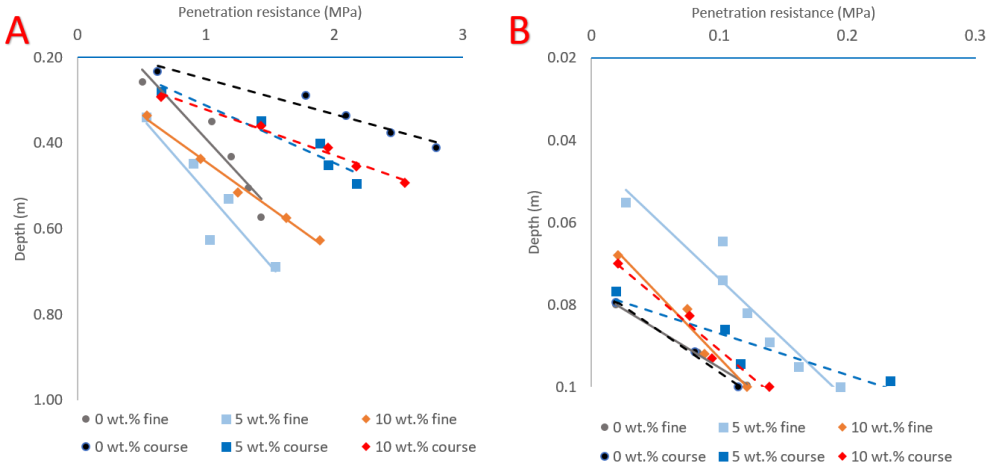

Figure 3.21: Penetration resistance with different mediums of the DCP (A) and scaled model (B).

For the purpose of empirical modelling, the S value (soil resistance) for each medium has been calculated for the solid spheres using Equations 3-9 and 3-14. The mass used was 2 g, a projected area of 238 mm^2 and a nose shape factor of 0.69 for Young's model. Table 3.4 shows the S values for the solid sphere after high velocity penetration into the different mediums. It can be seen that the two models predicted significantly different S values although they were of the same order of magnitude. More importantly, all the values were much higher than 60, which was stated as one of the boundary conditions set by Young, after which the model becomes inaccurate.

Table 3.4: Theoretically calculated S values for Young and Lorenz empirical formula from penetration depth of the solid sphere.

Medium	Penetration depth (mm)	S_{Young}	S_{Lorenz}
0 wt.% fine	20	239	102
5 wt.% fine	38	458	375
10 wt.% fine	41	493	436
0 wt.% coarse	25	299	160
5 wt.% coarse	35	415	308
10 wt.% coarse	37	439	345

Using the theoretical S values, Equation 3-8 can be rearranged to calculate the theoretical number of impacts (N_D). The method used to calculate the S number using Equation 3-8, uses a DCP with a 5 kg weight to reach 0.3 m. During this experiment, a 9 kg weight has been used. However, a linear correction factor of 0.55 $\left(\frac{5}{9}\right)$ was used to adjust the penetration depth for this calculation. Using the corrected penetration depth, the number of impacts to reach 0.3 m was interpolated. Figure 3.22 shows the corrected penetration depth for 0 wt.% moisture, the R^2 value is 0.99, indicating high accuracy of the linear trend line.

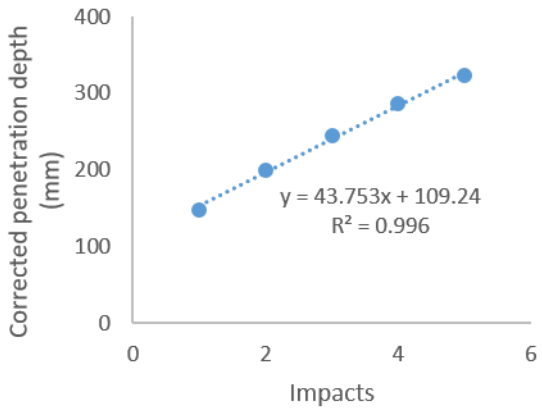

Figure 3.22: Number of drops to reach 0.3 m for 0 wt.% moisture content fine sand.

This was done for all six mediums to compare with the theoretical number of drops (Table 3.5). The percentage error was on average 24.7 % with the lowest being the 5 wt.% fine sand with an error of 1.64 %.

Table 3.5: Lorenz equation using a sphere: Comparison of theoretical N_D by the measured N_D using the correction factor.

Medium	Theoretical N_D	Corrected N_D	Percentage error
0 wt.% fine	5.63	4.36	29.07
5 wt.% fine	4.06	3.99	1.64
10 wt.% fine	3.98	5.66	29.69
0 wt.% coarse	4.82	7.60	36.57
5 wt.% coarse	4.18	5.56	24.90
10 wt.% coarse	4.10	5.58	26.45

Although a correlation between the depth of penetration for the standard DCP and the scaled model, this calculation shows a relatively consistent level or error, excluding the 5 wt.%. The standard deviation of error when excluded was 4.5 %, which is well within an acceptable level of error. This was repeated for both Young and Lorenz for the three different shapes (Sphere, parabolic, pointed) with their respective masses and nose shapes (Table 3.6).

Table 3.6: Variables effecting the theoretical S calculation for Young and Lorenz depth penetration predictions.

Shape	Nose shape factor	Mass (g)
Sphere	0.69 (3-12)	1.97
Parabolic	0.85 (3-12)	2.60
Pointed	1.55 (3-11)	2.30

The theoretical S values calculated for the range of projectiles were all above 60 and varied between 92 and 493. The percentage error was relatively consistent and in the same magnitude with an average of 22.3 %. The average percentage error for Young's model was 21.1 ± 13.0 %, Lorenz was 23.4 ± 11.0 %. The lowest percentage error was for 5 wt.% moisture fine sand with 5.3 ± 5.19 %, the least accurate was 0 wt.% coarse sand with 26.0 ± 5.2 %. The full list of results can be found in Appendix C.

3.4 Product Design Evaluation

The aim of this chapter was to evaluate a method to accurately penetrate the soil to allow for effective germination of seedlings. To evaluate the feasibility of this product, a method for testing the penetration resistance of soil had to be investigated and the ability to use this method to relate to a depth penetration prediction. This was done by investigating the relationship around a dynamic cone penetrometer

with a scaled model that penetrated the topsoil. Evaluating this with the effect of different moisture contents, sand types and nose shapes. This was compared to high velocity testing to determine the accuracy of the prediction. Lorenz and Young both laid the groundwork for solving this problem to be achievable; the boundary conditions were widely outside the scope of the project but was a credible starting point.

Using a DCP to test the soil's resistance to penetration, it was found that the field tests performed at a sandy river bank validated the results of the controlled experiment. The initial testing showed that the coarse sand was considerably harder to penetrate than the fine sand, even though when categorised using ASTM D2487 - 11, they were not different enough in particle diameter to warrant a different grading. It appeared that increasing the moisture content made it considerably easier to penetrate the coarse sand, as expected, but had little effect on the fine sand. When comparing to the scaled model, it was found that the logarithmic results were consistent, however, no relative difference was observed for the coarse and fine sand as in the previous experiment. If the results of the scaled experiment were to be used when modelling the penetration depth, relatively no difference would be expected. The results of the high velocity testing did not agree, the penetration depth increased by 92 % for fine sand and 40 % for coarse sand with the addition of 5 wt.% moisture. The addition of another 5 % only slightly increased penetration depth. For high velocity testing, the moisture content had more effect on the penetration depth for the fine sand opposed to the coarse, in contrast to the results of the standard DCP, where the coarse sand was more influenced by moisture content.

When the effect of nose shape was investigated for the scaled models it proved that by moving away from a tangent nose (pointed) towards conical, the energy required to penetrate the same depth was consequently increased, this was to be expected. The penetration depth for the scaled experiment with the hemisphere and parabolic nose showed very little effect on the change in sand type and moisture. Whereas, as it has been discussed the high velocity spherical samples were heavily affected by moisture content. The addition of 5 wt.% moisture greatly increased the penetration depth of the pointed nose during high velocity but the addition of 10 wt.% decreased the depth, for both coarse and fine sand. This was also observed for the standard DCP in the coarse sand. Interestingly there is potentially more observation in

common with the standard DCP than with the scaled model due to the lack of variation for the scaled model.

When using the empirical formulae proposed by Young and Lorenz, the number of drops of a DCP to reach 0.3 m was an integral part of the prediction. In the interest of this project, the aim was to evaluate if there was any relationship between penetrating a large steel rod, deep into the soil, and a small projectile penetrating the topsoil. This was done by using the results of the penetration depth from the high velocity testing to theoretically calculate what the S value would have been for a model with 100 % accuracy. When comparing to the measured number of drops for both Young and Lorenz, model a surprising accuracy of 22.3 % was found for both models, over the different soil types with the different nose shapes. A considerably positive result for the feasibility of the project, especially considering that Young's equation originally had a 15 % error in accuracy. If the window for successful germination is between 3 and 16 mm, adjusting the impact velocity to aim for a penetration of 9.5 mm gives an acceptable level of error at even up to 50 %. Although this was proven successful for multiple different moisture contents, at a varied particle size with different nose shapes, this was done with extremely homogenous sand. The soil has stratification layers that could easily introduce significant error. The layer above the soil would also be a highly situation dependent, whether it be healthy grass or barren soil. However, if the DCP can successfully predict the penetration of a homogenous medium then it gives confidence that by using a scaled model on more diverse soil mediums, an appropriate correction factor will ensure that the models used will yield the same results with more complex soils, as they have already proved with larger projectiles.

Conclusions

The purpose of this thesis was to develop a proof of concept for automated industrial seed planting which will increase productivity significantly and reduce labour costs. The concept was to use Novatein, a protein-based polymer, in conjunction with drone technology to develop an aerial seed planting device. Three key challenges were identified and evaluated further:

- The biodegradability of the Novatein blended with PBAT was to be tested in real-world conditions.
- Establishment of a realistic method of mass manufacturing and assessing the parameters influencing this process.
- Determining if a seed capsule can be consistently delivered into soil.

The biodegradability of Novatein, PBAT and blends thereof was evaluated by measuring the ability of bacteria and fungi to metabolise the polymers into CO_2 in soil at 25 °C. Pure Novatein had the greatest level of biodegradation and PBAT had very little. Furthermore, the presence of fungi on the Novatein blends and not pure PBAT, was a good indicator that the blends were potentially biodegradable. Although none of the samples tested reached the ASTM standard for biodegradation, it was concluded that PBAT could be used to control the rate at which biodegradation occurs in blends with Novatein. More extensive testing would be confirm the absolute degree of biodegradation of these materials, but was beyond the scope of this project.

To investigate the feasibility of mass manufacturing, compression moulded and lap welded joints of Novatein and Novatein/PBAT blends were tested. Welding and moulding were successful, provided it occurred above the glass transition temperature of the material. The weld quality improved with holding time and the gap between the mould and material had a significant effect on the ability to be moulded. However, long cycle times are not economically feasible, and the dependence on having a mould insert (ball bearing) can be replaced by vacuum forming the sheets during full scale manufacture. Using a more controlled experiment, testing lap welded joints showed that the cycle time could be reduced considerably. Tensile testing was used to establish a processing window for welding, where optimal conditions only had a 12 % reduction in tensile strength compared

to unwelded samples. Increasing sheet thickness and weld force increased the peel force, however, high weld force reduced tensile strength. If capsules were to be produced, increasing the sheet thickness and weld force would result in capsules harder to peel apart, but not necessarily stronger. Although it was difficult to identify which parameters were better for improving weld quality, further testing with a better suited heated press or with a hot plate welding machine would allow the temperature variable to be removed and will give a better understanding of how to optimise the weld quality.

Finally, the accuracy of using a paintball gun to deliver seed capsules into soil was evaluated against the accuracy of predictions using two empirical models. These models used a dynamic cone penetrometer to measure soil resistance against penetration to predict penetration depth of a known projectile. These models were developed for considerably heavier projectiles (> 2.2 kg) and penetration depths much greater than considered here. It was found that homogenous course and fine sand displayed similar relationships relating penetration depth to soil resistance; i.e. as penetration depth increased, soil resistance increased. To account for the shallow penetration required in this study, a 10^{th} scale DCP was used to evaluate the same sand samples. The scaled DCP did not show any dependence on the sand type or moisture content, whereas, the standard DCP showed clear a difference between coarse and fine sand. Although a similar dependence of soil resistance with penetration depth was observed. Although a clear relationship was not established between the standard DCP and the scaled model, at high impact velocity the standard DCP predicted the depth to sufficient accuracy of 22%.

It was concluded that PBAT may not be the best choice for blending with Novatein, considering its slow rate of biodegradation in soil. If PBAT is to be used, more testing would be required to confirm literature and manufacturers claims of its biodegradability. It was proven that a Novatein and PBAT blend can be successfully welded and formed, which validates the chosen method of manufacturing. Further testing using vacuum forming would be required. Using a paintball gun as the mechanism for thrust for the capsule to penetrate soil was proven to be sufficiently accurate when using homogenous sand, however, one has to recognise that non-homogenous soil types have significantly different properties and the mechanism will need further validation.

Further work is required for developing this concept but the results would indicate that it should be achievable. The most important aspects not considered here are testing capsule delivery in forestry soil and designing an integrated product, i.e. combining the seed capsule, thrust mechanism with a suitable drone.

References

[1] Lawrence, D., & Vandecar, K. (2014). Effects of tropical deforestation on climate and agriculture. *Nature Climate Change, 5*, 27.

[2] Association, F. O. (2016). Facts & Figures: New Zealand Plantation Forest Industry.

[3] Hodges, A. N., & Kennedy, M. D. (2011). Physical exertion and working efficiency of reforestation workers. *Journal of Occupational Medicine and Toxicology, 6*(1), 20.

[4] Hargreaves, C., Grace, L., van der Maas, S., Reeves, C., Holden, G., Menzies, M., Kumar, S., & Foggo, M. (2011). *Cryopreservation of Pinus radiata zygotic embryo cotyledons: Effect of storage duration on adventitious shoot formation and plant growth after 2 years in the field*. (Vol. 34).

[5] Burdon, R. D., Carson, M. J., & Shelbourne, C. J. A. (2008). Achievements in forest tree genetic improvement in Australia and New Zealand 10: Pinus radiata in New Zealand. *Australian Forestry, 71*(4), 263-279.

[6] Carson, M. (1986). Advantages of clonal forestry for Pinus radiata—real or imagined. *NZ J For Sci, 16*(3), 403-415.

[7] Mead, D. J. (2013). *Sustainable Management of Pinus Radiata Plantations*. Food and Agriculture Organization of the United Nations.

[8] Neumann, W. P., Kihlberg, S., Medbo, P., Mathiassen, S. E., & Winkel, J. (2002). A case study evaluating the ergonomic and productivity impacts of partial automation strategies in the electronics industry. *International Journal of Production Research, 40*(16), 4059-4075.

[9] Verma, S. (2008). Impact of agricultural mechanization on production, productivity, cropping intensity income generation and employment of labour. *Punjab Agricultural University, Ludhiana*, 133-153.

[10] Axelsson, S.-Ă. (1998). The mechanization of logging operations in Sweden and its effect on occupational safety and health. *Journal of Forest Engineering, 9*(2), 25-31.

[11] Ortiz Morales, D., Westerberg, S., La Hera, P. X., Mettin, U., Freidovich, L., & Shiriaev, A. S. (2014). Increasing the level of automation in the forestry logging process with crane trajectory planning and control. *Journal of Field Robotics, 31*(3), 343-363.

[12] Plant Tape. (2016). *Automated transplating system*. 2018, from http://www.planttape.com/the-process/.

[13] Plant Tape. (2015). *Plant Tape in the U.S*. Retrieved 2019, 2017, from https://www.youtube.com/watch?v=HohXkOvVFuU.

[14] BioCarbon Engineering. (2018). *Technologies*. 2018, from https://www.biocarbonengineering.com/technologies.

[15] Fletcher, L. E. Techniques for automated planting.

[16] BioCarbon Engineering (Compiler) (2018). *How BioCarbon Engineering's Drones Could Restore Earth's Forests*. Drone Below. Accessed 2018 from https://dronebelow.com/2018/05/24/drones-could-restore-forests-destroyed-by-fires/.

[17] DroneSeed. (2017). *How Drones are Helping to Plant Trees - A Cleaner Future*. Retrieved March, 2019, from https://www.youtube.com/watch?v=EkNdrTZ7CG4.

[18] PlasticsEurope (Compiler) (2017). *Plastics – the Facts 2017* Accessed 2018 from https://www.plasticseurope.org/application/files/5715/1717/4180/Plastics_the_facts_2017_FINAL_for_website_one_page.pdf.

[19] Brown, R. P. (2004). *Polymers in agriculture and horticulture*. Rapra Technology Limited.

[20] European Bioplastics. (2018). *Bioplastic material*. from https://www.european-bioplastics.org/bioplastics/materials/.

[21] Menzies, M., Van Dorsser, J., & Balneaves, J. M. (1985). Seedling quality–radiata pine as a case study. In *Proceedings of the international symposium on nursery manage. Practices for the Southern Pines, IUFRO Sub. Grp. S* (Vol. 3, pp. 202-03).

[22] Calvo, L., García-Domínguez, C., Naranjo, A., & Arévalo, J. R. (2013). Effects of light/darkness, thermal shocks and inhibitory components on germination of Pinus canariensis, Pinus halepensis and Pinus pinea. *European Journal of Forest Research, 132*(5), 909-917.

[23] Hazelton, P., & Murphy, B. (2016). *Interpreting soil test results: What do all the numbers mean?* CSIRO publishing.

[24] Vanags, C., Minasny, B., & McBratney, A. B. (2004). The dynamic penetrometer for assessment of soil mechanical resistance. In *Supersoil*

2004: Proceeding of the 3th Australian New Zealand Conference. University of Sydney, Australia.

[25] W. Young, C. (1970). *Penetration Equations*.

[26] Verbeek, C. J. R., Hicks, T., & Langdon, A. (2012). Biodegradation of Bloodmeal-Based Thermoplastics in Green-Waste Composting. *Journal of Polymers and the Environment, 20*(1), 53-62.

[27] Verbeek, C. J. R. S., J. M. Cozens. C. W. (2019). Rheology and Sheet Extrusion of Novatein Thermoplastic Protein/PBAT Blends. *Journal of Applied Polymer Science*.

[28] European Bioplastics e.V. (2016). *European Bioplastics Market (Online)*. 2017, from http://www.european-bioplastics.org/market/.

[29] Low-Tech Magazine (Compiler) (2017). *The monster footprint of digital technology*http://www.lowtechmagazine.com/2009/06/embodied-energy-of-digital-technology.html.

[30] EPA (Compiler). *Municipal Solid Waste Generation, Recycling, and Disposal in the United States*.

[31] Avérous, L., & Fringant, C. (2001). Association between plasticized starch and polyesters: Processing and performances of injected biodegradable systems. *Polymer Engineering & Science, 41*(5), 727-734.

[32] Sirisinha, K., & Somboon, W. (2012). Melt characteristics, mechanical, and thermal properties of blown film from modified blends of poly(butylene adipate-co-terephthalate) and poly(lactide). *Journal of Applied Polymer Science, 124*(6), 4986-4992.

[33] Ferreira, F. V., Cividanes, L. S., Gouveia, R. F., & Lona, L. M. F. (2019). An overview on properties and applications of poly(butylene adipate-co-terephthalate)–PBAT based composites. *Polymer Engineering & Science, 59*(s2), E7-E15.

[34] Lu, J., Tappel, R. C., & Nomura, C. T. (2009). Mini-Review: Biosynthesis of Poly(hydroxyalkanoates). *Polymer Reviews, 49*(3), 226-248.

[35] Zhu, Y., Romain, C., & K. Williams, C. (2016). *Sustainable polymers from renewable resources*. (Vol. 540).

[36] Iwata, T. (2015). Biodegradable and Bio-Based Polymers: Future Prospects of Eco-Friendly Plastics. *Angewandte Chemie International Edition, 54*(11), 3210-3215.

[37] Vert, M., Doi, Y., Hellwich, K.-H., Hess, M., Hodge, P., Kubisa, P., Rinaudo, M., & Schué, F. (2012). Terminology for biorelated polymers and applications (IUPAC Recommendations 2012). *Pure & Applied Chemistry, 84*(2), 377-410.

[38] Verbeek, C. J. R., & Uitto, J. M. (2002). Bioplastics. In *Encyclopedia of Polymer Science and Technology*. John Wiley & Sons, Inc.

[39] Thunwall, M., Kuthanová, V., Boldizar, A., & Rigdahl, M. (2008). Film blowing of thermoplastic starch. *Carbohydrate Polymers, 71*(4), 583-590.

[40] Coltelli, M.-B., Wild, F., Bugnicourt, E., Cinelli, P., Lindner, M., Schmid, M., Weckel, V., Müller, K., Rodriguez, P., Staebler, A., Rodríguez-Turienzo, L., & Lazzeri, A. (2016). State of the Art in the Development and Properties of Protein-Based Films and Coatings and Their Applicability to Cellulose Based Products: An Extensive Review. *Coatings, 6*(1), 1.

[41] University, C. S. *Organic Fertilizers.*

[42] Bier, J. M., Verbeek, C. J. R., & Lay, M. C. (2014). Thermal and Mechanical Properties of Bloodmeal-Based Thermoplastics Plasticized with Tri(ethylene glycol). *Macromolecular Materials and Engineering, 299*(1), 85-95.

[43] Marsilla, K. I. K. (2015). *Development of Bloodmeal Protein Thermoplastic Blends.* Doctoral thesis, University of Waikato, Hamilton, New Zealand.

[44] Gavin, C., Lay, M. C., Verbeek, C. J., & Walallavita, A. (2017). Protein Plastic Foams. *Advances in Physicochemical Properties of Biopolymers (Part 2)*, 371.

[45] Bonhomme, S., Cuer, A., Delort, A. M., Lemaire, J., Sancelme, M., & Scott, G. (2003). Environmental biodegradation of polyethylene. *Polymer Degradation and Stability, 81*(3), 441-452.

[46] Shah, A. A., Hasan, F., Hameed, A., & Ahmed, S. (2008). Biological degradation of plastics: A comprehensive review. *Biotechnology Advances, 26*(3), 246-265.

[47] Ray, S., & Cooney, R. P. (2012). 7 - Thermal Degradation of Polymer and Polymer Composites A2 - Kutz, Myer. In *Handbook of Environmental Degradation of Materials (Second Edition)* (pp. 213-242). Oxford: William Andrew Publishing.

[48] Kiran, N., Ekinci, E., & Snape, C. E. (2000). Recyling of plastic wastes via pyrolysis. *Resources, Conservation and Recycling, 29*(4), 273-283.

[49] Rabek, J. F. (2012). *Photodegradation of polymers: physical characteristics and applications*. Springer Science & Business Media.

[50] Song, Y. K., Hong, S. H., Jang, M., Han, G. M., Jung, S. W., & Shim, W. J. (2017). Combined effects of UV exposure duration and mechanical abrasion on microplastic fragmentation by polymer type. *Environmental science & technology, 51*(8), 4368-4376.

[51] Viljoen, C. (2011). *Development of a Bioderived Unsaturated Polyester Resin for Use in the Composites Industry*. thesis, University of Waikato, Waikato, New Zealand.

[52] Gu, J.-G., & Gu, J.-D. (2005). Methods Currently Used in Testing Microbiological Degradation and Deterioration of a Wide Range of Polymeric Materials with Various Degree of Degradability: A Review. *Journal of Polymers and the Environment, 13*(1), 65-74.

[53] Kijchavengkul, T., & Auras, R. (2008). Compostability of polymers. *Polymer International, 57*(6), 793-804.

[54] Aminabhavi, T. M., Balundgi, R. H., & Cassidy, P. E. (1990). A Review on Biodegradable Plastics. *Polymer-Plastics Technology and Engineering, 29*(3), 235-262.

[55] Griffin, G. (1973). Biodegradable fillers in thermoplastics. *Am. Chem. Soc. Div. Org. Coatings. Plast. Chem., 33*(2), 88-96.

[56] Lopezllorca, L., Colom Valiente, M., & Gascon, A. (1993). *A study of biodegradation of poly-β-hydroxyalkanoate (PHA) films in soil using scanning electron microscopy*. (Vol. 24).

[57] Weng, Y.-X., Wang, L., Zhang, M., Wang, X.-L., & Wang, Y.-Z. (2013). Biodegradation behavior of P(3HB,4HB)/PLA blends in real soil environments. *Polymer Testing, 32*(1), 60-70.

[58] Weng, Y.-X., Jin, Y.-J., Meng, Q.-Y., Wang, L., Zhang, M., & Wang, Y.-Z. (2013). Biodegradation behavior of poly(butylene adipate-co-terephthalate) (PBAT), poly(lactic acid) (PLA), and their blend under soil conditions. *Polymer Testing, 32*(5), 918-926.

[59] Luo, S., & Netravali, A. N. (2003). A study of physical and mechanical properties of poly(hydroxybutyrate-co-hydroxyvalerate) during composting. *Polymer Degradation and Stability, 80*(1), 59-66.

[60] Sabo, R., Jin, L., Stark, N., & Ibach, R. E. (2013). Effect of environmental conditions on the mechanical properties and fungal degradation of

polycaprolactone/microcrystalline cellulose/wood flour composites. *BioResources, 8*(3), 3322-3335.

[61] Hicks, T. (2010). *Environmental Aspects of Proteinous Bioplastic*. thesis, University of Waikato.

[62] Huang, J., Cui, C., Yan, G., & Zhang, M. (2016). *A Study on Degradation of Composite Material PBS/PCL*. (Vol. 24).

[63] ASTM *Standard Test Method for Determining Aerobic Biodegradation of Plastic Materials in Soil.*

[64] Bellis, M. (2011). The History of Plastics. *About. com Inventors*.

[65] OECD Guidelines for the Testing of Chemicals *Test No. 301: Ready Biodegradability*.

[66] Münstedt, H., Kurzbeck, S., & Stange, J. (2006). Importance of elongational properties of polymer melts for film blowing and thermoforming. *Polymer Engineering & Science, 46*(9), 1190-1195.

[67] Feuilloley, P., César, G., Benguigui, L., Grohens, Y., Pillin, I., Bewa, H., Lefaux, S., & Jamal, M. (2005). *Degradation of Polyethylene Designed for Agricultural Purposes*. (Vol. 13).

[68] Gerulová, K., Tatarka, O., Štefko, T., & Škulavík, T. (2015). The Study Of Metalworking Fluids Biodegradability By Indirect Measurement Of Bacterial Inoculum Respiration. *23*(36), 65.

[69] Briassoulis, D., & Dejean, C. (2010). Critical Review of Norms and Standards for Biodegradable Agricultural Plastics Part I. Biodegradation in Soil. *Journal of Polymers and the Environment, 18*(3), 384-400.

[70] Biodegradability, R. (1992). OECD Guideline for testing of chemicals. *Organisation for Economic Co-operation and Development, Paris*.

[71] ASTM *Standard Test Method for determining the Aerobic biodegradation of Plastic Materials in the Presence of Municipal Sewage Sludge1*.

[72] Sanctuary Mountain. (2018). *About Us*. Retrieved 2018, from https://www.sanctuarymountain.co.nz/about-us.

[73] Landcare Research. (2019). *New Zealand Soil Classification*. 2019, from https://soils-maps.landcareresearch.co.nz/.

[74] Crawford, R. J. (1998). *Plastics engineering*. Elsevier.

[75] Wikipeida. (2016). *Principe extrusion soufflage polymere*. 2019, from https://commons.wikimedia.org/wiki/File:Principe_extrusion_soufflage_polymere.svg.

[76] GWP Plastics. (2018). *Extruders of Plastic Profile and Plastic Tubing*. 2019, from https://www.plastixportal.co.za/css_pages/gwp_plastics.html.

[77] Wikipeida. (2016). *Injection molding diagram*. 2019, from https://commons.wikimedia.org/wiki/File:Injection_molding_diagram.svg.

[78] Verbeek, C. J. R., & van den Berg, L. E. (2010). Extrusion Processing and Properties of Protein-Based Thermoplastics. *Macromolecular Materials and Engineering*, *295*(1), 10-21.

[79] Martinez, R. (21-03-2001). Method for manufacturing a projectile containing chemiluminescent compounds.

[80] Sun, T. L., Kurokawa, T., Kuroda, S., Ihsan, A. B., Akasaki, T., Sato, K., Haque, M. A., Nakajima, T., & Gong, J. P. (2013). Physical hydrogels composed of polyampholytes demonstrate high toughness and viscoelasticity. *Nature Materials*, *12*, 932.

[81] Yousefpour, A., Hojjati, M., & Immarigeon, J.-P. (2004). Fusion Bonding/Welding of Thermoplastic Composites. *Journal of Thermoplastic Composite Materials*, *17*(4), 303-341.

[82] Barmouz, M., Shahi, P., & Asadi, P. (2014). 14 - Friction stir welding/processing of polymeric materials. In M. K. B. Givi & P. Asadi (Eds.), *Advances in Friction-Stir Welding and Processing* (pp. 601-670). Woodhead Publishing.

[83] Wikipeida. (2018). *Hot plate welding pressure history.svg*. Retrieved 19/3/19, 2019, from https://commons.wikimedia.org/wiki/File:Hot_plate_welding_pressure_history.svg.

[84] Liu, S.-J., & Cheng, H.-F. (2010). The Influence of Interface Geometry on the Joint Strengths of Hot Plate Welded Composites. *Journal of Reinforced Plastics and Composites*, *29*(4), 497-509.

[85] Nonhof, C. J. (1996). Optimization of hot plate welding for series and mass production. *Polymer Engineering & Science*, *36*(9), 1184-1195.

[86] Ülker, A., Öztoprak, N., Sayer, S., & Yeni, C. (2018). Optimization of welding parameters of hot plate welded PC/ABS blends by using the Taguchi experimental design method. *Journal of Elastomers & Plastics*, *50*(2), 162-181.

[87] BASF (Compiler) (2016). *Laser Welding of Engineering Plastics*. Accessed 2018 from

http://www8.basf.us//PLASTICSWEB/displayanyfile?id=0901a5e18045b8d9.

[88] Knapp, W., Clement, S., Franz, C., Oumarou, M., & Renard, J. (2010). Laser-bonding of long fiber thermoplastic composites for structural assemblies. *Physics Procedia, 5*, 163-171.

[89] Wikipeida. (2018). *Transmission welding diagram.png*. 2019, from https://commons.wikimedia.org/wiki/File:Transmission_welding_diagram.png.

[90] Chapter 10 - Resistive Implant Welding. (2009). In M. J. Troughton (Ed.), *Handbook of Plastics Joining (Second Edition)* (pp. 105-111). Boston: William Andrew Publishing.

[91] Stavrov, D., & Bersee, H. E. N. (2005). Resistance welding of thermoplastic composites-an overview. *Composites Part A: Applied Science and Manufacturing, 36*(1), 39-54.

[92] Zafar, A., Awang, M., & Khan, S. (2017). Friction Stir Welding of Polymers: An Overview. In (pp. 19-36).

[93] Kalas, V., & Roos, L.-J. (2016). *Welding of thermoplastic composites*.

[94] Gatwick Technologies. (2019). *FRICTION WELDING*. from http://www.gatwicktechnologies.com/processes/friction-welding.

[95] Weman, K. (2012). 11 - Pressure welding methods. In K. Weman (Ed.), *Welding Processes Handbook (Second Edition)* (pp. 119-132). Woodhead Publishing.

[96] Miller Weldmaster. (2018). *Weld Types*. 2019, from https://www.weldmaster.com/technology/weld-types/#.

[97] Hattori, K., Tomita, N., Tamai, S., & Ikada, Y. (2000). Bioabsorbable thread for tight tying of bones. *Journal of Orthopaedic Science, 5*(1), 57-63.

[98] Troughton, M. J. (2009). Chapter 16 - Solvent Welding. In M. J. Troughton (Ed.), *Handbook of Plastics Joining (Second Edition)* (pp. 139-143). Boston: William Andrew Publishing.

[99] Haverhals, L. M., Sulpizio, H. M., Fayos, Z. A., Trulove, M. A., Reichert, W. M., Foley, M. P., De Long, H. C., & Trulove, P. C. (2012). Process variables that control natural fiber welding: time, temperature, and amount of ionic liquid. *Cellulose, 19*(1), 13-22.

[100] Russell, R. A., Fox, E. T., Nolan, R., Chandler, M., Head, A. C., Brusoski, M., De Long, H. C., & Trulove, P. C. (2016). Natural Fiber Welding of

Chitin and Chitosan on a Cotton Cloth Substrate: Novel Materials Displaying Antimicrobial Properties. *ECS Transactions, 75*(15), 693-700.

[101] Verbeek, C. J. R., Lay, M. C., & Bier, J. M. (2013). Plasticization of Bloodmeal-based Thermoplastics. In *CHEMECA 2013: Challenging Tomorrow*: CHEMECA 2013.

[102] Verbeek, C. J. R., & van den Berg, L. E. (2011). Mechanical Properties and Water Absorption of Thermoplastic Bloodmeal. *Macromolecular Materials and Engineering, 296*(6), 524-534.

[103] Arruda, L. C., Magaton, M., Bretas, R. E. S., & Ueki, M. M. (2015). Influence of chain extender on mechanical, thermal and morphological properties of blown films of PLA/PBAT blends. *Polymer Testing, 43*, 27-37.

[104] Tavares, L. B., Ito, N. M., Salvadori, M. C., dos Santos, D. J., & Rosa, D. S. (2018). PBAT/kraft lignin blend in flexible laminated food packaging: Peeling resistance and thermal degradability. *Polymer Testing, 67*, 169-176.

[105] Grouve, W. J. B., Warnet, L. L., & Akkerman, R. (2013). Critical assessment of the mandrel peel test for fiber reinforced thermoplastic laminates. *Engineering Fracture Mechanics, 101*, 96-108.

[106] Zhao, T., Palardy, G., Villegas, I., Rans, C., Martinez, M., & Benedictus, R. (2016). *Mechanical Behaviour of Thermoplastic Composites Spot-Welded and Mechanically Fastened Joints: A Preliminary Comparison*.

[107] Ebnesajjad, S., & Landrock, A. H. (2015). Chapter 12 - Testing of Adhesive Bonds. In S. Ebnesajjad & A. H. Landrock (Eds.), *Adhesives Technology Handbook (Third Edition)* (pp. 339-352). Boston: William Andrew Publishing.

[108] McKeen, L. W. (2016). 13 - Measurement of Coating Properties and Performance. In L. W. McKeen (Ed.), *Fluorinated Coatings and Finishes Handbook (Second Edition)* (pp. 227-259). Oxford: William Andrew Publishing.

[109] Morris, B. A. (2017). 10 - Adhesion. In B. A. Morris (Ed.), *The Science and Technology of Flexible Packaging* (pp. 351-400). Oxford: William Andrew Publishing.

[110] ASTM *Standard Test Method for tensile Properties of Plastics.*

[111] Donald R. Franceschetti, P. (2016). *Principles of Physics*. Ipswich, UNITED STATES: Salem Press.

[112] Kaminski, D. A., & Jensen, M. K. (2004). *Introduction to Thermal and Fluids Engineering*. Wiley.

[113] Wikipeida. (2016). *File:14ilf1l.svg*. 2018, from https://commons.wikimedia.org/wiki/File:14ilf1l.svg.

[114] Wikipeida. (2017). *File:Steady flight.png*. 2018, from https://commons.wikimedia.org/wiki/File:Steady_flight.png.

[115] Gamo Precision Airguns. (2006). *Handbook - Break Barrel Rifle*. South America: Industrias El Gamo.

[116] Airgun Academy. (2008). *How a spring-piston airgun works*. Retrieved March, 2019, from https://www.pyramydair.com/blog/2008/12/how-a-spring-piston-airgun-works/.

[117] Tavella, D. (2015). *Internal Ballistics of Spring Piston Airguns*. Retrieved March, 2019, from https://www.researchgate.net/publication/274638905_Internal_Ballistics_of_Spring_Piston_Airguns.

[118] Werner, R., Schultz, B., Bockholdt, B., Ekkernkamp, A., & Frank, M. (2017). Energy-dependent expansion of .177 caliber hollow-point air gun projectiles. *International Journal of Legal Medicine, 131*(3), 685-690.

[119] Terminal Ballistics Research (Compiler) (2007). *.243 Winchester*. Accessed March 2019 from https://www.ballisticstudies.com/Knowledgebase/.243+Winchester.html.

[120] Deak, B. A. W. O. D., Chagrin Falls, OH, US). (2007). Paintball gun.

[121] Chiarawongse, P., & Chirathivat, A. (2008). Paintball velocity as a function of distance traveled. *International School Bangkok Journal of Physics, 2*(2), 2-2.

[122] Lyon, D. H. (1999). *Ballistic Evaluation of the Under-Barrel Tactical Paint Ball System.* Army Research Lab Aberdeen Proving Ground, Aberdeen, MD.

[123] Ogunjimi, L. A. O., Aviara, N. A., & Aregbesola, O. A. (2002). Some engineering properties of locust bean seed. *Journal of Food Engineering, 55*(2), 95-99.

[124] Voicu, G., Tudosie, E. M., Ungureanu, N., & Constantin, G. (2013). *Some mechanical characteristics of wheat seeds Obtained By Uniaxial Compression Tests*. (Vol. 75).

[125] Szczyglak, P., & Żuk, Z. (2012). Method of Determining the Minimum Breaking Strength of the Mustard Seed Coat. *Technical Sciences/University of Warmia and Mazury in Olsztyn*, 243-249.

[126] Buttinoni, I., Cha, J., Lin, W.-H., Job, S., Daraio, C., & Isa, L. (2017). Direct observation of impact propagation and absorption in dense colloidal monolayers. *Proceedings of the National Academy of Sciences, 114*(46), 12150-12155.

[127] Børvik, T., Langseth, M., Hopperstad, O. S., & Malo, K. A. (2002). Perforation of 12mm thick steel plates by 20mm diameter projectiles with flat, hemispherical and conical noses: Part I: Experimental study. *International Journal of Impact Engineering, 27*(1), 19-35.

[128] Mitrevski, T., Marshall, I. H., Thomson, R., Jones, R., & Whittingham, B. (2005). The effect of impactor shape on the impact response of composite laminates. *Composite Structures, 67*(2), 139-148.

[129] Wingrove, A. L. (1973). The influence of projectile geometry on adiabatic shear and target failure. *Metallurgical Transactions, 4*(8), 1829-1833.

[130] Wilkins, M. L. (1978). Mechanics of penetration and perforation. *International Journal of Engineering Science, 16*(11), 793-807.

[131] Omidvar, M., Iskander, M., & Bless, S. (2014). Response of granular media to rapid penetration. *International Journal of Impact Engineering, 66*, 60-82.

[132] Raie, M. S., & Tassoulas, J. L. (2009). Installation of Torpedo Anchors: Numerical Modeling. *Journal of Geotechnical and Geoenvironmental Engineering, 135*(12), 1805-1813.

[133] Freeman, T. J., Murray, C. N., Francis, T. J. G., McPhail, S. D., & Schultheiss, P. J. (1984). Modelling radioactive waste disposal by penetrator experiments in the abyssal Atlantic Ocean. *Nature, 310*(5973), 130-133.

[134] Zacny, K., Bualat, M., Lee, P., Alvarez, L., Fong, T., Deans, M., VanGundy, L., & Lees, D. (2012). Using percussive, dynamic, and static soil penetrometers to assess geotechnical properties and the depth to ground ice of the mars and lunar analog terrains on the Devon Island, Canadian Arctic. In *Earth and Space 2012: Engineering, Science, Construction, and Operations in Challenging Environments* (pp. 284-294).

[135] Lorenz, R. D., Moersch, J. E., Stone, J. A., Ron Morgan, A., & Smrekar, S. E. (2000). Penetration tests on the DS-2 Mars microprobes: penetration

depth and impact accelerometry. *Planetary and Space Science, 48*(5), 419-436.

[136] B Berrill, P. M., ETC Ooi, J-L Pautre. (1994). Liquefaction at Kaiapoi in the 1901 Cheviot, New Zealand, earthquake.

[137] Kumar, A., Chen, Y., Sadek, M. A.-A., & Rahman, S. (2012). Soil cone index in relation to soil texture, moisture content, and bulk density for no-tillage and conventional tillage. *Agricultural Engineering International: CIGR Journal, 14*(1), 26-37.

[138] Campbell, D., Stafford, J., & Blackwell, P. (1980). The plastic limit, as determined by the drop-cone test, in relation to the mechanical behaviour of soil. *Journal of Soil Science, 31*(1), 11-24.

[139] Busscher, W. J., Bauer, P. J., Camp, C. R., & Sojka, R. E. (1997). Correction of cone index for soil water content differences in a coastal plain soil. *Soil and Tillage Research, 43*(3), 205-217.

[140] Vaz, C. M. P., Bassoi, L. H., & Hopmans, J. W. (2001). Contribution of water content and bulk density to field soil penetration resistance as measured by a combined cone penetrometer–TDR probe. *Soil and Tillage Research, 60*(1), 35-42.

[141] Wieder, W., Shoop, S., Barna, L., Franz, T., & Finkenbiner, C. (2018). Comparison of soil strength measurements of agricultural soils in Nebraska. *Journal of Terramechanics, 77*, 31-48.

[142] Anderson, S. J. (Compiler) (2011). *Scala Dynamic Cone Penetrometer Irregularity*http://www.cetanz.org.nz/Publications/TR1_Scala_Dynamic%20Cone_Penetrometer_Cone_Irregularity_230911_Rev3.pdf.

[143] Wikipeida. (2019). *Paintball marker*. 2019, from https://en.wikipedia.org/wiki/Paintball_marker.

[144] Standards New Zealand NZS 4402.6.5.2:1988, *NZS - 4402 - Methods of testing soils for civil engineering purposes - Soil strength tests - Determination of the penetration resistance of a soil.*

Appendices

4.1 Appendix A

4.1.1 Equipment

- 19 x 500ml Schott bottles
- 38 x 250ml Schott bottles
- 57 x 250mm long stainless tube (5mm OD)
- 57 x 100mm long stainless tube (5mm OD)
- 20m Tygon S3 E-3603 flexible tubing (4mm ID)
- 1 x Stainless water bath of 500l x 500w x 200h (mm)
- 1 x Grant T100-ST18 Stirred Water Bath
- 3 x G sized BOC dry air, gas code 108
- 1 x MagMate C Oxygen Regular Type 17
- 1 x Norgren R07 Miniature ported pressure regulator
- 1 x DWYER Series VF Visi-Float® Acrylic Flowmeter. Range: 0.06-0.5L/min
- 1 x Eutech Instruments Ph150
- Associated fittings

- Manifold:
    - 19 x Male Hose Tail, 1/8, 1/8 BSPT
    - 19 x Ball Valve Mini Male/Female, 1/8 BSP
    - 1 x Ball Valve Mini Male/Female, 1/4 BSP
    - 1 x Male Hose Tail, 1/4, 1/4 BSPT
    - 1 x 300mm how bar, 10 mm thick
- 320 x 200ml alkaline soln, 0.1N NaOH, 0.05N HCl
- Titration equipment:
    - Alkaline Solution 0.1 M NaOH
    - 5.6 kg of NaOH
    - Titrant Soln 1.0 M HCL
    - 38 x 100 mL conical flasks
    - 5 mL Eppendorf Research® plus, single-channel, variable

4.1.2 Biodegradation apparatus

Figure 4.1: Physical set-up of biodegradation experiment.

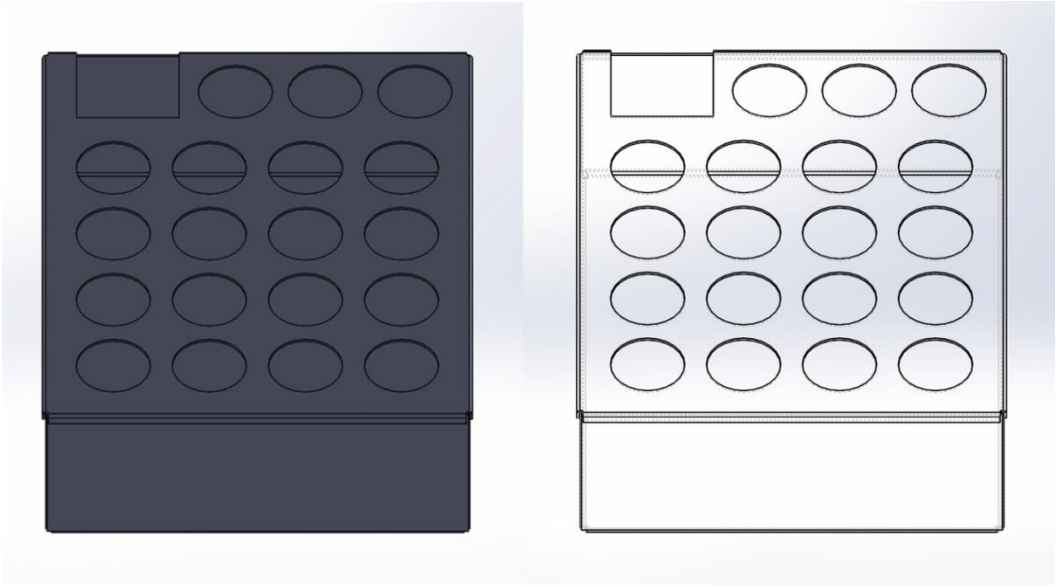

Figure 4.2: SolidWorks images of biodegradation experimental water bath.

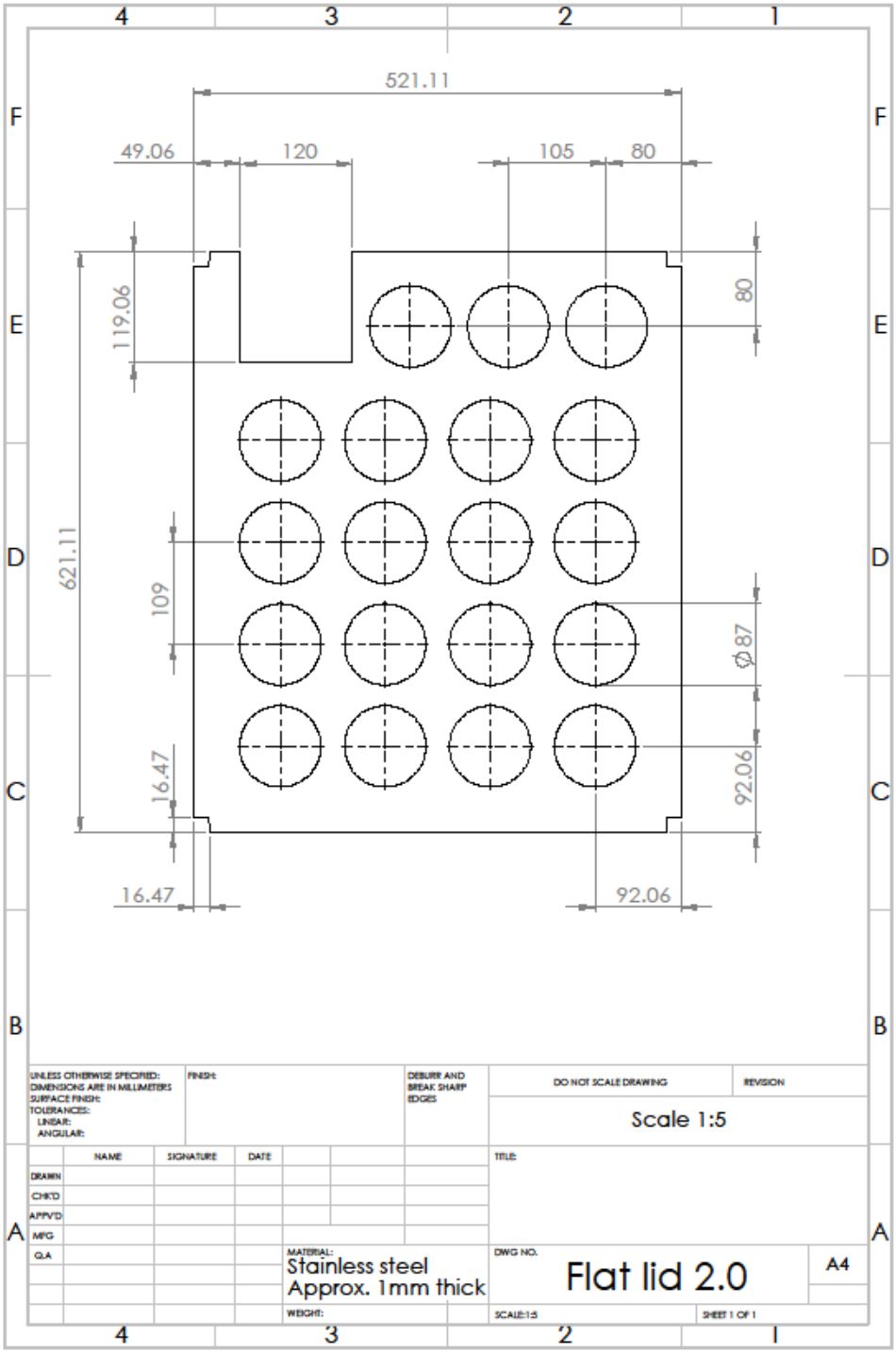

Figure 4.3: PDF of SolidWorks drawing for biodegradation water bath lid.

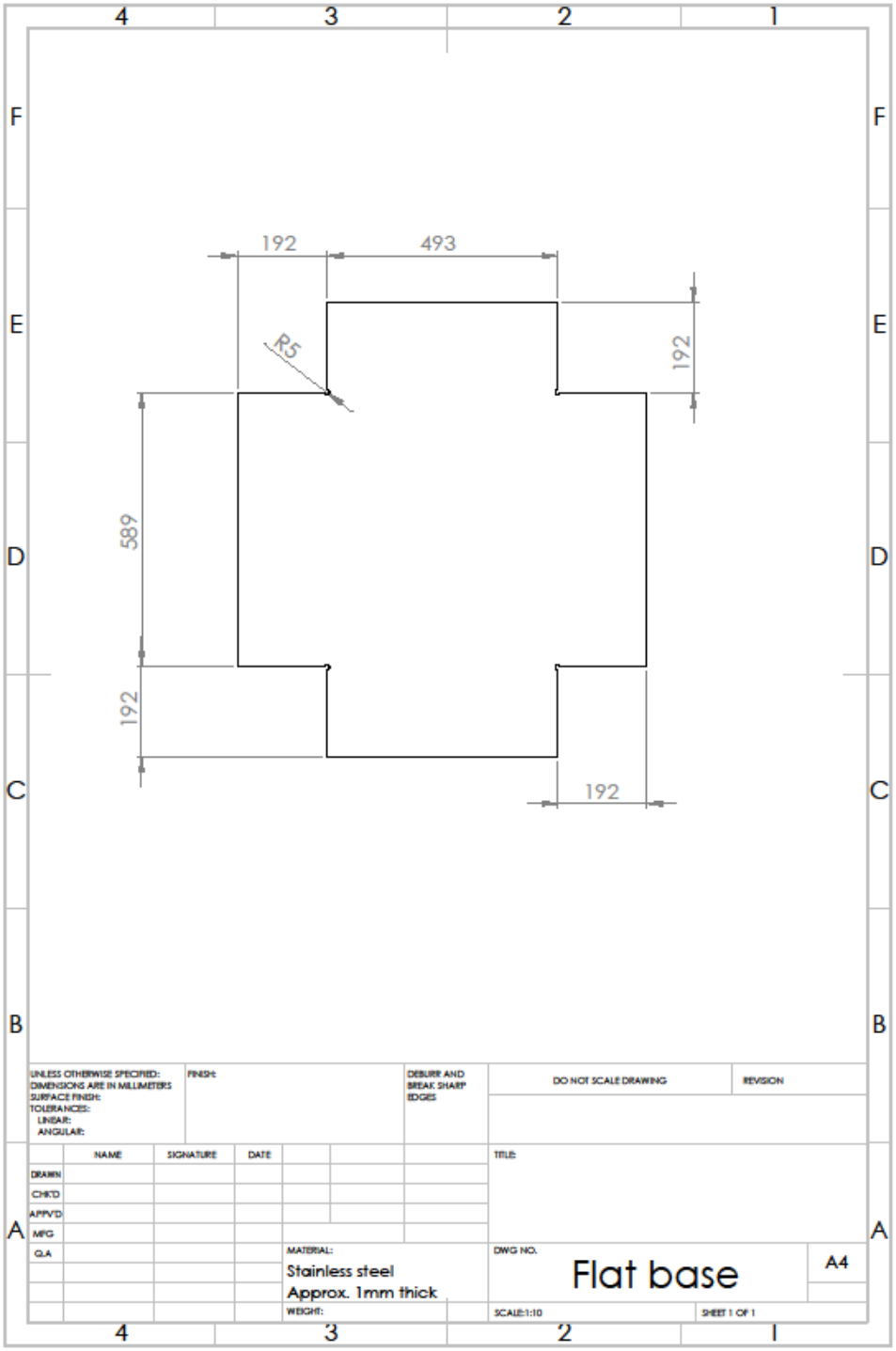

Figure 4.4: PDF of SolidWorks drawing for biodegradation water bath base.

4.1.3 Carbon content calculations

The carbon content of PBAT and glucose were calculated by calculating the mass fraction of organic carbon using Table 4.1.

Table 4.1: Table for calculating the mass fraction of carbon in PBAT and Glucose.

	g/mol	12	1	16	
	Periodic Element	**C**	**H**	**O**	
PBAT	component n	9	16	4	
	component m	12	12	4	
					SUM
	component n	108	16	64	**188**
	component m	144	12	64	**220**
		Mass fraction			
	component n	0.58			
	component m	0.66			
	Mass fraction of carbon	**0.62**			
Glucose	Periodic Element	C	H	O	
	Repeating monomer	6	12	6	
		Mass fraction			**SUM**
	grams	72	12	96	**180**
	Mass fraction of carbon	**0.4**			

The organic carbon content mass fraction of Novatein was found to be 27.51 % by SEM. Using the mass fraction we can calculate the test mass of sample required which is 1 g per 500 g of soil. Table 4.2 is the mass of carbon required for 500 g of carbon, this was adjusted for 300 g of soil during the experiment, as seen in the Biodegradation method.

Table 4.2: Mass of sample required per 500 g of soil.

Sample	Carbon Content	grams
NTP	0.28	3.64
PBAT	0.61	1.63
Glucose	0.40	2.50

4.1.4 Scrubber efficiency testing

The dry air purchased had 0.2 % CO_2 in it. Therefore knowing this quantity we can calculate the total CO_2 entering the system from Table 4.2.

Table 4.3: Calculating the total mass of CO_2 entering the system.

Air Flow rate (L/min)	3.70E-01
flow rate (m^3/min)	3.70E-04
duration (mins)	2.69E+03
CO_2 Conc (%)	2.00E-01
Air density (kg/m^3)	1.23E+00
CO_2 mass total (g)	2.44E+00
CO_2 mass per sample (g) ($\boldsymbol{CO_{2\ total}}$)	**1.28E-01**

$$CO_{2\ Scrub}(g) = \frac{Moles\ CO_2 reacted}{MW_{CO_2}} \quad 4\text{-}1$$

$$Efficiency\ (f) = \frac{CO_{2\ Scrub}}{CO_{2\ Total}} \quad 4\text{-}2$$

From this, we get the scrubber efficiencies stated in Table 4.4. This was used as a correction factor during the experiment.

Table 4.4: Raw data for scrubber efficiency test.

Scrubber	Initial	Final	HCl added (mL)	NaOH reacted (M)	CO_2 reacted (M)	Mass of CO_2 (g)	Scrubber efficiency
9a	10.30	15.70	5.40	0.005	0.001	**0.062**	47.977
9	5.10	10.30	5.20	0.005	0.002	**0.070**	54.831
10a	21.20	26.80	5.60	0.006	0.001	**0.053**	41.123
10	15.70	21.20	5.50	0.006	0.001	**0.057**	44.550
11a	32.20	37.70	5.50	0.006	0.001	**0.057**	44.550
11	26.80	32.20	5.40	0.005	0.001	**0.062**	47.977
12a	43.20	48.60	5.40	0.005	0.001	**0.062**	47.977
12	37.70	43.20	5.50	0.006	0.001	**0.057**	44.550
13a	5.70	11.20	5.50	0.006	0.001	**0.057**	44.550
13	0.20	5.70	5.50	0.006	0.001	**0.057**	44.550
14a	16.60	22.00	5.40	0.005	0.001	**0.062**	47.977
14	11.20	16.60	5.40	0.005	0.001	**0.062**	47.977
15a	27.60	33.00	5.40	0.005	0.001	**0.062**	47.977
15	22.00	27.60	5.60	0.006	0.001	**0.053**	41.123
16a	38.60	44.10	5.50	0.006	0.001	**0.057**	44.550
16	33.00	38.00	5.00	0.005	0.002	**0.079**	61.684
17a	0.10	6.10	6.00	0.006	0.001	**0.035**	27.415
17	44.10	49.50	5.40	0.005	0.001	**0.062**	47.977
18a	6.10	11.60	5.50	0.006	0.001	**0.057**	44.550
18	11.60	17.00	5.40	0.005	0.001	**0.062**	47.977
19a	17.00	22.80	5.80	0.006	0.001	**0.044**	34.269
19	22.80	28.30	5.50	0.006	0.001	**0.057**	44.550
					Average Scrubber efficiency (%)		**45.48**
					Standard deviation		**6.53**

4.2 Appendix B

4.2.1 Sheet extrusion

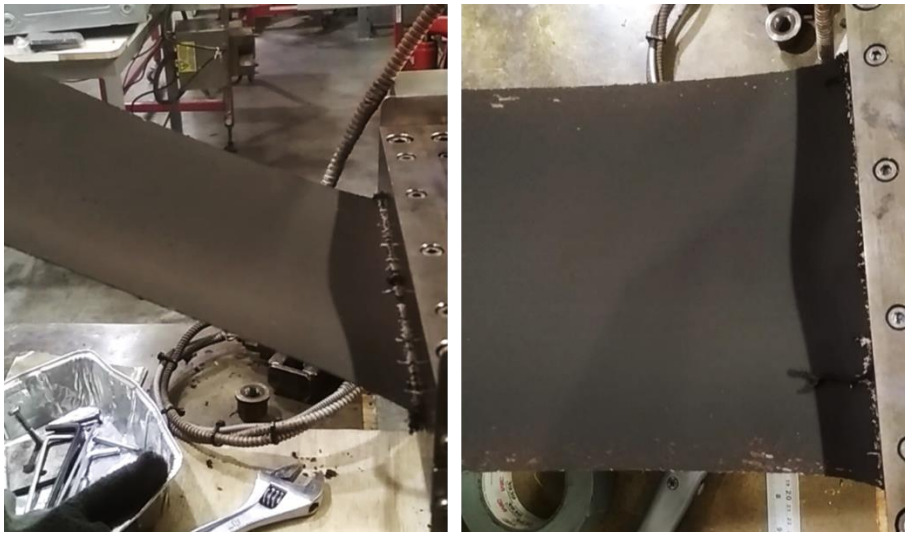

Figure 4.5: Sheet extrusion.

Figure 4.6: Sheet extrusion.

4.2.2 Aluminium mould

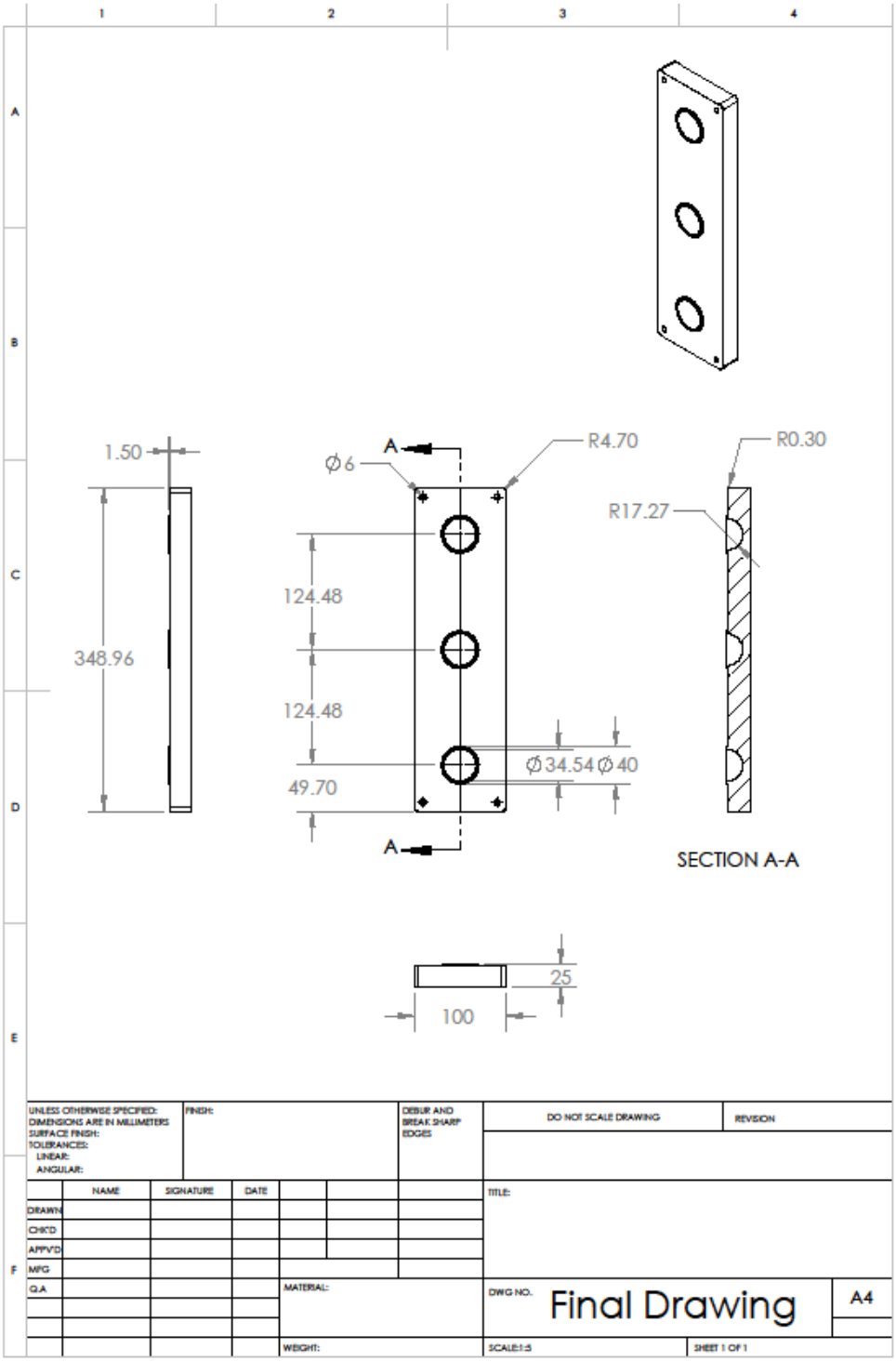

Figure 4.7: SolidWorks drawing with dimensions for the aluminium mould.

4.2.3 Welding data

Table 4.5: Feasibility weld data.

Test No.	Bearing Size (mm)	Approximate Press Temp (°C)	Approximate Release Temp (°C)	Press Time (min)	Average Sheet Thickness (mm)	Weld Adhesion (%)	Compression Force (N)	Compression Force (N)	Compression Force (N)	Compression Force (N)	Compression Force (N)	Compression Force (N)	Average (N)	Standard Deviation
1	14.3	15	15	0.5	1.25	0								
2	14.3	15	15	0.5	1.65	0								
3	15.9	100	100	1	1.25	0								
4	15.9	100	75	1	1.25	0								
5	14.3	100	75	1	1.25	0								
6	14.3	100	75	3	1.25	0								
7	14.3	100	75	1	1.35	0								
8	14.3	100	75	3	1.35	0								
9	15	75	60	1	1.15	0								
10	15	75	60	3	1.15	0								
12	15.9	75	60	1	0.45	0								
13	15.9	75	60	3	0.5	0-50								
15	14.3	75	60	3	0.5	20								
16	15.9	75	60	3	0.55	0-20								
17	15.9	75	25	3	0.55	50-100								
18	15.9	125	24	3	0.85	100	33.4**	33.4	DNS	DNS	DNS	DNS	**33.4**	**N/A**
19	15.9	110	21	1	1	100	23.5	36.3	35.3	DNS	DNS	DNS	**31.7**	**7.11898869**
20	15.9	105	30	3	1	100	20.6**	47	11.8**	49.1	40.2	48	**44.88**	**4.00946796**
21	15	120	29	3	0.9	0								
22	15	120	29	1	1	0								
23	15	95	34	3	0.95	0								
24	15	90	28	1	0.55	0								

25	15	90	24	3	0.5	100								
26*	15	105	28	1	0.5	100								
27*	15	105	31	3	0.5	0-70	2	2	DNS	DNS	DNS	DNS	**2**	**0**
28*	15	105	30	1	1	0								
29*	15	105	25	3	1	0								
30*	15	105	39	3	1	0								
31*	15.9	105	27	3	0.9	100	19.6	26.5	11.8**	4.9**	DNS	DNS	**23.05**	**4.87903679**
32*	15.9	90	33	3	1.05	0								
33*	15.9	115	28	3	1.1	100	31.4	15.7**	33.4	DNS	DNS	DNS	**32.4**	**1.41421356**
34*	15.9	115	30	3	1.15	100	15.7**	28.4**	33.4	33.4	DNS	DNS	**33.4**	**0**
35*	15.9	16	20	0.5	1.05	0								
36*	15.9	16	20	1	1.05	0								
37*	15.9	16	20	3	1	0								
38*	15.9	90	28	0.5	1.05	0								
39*	15.9	90	25	1	1.1	0-10								
40*	15.9	105	31	0.5	0.95	0-70	25.5	DNS	DNS	DNS	DNS	DNS	**25.5**	**N/A**
41*	15.9	105	26	1	1.05	60-80	15.7	DNS	DNS	DNS	DNS	DNS	**15.7**	**N/A**
42*	15.9	115	33	0.5	1	80-100	26.5	16.7	DNS	DNS	DNS	DNS	**21.6**	**6.92964646**
43*	15.9	115	32	1	1	100	48.1	49	20.6	DNS	DNS	DNS	**39.2**	**16.1432132**
44*	15.9	115	27	1	1.05	100	13.7	6.9**	13.7	18.6	37.3	DNS	**20.8**	**11.2235987**
45*	15.9	105	30	3	1.1	50-90	22.6	18.6	8.8**	7.8**	23.5	DNS	**21.6**	**2.60832002**

**Denotes use of CRC 808 Silicone Spray, **Denotes torn or otherwise damaged test samples, DNS = Did Not Survive*

Table 4.6: Tensile data for welded dog bones.

Sample No.	Sample reference	Weld load (N)	Load at maximum (N)	Extension at maximum (mm)	Tensile strength (MPa)
114	T1	500	37.20		2.95
134		500	40.52	4.61	4.59
140		500	47.41	4.04	4.70
142		750	36.04	2.75	4.09
143		750	52.90	5.63	6.00
115	T2	500	52.60		3.48
116		500	59.60		3.78
121		750	69.68	5.40	5.03
122		750	69.14	5.17	4.77
162		900	66.95	4.85	4.43
177		900	39.48	2.49	2.85
171	T3	500	91.26	4.66	4.67
172		500	79.88	3.30	4.23
173		500	77.36	4.20	4.39
168		750	82.02	3.60	4.20
169		750	83.79	4.32	4.59
170		750	70.79	3.03	3.87
137		900	84.86	4.90	4.64
138		900	41.22	1.76	2.26
2	1.44mm	N/A	95.64	8.94	5.27
3	0.57mm	N/A	32.67	2.79	4.55
6	1.33mm	N/A	99.60	11.22	5.94
8	1.0mm	N/A	77.95	7.38	6.19
9	1.2mm	N/A	103.42	15.64	6.84

Table 4.7: Peel data.

Sample reference	Weld force (N)	Load at maximum (N)
T1	500	6.89
	500	2.64
	750	4.88
	750	8.60
	750	8.60
T2	500	9.35
	500	8.37
	750	11.61
	750	9.34
	750	9.79
	750	7.36
	900	10.76
	900	11.14
T3	500	10.21
	500	8.07
	500	5.34
	750	9.97
	750	8.16
	750	9.93
	900	8.45
	900	11.98
	900	14.51

4.2.4 Welding images

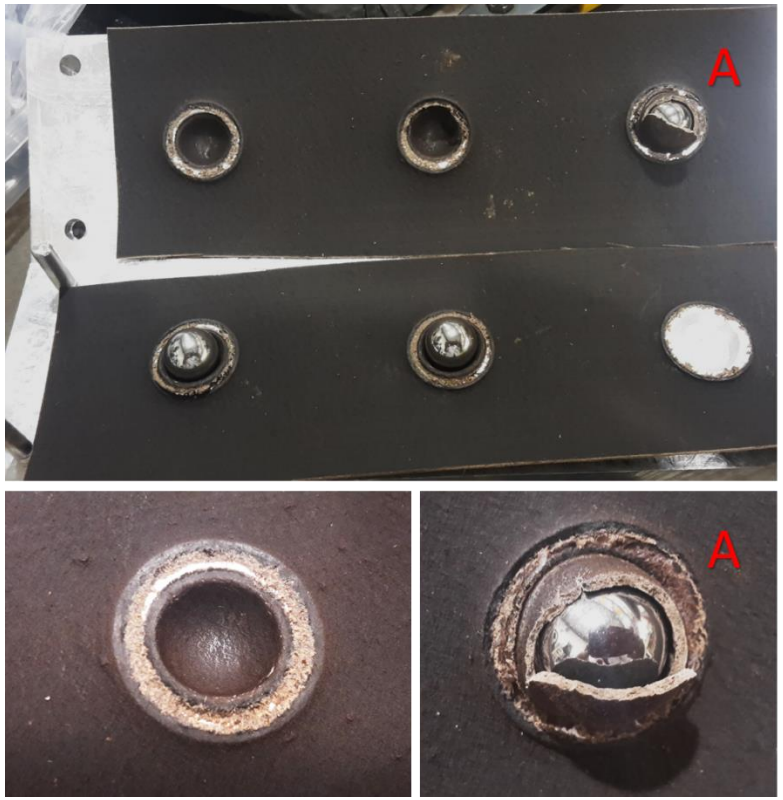

Figure 4.8: Unsuccessful weld samples.

Figure 4.9: Progression of improved of feasibility welds, left to right.

Figure 4.10: Successful scoping welds on left, unsuccessful scoping welds on right.

4.3 Appendix C

4.3.1 Penetrometer method

PART 2 – SCALA PENETROMETER (DYNAMIC CONE PENETROMETER)

The Scala (or dynamic cone) penetrometer is widely used in NZ to obtain field strength data for soils. It involves dropping a known weight and fixed distance and measuring the penetration of a standard tip into the soil. Slightly different procedures are used depending on the end use of the data, and all consultancies will have their own internal methods. The method below is a simplified one for demonstration of the use of the equipment.

1. Hold the Scala penetrometer vertical and gently tap the hammer on the anvil until the top of the cone is flush with the soil surface (bedding in).
2. Use a tape measure and board on the ground to record this zero position.
3. Raise the hammer to the top of the rod (full 508 mm) and let it drop to the anvil.
4. If the penetration is less than 20 mm make more hammer blows until the depth is 20 mm or until there have been 8 blows without getting 20 mm penetration
    a. if less than 20 mm after 8 blows, STOP before you break something.
5. If the penetration is greater than 20 mm, continue using the hammer to drive the penetrometer to the desired depth (based on purpose – eg. buildings, road subgrade)
6. Take depth readings to the nearest 1 mm for each blow or series of blows, recording the depth and number of blows:
    a. the penetration should not exceed 300 mm for any one blow;
    b. stop if at any time it takes more than 8 blows for 20 mm penetration.

These data can be used to identify strength changes down the profile and estimate bearing strengths. An auger hole should be completed nearby to verify the stratigraphy seen in the penetrometer data.

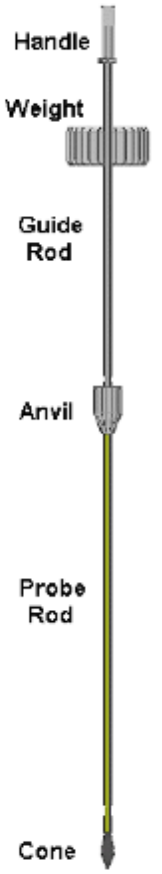

http://groundtest.co.nz/scala/scalapage2.php

Figure 4.11: Dynamic cone penetrometer method.

4.3.2 Example calculations

Below is example calculations for the Results in Table 4.8. Equation 3-9 is rearranged to make S the subject in Equation 4-3.

$$S_{Young} = \frac{D}{\left((0.000178 * N * \left(\frac{W}{A}\right)^{(0.7)} * (V - 30.5)\right)} \quad 4\text{-}3$$

Equation 3-14 is rearranged to make S the subject in Equation 4-4

$$S_{Lorenz} = \left(\frac{D}{\left((4.5 * 10^{-8} * \left(\frac{W}{A}\right)^{(0.7)} * (V)^2\right)}\right)^2 \quad 4\text{-}4$$

Using Equation 4-3 with the 0 wt.% moisture fine sand with the sold sphere you get Equation 4-5

$$S_{Young} = \frac{0.02}{\left((0.000178 * 0.685 * \left(\frac{0.002}{0.00024}\right)^{(0.7)} * (100 - 30.5)\right)} \quad 4\text{-}5$$

Resulting in a S_{Young} value of 239. Using this in the rearranged Equation 3-8, Equation 4-6 gives the theoretical N (number of drops to 0.3 m)

$$N_{theoretical} \sim \left(\frac{60}{S} + 2\right)^{\frac{1}{0.55}} \quad 4\text{-}6$$

Resulting in a $N_{theoretical}$ of 4.37. Calculating the percentage error from the $N_{experimental}$ of 4.36, gives an percentage error of 0.28 %.

For the same example for Lorenz, Equation 4-4 results in Equation 4-7.

$$S_{Lorenz} = \left(\frac{0.02}{\left((4.5 * 10^{-8} * \left(\frac{0.002}{0.00024}\right)^{(0.7)} * (100)^2\right)}\right)^2 \quad 4\text{-}7$$

Resulting in a S_{Lorenz} value of 102. The $N_{theoretical}$ was calculated with Equation 4-6 and compared with the $N_{experimental}$ as seen for the Young example.

4.3.3 Percentage error results

Table 4.8: Theoretical S and N_D values for the three different shapes investigated over the different mediums.

Sand	Circle			Parabolic			Pointed			Circle			Parabolic			Pointed		
	$S_{(Young)}$	theoretical N_D	% error	$S_{(Young)}$	theoretical N_D	% error	$S_{(Young)}$	theoretical N_D	% error	$S_{(Lorenz)}$	theoretical N_D	% error	$S_{(Lorenz)}$	theoretical N_D	% error	$S_{(Lorenz)}$	theoretical N_D	% error
0 % fine	239	4.37	0.28	183	4.65	6.60	228	4.42	1.26	102	5.63	29.07	92	5.90	35.26	161	4.81	10.25
5 % fine	458	3.96	0.80	310	4.17	4.53	334	4.12	3.35	375	4.06	1.64	264	4.29	7.49	346	4.10	2.79
10 % fine	493	3.93	30.64	350	4.10	27.65	293	4.21	25.62	436	3.98	29.69	336	4.12	27.21	267	4.28	24.38
0 % coarse	299	4.20	44.78	199	4.55	40.09	244	4.35	42.72	160	4.82	36.57	108	5.50	27.66	185	4.63	39.05
5 % coarse	415	4.00	27.99	326	4.14	25.57	366	4.07	26.82	308	4.18	24.90	292	4.21	24.22	417	4.00	28.04
10 % coarse	439	3.98	28.72	350	4.10	26.61	269	4.27	23.39	345	4.10	26.45	336	4.12	26.17	224	4.43	20.60